

Volume: 24/ 1&2

JANUARY 2012

ISRAPS Bulletin

TSRP - 2012 SPECIAL ISSUE

SUPRAMOLECULAR CHEMISTRY

&

ITS APPLICATIONS



Guest Editor

Dr. A. C. Bhasikuttan

A Publication of
Indian Society For
Radiation & Photochemical Sciences

Fluorescence & Phosphorescence Spectrometers

FLS920 Series

Steady state, fluorescence lifetime (using TCSPC) and phosphorescence (MCS) decay measurements

Modular architecture gives you the choice and flexibility to build a system to suit your application needs

Ultrafast data acquisition lets you watch profiles build in real time on your computer screen

High performance monochromators with high stray light rejection

Control your choice of measurement using a single data acquisition and analysis software package

A microscope attachment is available to complement your research



Software

Spectral correction

Fitting of single and multi-exponential decays

Eleven measurement modes including

synchronous spectra, anisotropy spectra and time resolved spectra

Advanced Analysis Package

Discrete component analysis of multiple exponential terms

Fluorescence lifetime distribution analysis

Global lifetime analysis

Advanced analysis of time resolved fluorescence anisotropy

TCSPC Time-correlated single photon counting
Fluorescence decays 100ps – 50ps

MCS Multi-Channel Scaling, Phosphorescence decays 1ps – 10s

Steady State Sensitivity (Water Fluorescence) > 10000:1

Edinburgh Photonics

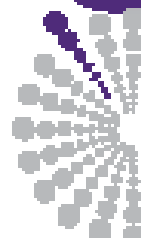
2 Blair Square, Kirkton Campus,
Livingston, EH54 7DQ,
United Kingdom

Telephone:
+44(0) 1506 425 300

Facsimile:
+44(0) 1506 425 300

Email:
sales@edinet.com/ specialise@edinet.com

Website:
www.edinburghphotonics.com
www.specialisedinstruments.com



**EDINBURGH
PHOTONICS**

A Division of
EdinburghInstruments Ltd.

Accessories

Temperature control options

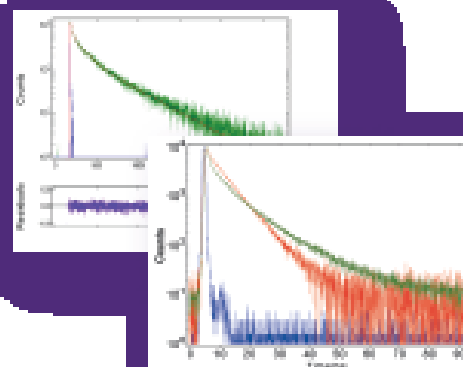
Polarisers

Integrating sphere

Pulsed diode lasers and LEDs

Stopped flow system

Photocounter module



Pride in Precision

Supramolecular Chemistry & its Applications

A Publication of Indian Society for Radiation & Photochemical Sciences

CONTENTS

| | |
|---|----|
| Editorial..... | 3 |
| Message from the President & Secretary, ISRAPs..... | 5 |
| Supramolecular Chemistry: Physico-Chemical Properties and Prospects of Cucurbituril Based Molecular Assemblies <i>Jyotirmayee Mohanty, Sharmistha Dutta Choudhury, Haridas Pal and Achikanath C. Bhasikuttan.....</i> | 6 |
| Grappling with Molecular Design: Attempts at Creating Potential Optical Probes for Targeting Zn (II) <i>Sabir H. Mashraqui</i> | 20 |
| Molecular Recognition by Calix[4]arene Scaffolds <i>Jugun Prakash Chinta and Chebrolu P. Rao</i> | 31 |
| Role of Crown Ethers and Calixarenes in Radioactive Waste Remediation <i>P.K. Mohapatra.....</i> | 43 |
| Functionalized Boron-dipyrromethenes and their Applications in the Synthesis of New BODIPY Systems <i>Tamanna K. Khan and M. Ravikanth</i> | 51 |
| Radiation Induced Grafting for Surface Modification of Macromolecules <i>N. K. Goel, Virendra Kumar, Y. K. Bhardwaj, L. Varshney.....</i> | 70 |

ISRAPS EXECUTIVE COUNCIL

President:

Dr. Tulsi Mukherjee

Vice-Presidents:

Dr. Sisir K. Sarkar

Dr. P.N. Bajaj

Secretary:

Dr. Tapan K. Ghanty

Treasurer:

Dr. S. Dhanya

Executive Members

Co-opted Members

Prof. Samita Basu
Dr. D.B. Naik
Dr. Haridas Pal
Prof. K. Pitchumani
Prof. B.S.M.Rao
Prof. Anunay Samanta
Dr. R.K. Vatsa

Dr. C.T. Aravindakumar
Dr. T. Bandyopadhyay
Dr. H.N. Ghosh
Dr. Sanjay Pant
Dr. C.N. Patra
Prof. P. Ramamurthy
Dr. Sunil Sabharwal
Dr. A.V. Sapre
Prof. A. K. Singh
Dr. H. P. Upadhyaya

ISRAPS EDITORIAL COMMITTEE:

S. K. Sarkar

P. N. Bajaj

K. I. Priyadarshini

Tusar Bandyopadhyay



ISRAPS Bulletin
A Publication of
Indian Society for Radiation and Photochemical Sciences

Editorial

Dear ISRAPS Members

It gives me immense pleasure to edit this special bulletin featuring the science of macromolecules and their relevance in the wide area of supramolecular chemistry. This collection of articles originated from the presentations at the thematic discussion meeting on 'Supramolecular Chemistry and its Applications' organized by the ISRAPS some time back. Supramolecular chemistry embodies the creative power of chemistry. Indeed, it fashions entire new worlds that do not exist before they are shaped by the hand of the chemists. Ever since the award of the 1987 Nobel Prize to Cram, Lehn, and Pedersen for their development and use of *molecules with structure-specific interactions of high selectivity*, studies of supramolecular sciences have become one of the major areas of scientific endeavor involving scientists from virtually all areas of sciences. Macro-polycyclic structures meet the requirements for designing artificial receptors, which may be considered as a generalized coordination chemistry, not limited to transition metal ions but extending to all types of substrates: cationic, anionic or neutral species of organic, inorganic or biological nature. They are large and may therefore contain cavities and clefts of appropriate size and shape to allow the arrangement of structural groups, binding sites and reactive functions with pre-designed tunability.

This issue provides a glimpse of applications of various cavitand macrocycles like *Cyclodextrins*, *Cucurbiturils*, *Calixarenes*, and other polycyclic ligating macromolecules like *Crown ethers*, *Porphyryns*, *Grafted macromolecules*, which are tailored to function for specific chemical interactions. Their indisputable command in stimulus responsive molecular assemblies, drug delivery, sensors, photoreceptors, recognition of aminoacids/proteins, separation of radionucleotides, surface modified macromolecules through radiation-induced grafting etc. are a few among their vast potential. Though this collection is only a glimpse of the vast field of supramolecular chemistry, I am sure that the contents will certainly boost up active research on such supramolecularly assembled systems and their photochemical and radiation chemical advantages in multidisciplinary areas. I gratefully acknowledge the active cooperation from all the contributors and thank the office bearers of ISRAPS for entrusting this job to me.

A.C. Bhasikuttan (Guest Editor)
Radiation & Photochemistry Division
Bhabha Atomic Research Centre, Mumbai, INDIA



Achikanath C. Bhasikuttan obtained his M.Sc. in Chemistry from Calicut University, Kerala in 1989 and joined Bhabha Atomic Research Centre, Mumbai, India, in 1991 after one year advanced orientation course conducted by the BARC Training School (34th Batch). After his Ph.D. from the University of Mumbai in- 1998 he joined as a JSPS postdoctoral fellow at Osaka University, Japan, 1999-2001. He was at the Heidelberg University, Germany as a visiting scientist during 2006. His research interests include the time resolved excited state molecular dynamics and the intricacies of non-covalent interactions in supra-biomolecular systems. He is a recipient of the Scientific & Technical Excellence Award -2009 from the Department of Atomic Energy, India and a Fellow of the Maharashtra Academy of Sciences & the National Academy of Sciences, India.



INDIAN SOCIETY FOR RADIATION AND PHOTOCHEMICAL SCIENCES

(Reg. No. 617/1985, GBBSD, Bombay; Trust No. F-10965) (Affiliated to IARR)

Radiation & Photochemistry Division

Bhabha Atomic Research Centre, Mumbai - 400 085

Member Enrolment Form

1. Name in Block Letters:

2. Date of Birth:

3. Highest Academic Qualification:

4. Present Position:

5. Addresses:

Photograph

| Office | Residence |
|-----------------------|-----------------------|
| Put your address here | Put your address here |
| Telephone | Telephone |
| Fax | Fax |
| E-mail | E-mail |

6. Address for Correspondence: Office / Residence

7. Category of Membership Applied for: Annual / Life / corporate member

8. Remittance (DD only) payable to ISRAPS, Mumbai

| Category | Fees | Admission fee | Total Amount |
|------------------|------------|---------------|--------------|
| Annual | Rs 200/- | Rs 100/- | Rs 300/- |
| Life Member | Rs 1500/- | Rs 100/- | Rs 1600/- |
| Corporate Member | Rs 20000/- | Rs 1000/- | Rs 21000/- |

9. Brief Resume of activities and research interests:

10. List of memberships of other professional bodies, if any:

11. List of prizes/awards/fellowships received, if any:

12. Number of Publications:

I agree to abide by the constitution and bye-laws, and rules and regulations of the SOCIETY.

Place:

Signature

Date

Message from the President and Secretary

Greetings from the Executive Council of ISRAPS for a very happy and prosperous new year 2012! In the year 2011 we have held the National Symposium on Radiation and Photochemistry (NSRP-2011) at JNV University, Jodhpur during March 2011. It was a great success with almost 200 participants from various universities and institutes. Leading experts in their respective areas delivered talks emphasizing current developments in both the field..

All our efforts in recent months have been focused on the preparation for organizing Trombay Symposium on Radiation & Photochemistry to be held during January 4-7, 2012, at Bhabha Atomic Research Centre, Mumbai. Radiation and Photochemistry Division of BARC and ISRAPS are jointly organizing this symposium. On behalf of ISRAPS and symposium organizing committee we extend our warm welcome to all the delegates of the symposium and wish them a very interactive and fruitful meeting. This is a special issue of ISRAPS Bulletin, which is being published on the eve of TSRP-2012. Finally, we like to thank Dr. A. C. Bhasikuttan, the Guest Editor of this special issue, for his efforts in bringing out a scientifically rich issue of ISRAPS bulletin containing six articles on the theme "Supramolecular Chemistry & its Applications". Thanks are also due to all the authors for contributing articles.

With great pleasure, we like to inform our members that BRNS has agreed to give a grant for the publication of ISRAPS bulletin.

We wish to express our gratitude to each and every member of ISRAPS for their continued support and cooperation in carrying out the activities of the society.

(Dr. Tulsi Mukherjee)
President

(Dr. Tapan K. Ghanty)
Secretary



(Dr. Tulsi Mukherjee)
President



(Dr. Tapan K. Ghanty)
Secretary

Supramolecular Chemistry: Physico-Chemical Properties and Prospects of Cucurbituril Based Molecular Assemblies

Jyotirmayee Mohanty, Sharmistha Dutta Choudhury, Haridas Pal and Achikanath C. Bhasikuttan*

Bhabha Atomic Research Centre, Trombay, Mumbai, 400085, INDIA

E-mail: bkac@barc.gov.in

Abstract

This article provides an account of the recent research findings from our group on the spectacular physico-chemical properties of cucurbituril-based supramolecular assemblies of chromophoric dyes having technological and biological importance. Simultaneous association of multiple hosts or guests either by cooperative binding or competitive displacement is an applied strategy to construct novel functional assemblies with predesignated characteristics. Here, effort has been made to briefly discuss the diverse photophysical characteristics of several host-guest complexes and intriguing response of such molecular assemblies towards external stimulants like metal ions. The detailed experimentation on these assemblies project their applications in controlled uptake and release of drugs, fluorescence on-off systems, photofunctional devices and molecular architectures.

1. Introduction

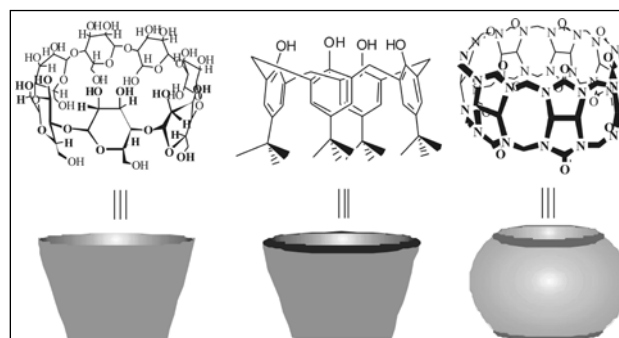
Supramolecular chemistry is the chemistry of large intermolecularly bound assemblies, covering the structures and functions of these entities formed by association of two or more chemical species, each designed to perform a specific task. More precisely, while the molecular chemistry rules the covalent bonds, the goal of supramolecular chemistry is to gain control over the intermolecular non-covalent bonds. Therefore, while a supramolecule is still a single molecule, it is engineered to function like a large complex compound [1]. The functional activities of such supermolecules formed by receptor-substrate (*host-guest*) binding rest on the molecular compatibility, transformation and translocation to effect the basic functions of such molecular assemblies, which got a shot in the arm ever since the award of the 1987 Nobel Prize to Cram, Lehn, and Pedersen for their development and use of molecules with structure-specific interactions of high selectivity.

In conceiving the same, chemists have often relied upon molecular recognition-guided supramolecular interactions, which allow rational control of the ensuing non-covalent interactions and its cooperativity, as a very powerful con-

struction principle for novel hierarchically ordered molecular assemblies with unprecedented physico-chemical properties [2]. In a supramolecular system, the components are held reversibly by intermolecular forces like, van der Waals molecular interaction, electrostatic interaction, hydrophobic interaction, hydrogen bonding interaction etc. Interplay of all such interactions and their implication in the desired applications makes the study of supramolecular sciences a highly interdisciplinary field of science and technology, bridging chemistry with biology and material science [1-3]. In the past decades, scientists have made enormous strides toward creating nanoscale assemblies and structures with aim to achieve applications ranging from targeted drug delivery to the development of functional materials [1-3]. The proliferation of such new assemblies have created immense interests to survey their mechanism of formation, the structural layout of their constituent components and the modulation in molecular properties [1]. Harnessing the full functionality of these nanostructures requires control over their intricate molecular dynamics. Since host-guest complexation is driven by non-covalent interactions that are much weaker than covalent bond strengths, the stability of the host-guest complexes is based on the cooperative

effect of multiple interactions. This is a favorable situation because it imparts flexibility to the systems and makes them amenable to desired modifications by external stimuli like light, temperature, pH or other additives [4-7]. Moreover, encapsulation of guest molecules within the host cavities can bring forth many interesting changes in their physicochemical properties, without any covalent modifications [8-11].

Many attempts have been made over the last few decades to realize such non-covalently linked host-guest complexes using classical macrocyclic host molecules like cyclodextrins (CDs, Chart 1), calixarenes (CXs, Chart 1), and other macrocyclic ligating hosts like crown ethers, porphyrins etc. Among the well known classical cavitand macrocycles, the homologues of cyclodextrins are naturally occurring cyclic oligosaccharides composed of D-glucofuranose units joined by ether linkages and the most common members of this family being α -, β -, and γ -CDs, which are made up of six, seven and eight D-glucofuranose units, respectively [12]. The structure of the CDs is that of a truncated cone, having an inner hydrophobic cavity and outer hydrophilic edges consisting of hydroxyl groups as show in Chart 1. Calixarenes (Chart 1), are the synthetic cavitand macrocycles, obtained by the oligomerisation of phenol and formaldehyde. While the stereochemical orientation of the ligating arms can be properly tuned, the larger homologues like calix[6/8]arenes can also be easily functionalised and adapt their conformations to the stereochemical request of the multivalent receptor entity [13]. There are several other macrocyclic ligands which can form metal complexes exclusively and are being extensively studied for their variety of applications. The crown receptors, especially the aza-crown compounds have complexation properties that are intermediate between those of the all-oxygen crowns, and those of the all-nitrogen cyclams, which strongly complex heavy-metal cations [14]. Porphyrins and phthalocyanines, planar macrocyclic ligands, composed of four isoindole units are another group of ligating macrocyclic compounds, which exhibit immense potential for building extended



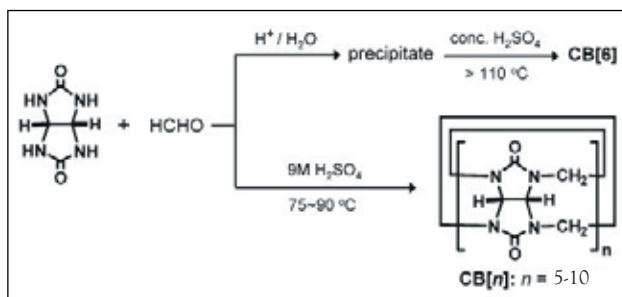
β -Cyclodextrin Calix[4]arene Cucurbit[7]uril
Chart 1: Chemical structures and typical representations of the cavitand macrocycles described.

functional assemblies, phototherapeutics and for bioanalytical applications.

Interestingly, relatively new entrant to the cavitand macrocycle family, the cucurbit[n]urils (CBn, Chart 1), have made excellent results in host-guest complexation, especially, involving cationic guest molecules [15,16]. In many cases, as compared to the cyclodextrin counterpart of comparable dimension, the cucurbiturils have shown over 100 fold enhancement in the binding interactions and remarkable change in the physico-chemical properties of the guests [8,17]. By harnessing the immense potential of such supramolecular host-guest interactions of cucurbiturils, several groups, including ours, have demonstrated many interesting attributes like, supramolecular pK_a shift [8,17,18], guest relocation [5], enhancer strategy [10], supramolecular architecture [19], fluorescence on-off systems [6], molecular capsule [4], aqueous dye laser systems [20], etc. In this article, we discuss the physico-chemical properties of some of these interesting cucurbit[n]uril based molecular assemblies and their prospects in comparison with that of cyclodextrins.

2. Cucurbit[n]urils: A class of versatile macrocycles

Cucurbit[n]urils are interesting class of macrocyclic receptor molecules composed of methylene-bridged glycoluril monomers having highly symmetrical hydrophobic cavities accessible through two identical carbonyl laced portals. Depending upon the number of monomer units, different homologues of cucurbit[n]urils



Scheme 2: Synthetic route for the preparation of CB_n

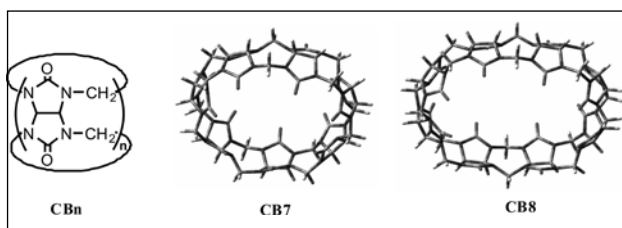


Chart 2: Structural formula of CB_n ($n = 5-10$) and energy optimized structures of CB_7 and CB_8 .

(CB_n ; $n = 5-10$, Chart 2) with varying cavity and portal dimensions are known [15,16].

A synthetic approach for cucurbit[n]urils involves the acidic condensation of glycoluril with formaldehyde at 75-90°C for ~72 hours to yield a mixture of $CB[n]$ homologues (Scheme 2). From the mixture of different CB s, the individual CB s are separated in pure form using fractional crystallization and dissolution using various solvent systems, such as acetone-water and methanol-water mixtures and involve multiple solvent-based separation cycles [21].

Cucurbiturils are proficient hosts to bind a range of guest molecules like organic dyes into their rigid cavities through hydrophobic interactions, or metal cations and protonated alkyl and aryl amines via ion-dipole interactions involving their carbonyl portal ends. Among the set of CB s, the complexation behavior of cucurbit[7]uril (CB_7), has been extensively studied due to its substantial solubility in water as compared to the other homologues like CB_5 , CB_6 , CB_8 and CB_{10} [15,16].

Among the CB series, going from CB_5 to CB_{10} , the cavity width increases gradually with a constant cavity height (9.1 Å). Though they have similar structural features, their varying inner and portal dimensions lead to remarkable molecular recognition behavior which are different from

each other. For example, the smallest homologue CB_5 binds small gas molecules like O_2 , N_2 , Ar inside the macrocyclic cavity and cations like NH_4^+ , and Pb^{2+} strongly at the portals [15,16]. The next higher homologue i.e. CB_6 forms stable complexes with protonated diaminoalkanes, benzyl amines and alkali metal ions, where as CB_7 forms stable inclusion complexes with larger guest molecules. On the other hand, the cavity of CB_8 being large enough, it can accommodate more than one guest molecules simultaneously to form 1:2 host-guest complexes or 1:1:1 ternary complexes. Interestingly CB_{10} , the largest CB homologue reported, is capable of encapsulating the smallest homologue, CB_5 as well as large chromophores like metalated tetra (N-methylpyridinium) porphyrins through its large ellipsoidal cavity [15,16].

3. Physico-chemical properties and prospects of CB_n based assemblies

In general the stability constants of the host-guest complexes formed by the cucurbituril macrocycles are higher than those of the corresponding cyclodextrins with the same guest, and can be several orders of magnitude larger when the guest is cationic [8,17]. Simultaneous association of multiple hosts or guests either by cooperative binding [10,19] or competitive displacement [5,6] mechanism is another idea to construct novel assembled systems involving cucurbiturils with diverse characteristics. On the other hand, the binding interactions being mainly non-covalent in nature, make it convenient to tune them by wide range of stimuli like competitive binders, pH, temperature, light, redox control, etc. Since the guest molecules experience low polarity [11], and an extremely low polarizability (close to the gas phase) inside the host cavity and strong ion-dipole interaction at the portal region (for cationic guests), the complexed guest molecules show fundamentally different photophysical chemical and physicochemical behaviors. Further, the cavity of cucurbiturils also provides an inert reaction medium and protects the guests from the interaction with the surrounding solvent molecules [11].

On the other hand, fluorogenic dyes find

many usages in technological, biological as well as medicinal applications. In the recent years, we have contributed towards the understanding of supramolecular interactions of number of the important chromophoric dyes with the cucurbituril hosts and explored their implications in several applied areas. Effectively, the promising modulation in the physico-chemical properties of the guests in the presence of CBs have been projected towards variety of possible applications (*vide supra*). The studies are mainly carried out using steady-state and time-resolved absorption and fluorescence techniques with support from ^1H NMR and computational inputs.

3.1. Prototropic guests: Supramolecular pK_a shifts

Controlling the protolytic equilibrium of drugs/dyes is useful in selected medicinal and biological applications to achieve controlled binding and release of the active form of the drugs. The prototropic equilibrium of dyes can be significantly altered upon complexation with macrocyclic hosts due to the differential binding affinity of the host molecules towards the different prototropic forms of the dyes (Chart 3). With these objectives, the effect of supramolecular host-guest interaction on the prototropic equilibrium of selected potential dyes, namely, Neutral Red (1) and Acridine Orange (2), (Chart 3), using cucurbit[7]uril and β -cyclodextrin (β -CD) hosts has been examined. These dyes have been extensively used as fluorescent probes, stains for biological systems and are the parent molecules for several drug systems. They exist in two different prototropic forms and depending upon the pH of the solution they show sharp color

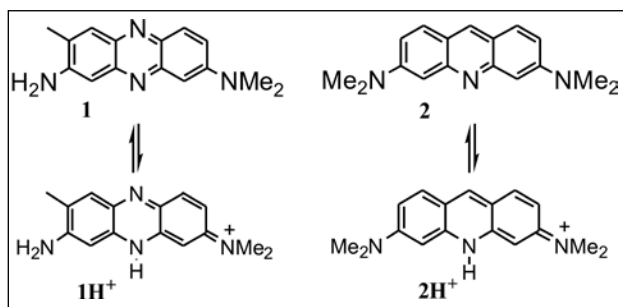


Chart 3: Chemical structures of dyes showing prototropic equilibrium.

changes or distinctive spectral changes around their ground-state pK_a values, especially in case of neutral red, pK_a 6.8 [8] and for acridine orange, pK_a 9.8 [17].

Shift in the absorption and fluorescence peaks and increase in the fluorescence quantum yield, lifetime and rotational correlation time of both the prototropic forms of the dyes in the presence of CB7 host confirm the formation of inclusion complexes. Here the interactions are seen much stronger for the protonated $\text{CB7} \cdot 1\text{H}^+ / 2\text{H}^+$ complexes ($K > 10^5 \text{ M}^{-1}$) than the neutral $\text{CB7} \cdot 1/2$ complexes ($K > 10^3 \text{ M}^{-1}$) [5,8]. Such differential binding encouraged the ideas to preferentially control the availability of different prototropic forms of the dyes in solution, resulting a shift in their pK_a values.. The ground-state pK_a values of

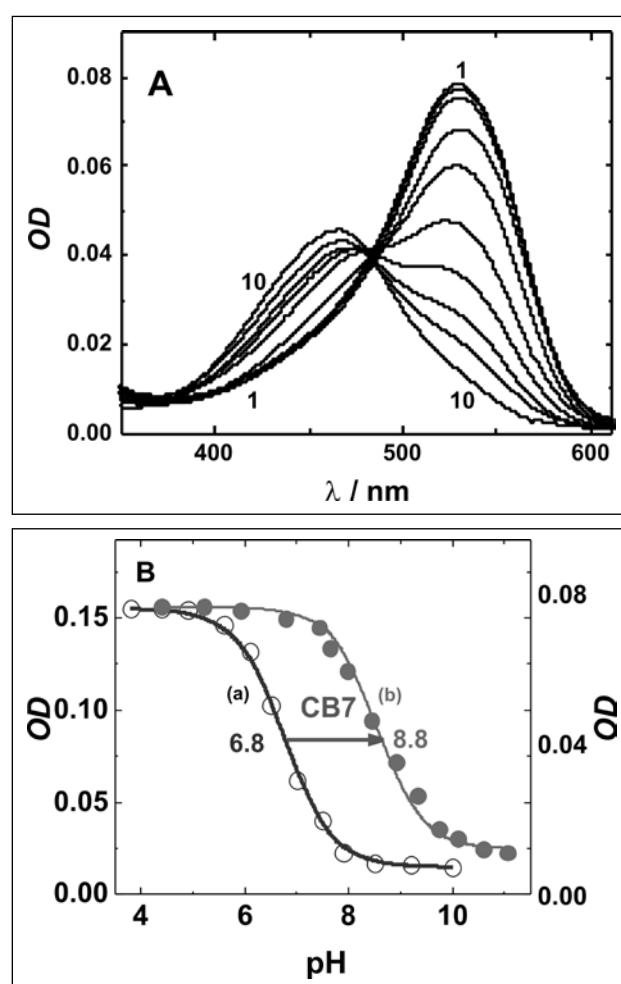
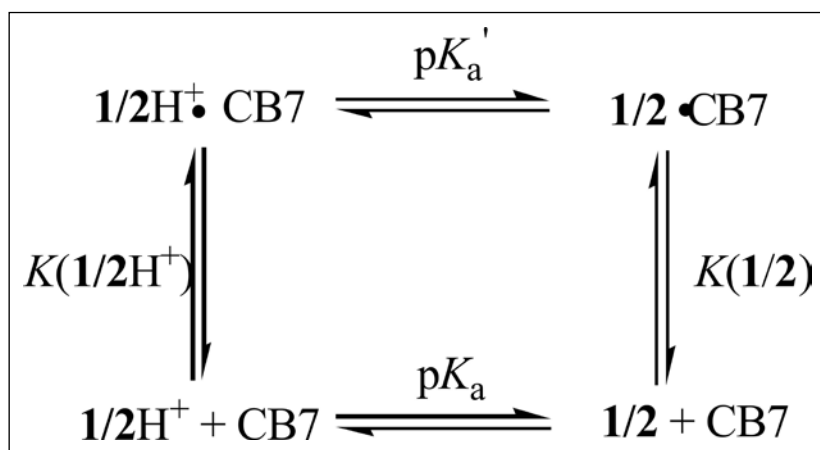


Figure 1: (A) Absorption spectra of neutral red (3uM) in water containing 150 μM CB7 at different pH: 3.5 (1) and 11.0 (10). (B) The variation in absorbance with pH at 530 nm in the absence (a) and presence (b) of 150 μM CB7.



Scheme 2: Four-state model for the feasible protonation equilibria with **1/2** dyes.

both the dyes in the presence of CB7 have been estimated using a four state model (scheme 2), revealing an exceptionally large upward $\text{p}K_a$ shift by more than two units (~ 2 units [8] for $\text{CB7}\cdot\text{1H}^+$ and ~ 2.6 units [17] for $\text{CB7}\cdot\text{2H}^+$ complexes), which make the CB7 bound guests more basic than the free dyes. The pH titration data in presence of CB7 presented for the NR dye (Fig.1), clearly emphasizes the increase in the $\text{p}K_a$ value of the protonated dye due to the strong affinity of CB7 towards the protonated form, which is stabilized in the complex by additional ion-dipole interactions with the ureido carbonyl rim of the macrocyclic host. For biological applications, the features of the protonated form of the dye are predominant and display its name-carrying red/orange colour. Thus, the prototropic equilibrium of the guest molecules can be significantly changed upon complexation with macrocyclic hosts and this property has been employed in selected medicinal and biological applications.

In contrast, the results obtained from the measurements on using β -CD host, having comparable cavity size as that of CB7, shows a downward $\text{p}K_a$ shift by ~ 0.8 unit and makes the protonated guest more acidic [8,17]. Here, only the neutral form (**1/2**) of the dye, forms an inclusion complex with β -CD. The measured $\text{p}K_a$ of **1**, in the presence of 10 mM β -CD is much lower than the $\text{p}K_a$ value of 6.8, measured in the absence of β -CD. The comparison of the complexation behavior of neutral red towards CB7 and β -CD reveals that although both hosts

have a hydrophobic cavity, additional recognition elements like cation receptor sites at the portals of the CB7 cavity are essential to promote a strong and selective binding of the protonated forms of these fluorescent dyes. The cationic form undergoes no significant complexation with β -CD, but binds strongly with CB7 ($K_{\text{eq}} = 2.0 \times 10^5 \text{ M}^{-1}$), causing a large enhancement in fluorescence intensity and lifetime of the dye in the latter host. In contrast, the neutral **2** form of the dye shows quite similar binding with both CB7 and β -CD, but the binding constants are lower by more than two orders of magnitude compared to that of the 2H^+ -CB7 system. Interestingly, CB7 and β -CD show a contrasting behavior in modifying the acid-base character of the dye, shifting its $\text{p}K_a$ by about 2.6 units upward and about 0.8 units downward, in the two respective cases [17]. These divergent $\text{p}K_a$ shifts of the dye arise from the differential affinity of the two host molecules to encapsulate the protonated and neutral form of the dye.

A spectacular example has recently been reported by Pluth et al., who demonstrated the possibility to perform acid catalysis under basic conditions in a supramolecular host cavity, owing to its ability to protonate (shift the $\text{p}K_a$) an included guest [22]. The use of chromophoric guests, such as the acridine orange dye investigated herein, provides a powerful method to quantify $\text{p}K_a$ shifts using macrocyclic hosts directly through optical spectroscopy, namely fluorescence and absorption. CB7 causes an upward $\text{p}K_a$ shift by

more than 2 units and makes the guest more basic, because it stabilizes the protonated form of the dye by ion-dipole interactions. In contrast, β -CD causes a downward pK_a shift by nearly 1 unit and makes the protonated guest more acidic, because this host lacks cation-receptor sites and cannot compete with the aqueous bulk phase in 'dissolving' the protonated form of the dye.

3.2 Supramolecular pK_a tuning: Salt-induced guest relocation

Specifically, it is known that cations bind competitively to the portals of cucurbiturils, which can cause a displacement of the included guest, particularly when its binding is driven by the Coulombic ion-dipole interactions with the portals, i.e., when the guest is positively charged (protonated form). The variation of the ionic strength of the medium by addition of NaCl, therefore, allows a tuning of the pK_a value of the CB7•1 complex down to the value of the uncomplexed dye (Fig. 2) [5]. Such a "supramolecular tuning" of the pK_a value of neutral red (between 6.8-8.8) has immediate relevance for biological applications. In the presence of divalent metal ions, i.e., Ca^{2+} , a sharper decrease in the pK_a value for CB7•1 complex was observed than in the presence of the monovalent alkali ions [5].

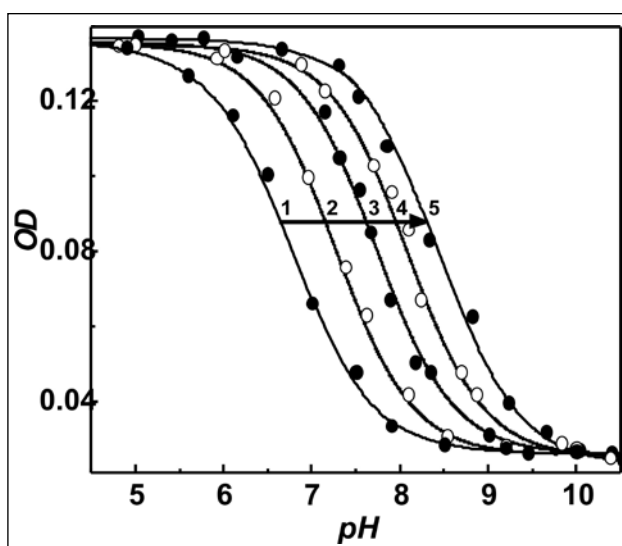


Figure 2: pH titration of the absorbance ($\lambda_{mon} = 535 \text{ nm}$) of 1 ($3 \mu\text{M}$), (1) in the absence of further additives, and (2-5) in the presence of CB7 ($150 \mu\text{M}$) with $[\text{NaCl}]/M$: (2) 0.5, (3) 0.1 (4) 0.01 and (5) 0.

Extending the methodology of pK_a tuning by a macrocyclic host and salt, the applicability of this method in a biological environment has been evaluated, where the unprotonated dye would tend to be noncovalently bound to a protein. With BSA protein, its binding with neutral red can be readily followed through the changes in the absorption and fluorescence characteristics. The fluorescence titrations established that BSA shows indeed an about one order of magnitude higher affinity for the neutral form (1) over the protonated form ($1H^+$). In the presence of BSA, the pK_a of the dye was estimated as 6.3 which could again be shifted by 2 units, i.e. to 8.3 upon addition of CB7. This shift corresponds to the relocation of the dye in the forward direction, from BSA to CB7, where the protonated dye is more tightly bound. Following the salt-induced tuning method, the pK_a value of the dye could be further tuned by addition of a salt to the 1•CB7•BSA ternary-system [5]. The pK_a curves generated at different salt concentrations confirm a tunability essentially over the entire range, from 8.3 to 6.8 (Fig. 3). This shift corresponds to the relocation of the dye in the backward direction, from CB7 to BSA, where the neutral dye is more tightly bound. The net effect of the addition of metal salt is illustrated by the vertical arrow in Fig. 3, which illustrates how the addition of salt - at a constant pH near 7.5 - converts the protonated (CB7-complexed) form (top curve) into the unprotonated (BSA-complexed) form [5]. Supporting evidence for this guest relocation came from the absorption spectra (inset of Fig. 3), whose maxima shifted upon addition of NaCl, from ca. 526 nm, (characteristic for the protonated form included in CB7) to 450 nm (characteristic for the neutral form in BSA). The net effect of the salt-induced transfer of 1 from CB7 to BSA is visualized in Scheme 3.

Though the transferability of this case study to drug delivery mechanism is far fetched, yet it deserves its conceptual attention. Moreover, since the stability and activity of drugs depend on their protonation state, the macromolecular encapsulation into CB7 could provide an interesting tool to improve drug stability through a host-assisted guest protonation. The

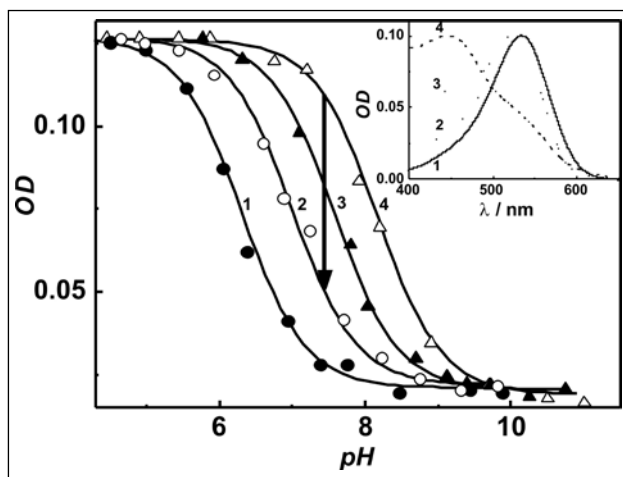
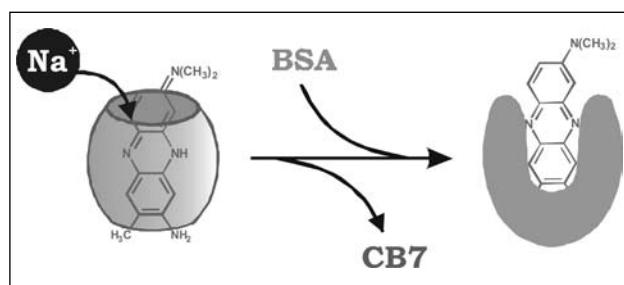


Figure 3: pH titration of the absorbance ($\lambda_{\text{mon}} = 535 \text{ nm}$) of **1** ($3 \mu\text{M}$) in the presence of $150 \mu\text{M}$ BSA (1) in the absence of CB7 and NaCl, and (2-4) in the presence of CB7 ($50 \mu\text{M}$) with $[\text{NaCl}]/\text{M}$: (2) 0.1, (3) 0.05 and (4) 0. Inset: Normalized absorption spectra of **1** in different environments at pH 7.5: (1) **1**, (2) CB7, (3) CB7-BSA and (4) CB7-BSA-NaCl.



Scheme 3: Schematic representation of the salt-induced transfer of a dye from CB7 to BSA near neutral pH.

addition of salts could then provide a simple stimulus for the controlled release of the potential drug, as well as for its activation owing to the accompanying deprotonation. Recently, Day *et al* [23], have examined the toxicity of CB7 and CB8 from *in vitro* studies on cell cultures and the bioadaptability of CB7/CB8 by *in vivo* studies. Intravenous administration of CB7 showed a maximum tolerated dosage of 250 mg kg^{-1} , while oral administration of a CB7/CB8 mixture showed a tolerance of up to 600 mg kg^{-1} . The sufficiently low toxicity of CB7/CB8, their strong ability to bind various guest molecules and the guest relocation methodology demonstrated here will be interesting to explore further, especially since drug delivery applications of CB7/CB8 are presently under investigation.

3.3. Advantages of larger host cavity: Guest exchange with CB8

We extended our study to see the effect of cavity size and portal charge density on the modulation of photophysical properties of neutral red dye (**1**) using higher homologue of CB7, i.e. CB8. A comparative analysis of the results with the complexation behaviour of the dye with CB7, indicates contrasting guest binding behaviour for CB8 with significant changes in the photophysical characteristics of the dye. While CB7 interaction leads to a 1:1 stoichiometry resulting in ~ 6 fold enhancement in the fluorescence emission of the dye [8], CB8 displays signature for a 1:2 host-guest stoichiometry with drastic reduction in the fluorescence emission [24].

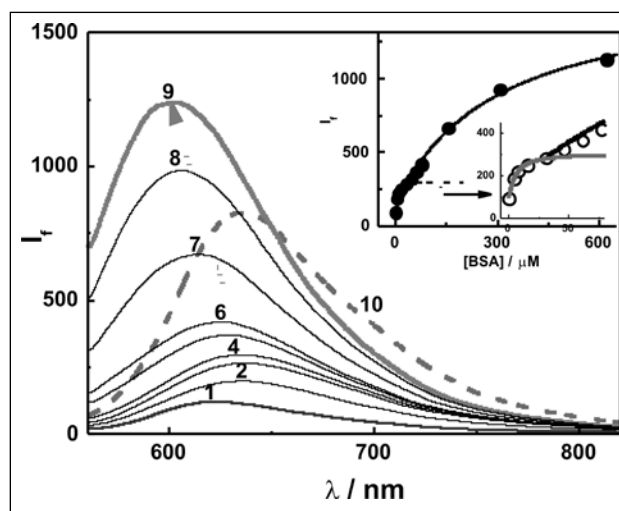


Figure 4: Fluorescence spectra recorded for $\text{CB8} \cdot (\text{1H}^+)_2$ complex alone (1), and with $[\text{BSA}]/\mu\text{M}$: (2) 4.5, and (9) 620. The dashed curve (10) shows the emission spectrum for 1H^+ in water. Inset: Fluorescence titration curve recorded at 600 nm for the $\text{CB8} \cdot (\text{1H}^+)_2$ complex with BSA at $\text{pH} \sim 5$. The solid line represents the fitted curve based on two-step binding interaction of BSA.

Apart from the evaluation of ~ 2 unit shift in the protolytic equilibrium on complexation with CB8 (pK_a shift), the measurements in the presence of tryptophan established a selective guest exchange to favour a co-localized hetero dimer inside the CB8 cavity. In a protein medium (BSA), the 1:2 complex was converted to a 1:1:1 $\text{CB8} \cdot \text{1H}^+ \cdot \text{BSA}$ complex (Fig. 4). The finding that 1H^+ can be transferred from CB8 to BSA even though the binding constant for $\text{CB8} \cdot \text{1H}^+$

is much higher than $\text{BSA} \cdot \text{1H}^+$, is projected for a slow release of 1H^+ towards BSA [24]. Since the release and activity of drugs can be controlled by regulating the protolytic equilibrium, the macromolecular encapsulation and release of 1H^+ provide information relevant to host-guest based drug delivery systems and its applications.

4. Interaction of Riboflavin and Flavin Adenine Dinucleotide with CB7 and β -CD hosts

Flavin mononucleotide (FMN) and flavin adenine dinucleotide (FAD), which consist of a heterocyclic isoalloxazine moiety tethered to a ribityl phosphate or ribityl adenine diphosphate chain, respectively, are the most commonly occurring flavins in flavoproteins (Chart 4). These flavin co-factors are derivatives of riboflavin (RF), a compound better known as Vitamin B2. Because of their chemical versatility, flavoproteins are ubiquitous and participate in a broad spectrum of biological activities. Flavoproteins are the ideal systems for studies of intraprotein electron transfer and conformational dynamics of biomacromolecules, not only because the flavin (isoalloxazine) moiety is a redox-active group suitably located in the heart of the active site, but also due to the fact that it is a fluorescent chromophoric group, which makes it amenable for various fluorescence studies [25,26].

The remarkably low fluorescence yield of FAD compared to RF or FMN is well understood as due to the photoinduced electron transfer from the adenine moiety to the isoalloxazine moiety. Based on different studies, it is confirmed that in solution, FAD exists in two conformations; an extended or "open" conformation in which the isoalloxazine and the adenine moieties are largely separated from each other, and a "closed" conformation in which the two aromatic rings are in close proximity and stacked together (Scheme 3). The "closed" conformation is preferred in aqueous solutions, and is stabilized by the combined effect of the π - π interaction between the isoalloxazine ring and the adenine moiety and the intramolecular H-bonding interactions along the phosphate sugar backbone. So we felt it was quite intriguing to investigate the conformational changes of FAD as well as the

modulation in its photophysical properties and intramolecular electron transfer behavior in the presence of the biomimetic binding pockets of CB and CD hosts.

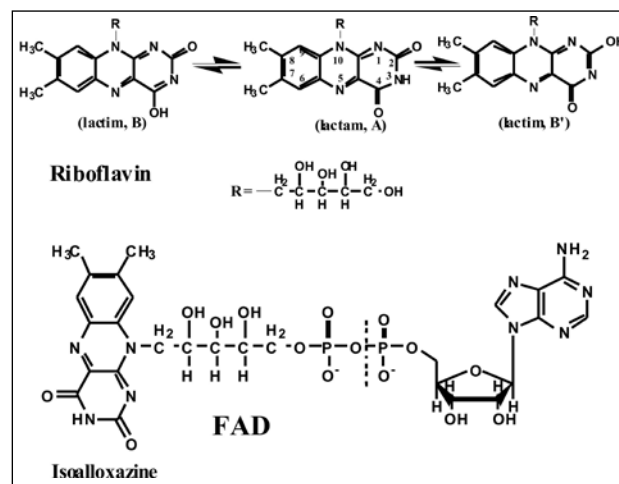
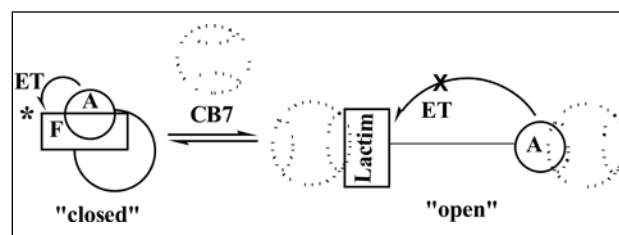


Chart 4: Structures of Riboflavin and the FAD



Scheme 3: The open and closed structures showing the proximity of the interacting groups.

Although both the host molecules provide a biomimicking environment and change the conformation of FAD from the "closed" to the more biologically predominant "open" form, thus inhibiting the intramolecular electron transfer from adenine to the isoalloxazine moiety of FAD, their effect on the photophysical properties of the parent molecule, RF, is markedly different. The host β -CD has no affinity for the isoalloxazine moiety and does not affect the absorption and fluorescence characteristics of RF at all. In the β -CD-FAD system, the primary interaction of the host takes place via the inclusion of the adenine moiety into the host cavity [25]. On the other hand, CB7 has a significant affinity toward the RF molecule and leads to interesting changes in the absorption and fluorescence characteristics of RF. Very surprisingly the fluorescence intensity of RF is quenched upon complexation with the

CB7 host. This interesting effect is attributed to the transformation of the lactam form of RF to the lactim forms, in the presence of CB7. Such a tautomerisation effect is possible due to the higher dipole moment of the two lactim forms of RF and thus highlights the important role played by the dipole-dipole forces in the host-guest interaction of CB7 [26]. Geometry optimization studies also reveal that for the RF-CB7 system, exclusion type complexes are formed rather than the more commonly encountered inclusion type host-guest complexes. Because of the affinity of CB7 toward the isoalloxazine ring, binding of CB7 can take place with both the isoalloxazine as well as with the adenine moieties of FAD. In the CB7-FAD system there is interplay between two opposing effects, namely, fluorescence quenching due to the lactam to lactim tautomerisation of the isoalloxazine ring bound to CB7 and the fluorescence enhancement due to the conformational change from "closed" to "open" form of FAD on its binding to CB7 host. Results indicate that the latter effect predominates, leading to a net fluorescence enhancement of FAD. These results are not only useful in the studies and interpretation of the conformational dynamics and the activity of FAD binding to proteins but also help to elucidate the dissimilar interactions of the two widely used macrocyclic hosts, β -CD and CB7, toward the same guest molecules [25,26].

5. Fluorescence behaviour of a fibril binder dye, Thioflavin T: Assemblies with CB7/CB8

It is possible that by proper selection of the structural criteria of hosts and guests, well ordered and directional assemblies can be achieved, which are promising as tunable functional materials. For these studies, guests

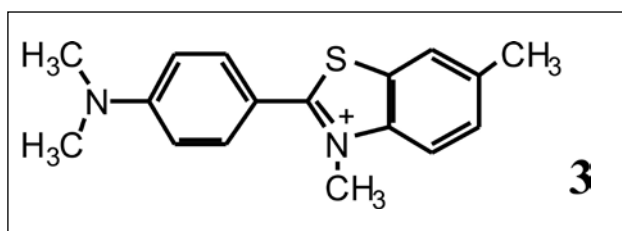


Chart 5: Chemical structure of Thioflavin T dye

with multiple binding sites (Chart 5) or hosts which can uptake multiple guests have been employed. Thioflavin T (**3**) is a benzthiazolium dye, that has been extensively applied in the early detection of amyloid fibril formation in tissues to diagnose chronic disorders such as Alzheimer's and Parkinson's diseases [27].

Detection is mainly based on the characteristic fluorescence of dye **3** ($\Phi_f = 0.0003$) at 490 nm which increases dramatically (~ 1000 fold) upon binding to the cavities of the amyloid fibrils [27]. Though the application of **3** for the analysis of different aggregating systems is rapidly rising, the exact mechanism for binding of **3** into the cavities of the amyloid fibrils causing dramatic changes in its fluorescence properties is still largely elusive. Apart from the restriction towards the torsional motion between the benzthiazole and dimethylaminobenzene groups, excimer formation within the binding site is also proposed to cause further enhancement in the fluorescence for **3** on binding with amyloid fibrils. Addressing this issue, rationalizations have been put forward considering the void volumes in amyloid fibrils and its probable binding interaction, in comparison with synthetic water soluble macrocyclic cavities. Several studies have been carried out on **3** with cyclodextrin (CD) hosts, to explore the binding interactions in restricted environments, where the driving force for inclusion complex formation is mainly hydrophobic in nature and subsequent fluorescence changes. We have exploited the cationic receptor behavior of cucurbituril hosts to introduce strong and multiple binding with the cationic dye **3**. CBs can encapsulate **3** from either ends and can provide a large stabilization of the inclusion complex via ion-dipole interaction between the carbonyl portals of CBs and the cationic charge on the dye along with the hydrophobic interaction exerted by the host cavity. The following sections summarize the distinct spectrochemical changes observed on interaction of ThT with CB7 and CB8 macrocycles in aqueous solution.

5.1 Interaction of ThT with CB7

Steady-state and time-resolved fluorescence studies illustrate significant enhancements/

modifications in the fluorescence yield (40-fold), lifetime and spectral features of dye **3** on interaction with CB7 and has been assigned to the formation of 1:1 and 2:1 complexes between the **3** and the CB7 leading to the specific structural arrangements [27]. The macrocyclic host-guest interactions impart structural rigidity bringing out restrictions on the torsional motion in the dye, thus modulating the excited state properties. The high binding constant values for the 1:1 complex ($K_1 \sim 10^5 \text{ M}^{-1}$) indicates the strong ion-dipole interaction between the host and guest molecules, whereas the 1:2 complex formation is mainly driven by weaker forces like hydrophobic interaction as evident from the lower binding constants ($K_2 \sim 10^3 \text{ M}^{-1}$) [27]. These contentions were further verified by the rotational relaxation dynamics, NMR and quantum chemical calculations on CB•**3** systems. The structural geometry of the proposed complexes were optimized computationally at PM3 level incorporating molecular mechanics (MM) correction and the most stable structures for 1:1 and 1:2 complexes (Fig.5) correspond quite nicely to those inferred from experimental results.

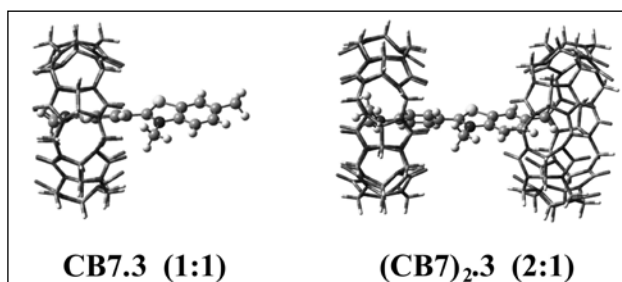


Figure 5: Geometry optimized structures for the 1:1 and 2:1 (CB7•**3**) complexes.

5.1.1 Stimulus responsive molecular assemblies: Action of metal ions

The binding interactions in host-guest complexes are mainly non-covalent in nature which makes it convenient to tune the complexes by wide range of stimuli including cooperative/competitive binding of guests/hosts, pH, temperature, light, redox control, etc. Considering the cases of cation receptor properties of CB hosts, an increase in the ionic strength of the solution

would lower the extent of ion-dipole interaction affecting the stability of the complex, especially for cationic guests, thus releasing the free dye in the solution. Advantage of the stimulus response, especially, the competing metal ion strategy has been explored in our studies, especially for CB7•**3** assemblies as summarized in the following sections.

5.1.2 Fluorescent molecular capsule and its rupture

After illustrating the structural arrangements of CB7•**3** assemblies, we attempted to see the effect of competitive binders like metal ions on these molecular assemblies. Addition of metal cations to the 1:1 CB7•**3** complex displays expected competitive binding interactions with CB7, leading to the decrease in the fluorescence intensity from **3**. However, addition of metal ions to the 2:1 (CB7)₂•**3** complex, leads to unusual enhancement in the fluorescence emission, ~270 fold in the presence of Ca²⁺ and ~160 fold in the presence of Na⁺ as shown in Fig.6. These contrasting observations on the fluorescence enhancement for the stoichiometrically different CB7•**3** complex have been investigated explicitly for a feasible binding model.

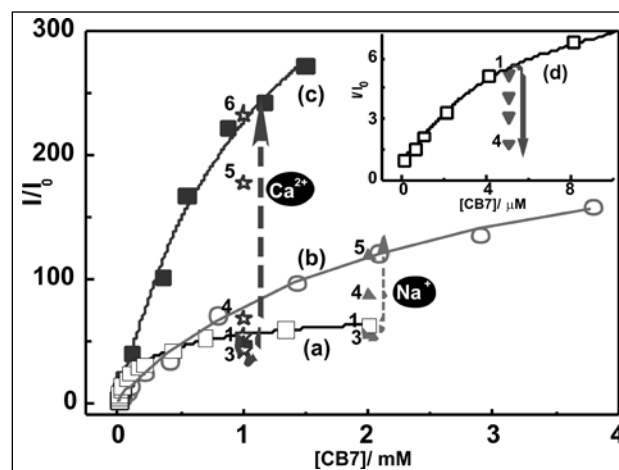


Figure 6: Fluorescence titration curves of ThT (3 μM) with CB7 in the absence of any metal ion (a), and in the presence of 1 M NaCl (b), 1 M CaCl₂ (c). (p) represents the intensity changes on (a) with NaCl/M; 1) 0.001, 2) 0.004, 3) 0.02, 4) 0.1, 5) 1.0 and (d) represents the intensity changes on (a) with CaCl₂/M; 1) 0, 2) 0.001, 3) 0.005, 4) 0.01, 5) 0.3, 6) 1.0, at the respective host concentration. Inset: Titration curve corresponding to 1:1 complex, (q) shows the intensity changes with NaCl/M; 1) 0.001, 2) 0.01, 3) 0.3, 4) 1.0.

A detailed photophysical characterization with supporting data from NMR and anisotropy measurements has led to the revelation of a novel stimulus responsive cooperative metal ion binding to the stoichiometrically selected $(\text{CB7})_2 \cdot \mathbf{3}$ complex, demonstrating a highly fluorescent supramolecular nano-capsule as shown in Scheme 4A [4,27]. The first example of a non-covalently packed fluorescent complex became feasible due to the structural arrangement of the host-guest complex in the 2:1 stoichiometry with two CB7 portals providing strong negative charge density for the metal ions to group and seal the complex, thus protecting the incorporated dye. This supramolecular structure provides vital lead for the design and synthesis of tailor-made dyes/drugs in tandem fashion for an extended chain. Moreover, the relative binding strengths of different noncovalent forces and the noteworthy modulation in the photophysical properties of the guest chromophore provides information on the understanding of the intramolecular motions and their remarkable contributions toward the radiative yield of the dye. In addition to the increase in the fluorescence intensity, the fluorescence lifetime of the molecular capsule with divalent metal ions closely matches with the fluorescence lifetime pattern recorded for **3** in insulin fibril. This result clearly shows that the inclusion of **3** into the supramolecular capsules mimics its confinement inside fibril cavities.

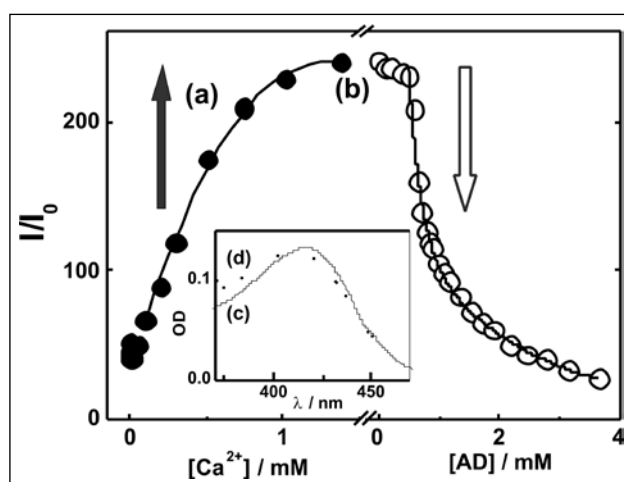
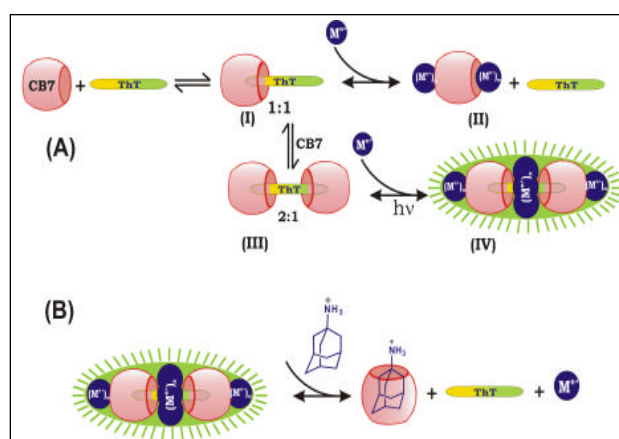


Figure 7: Changes in the fluorescence intensity of $(\text{CB7})_2 \cdot \text{ThT}$ complex in presence of Ca^{2+} (trace a) and followed by the addition of AD (trace b) **Inset:** The absorption spectrum of Ca^{2+} bound $(\text{CB7})_2 \cdot \text{ThT}$ complex (c) and after the addition of AD (d).

To further strengthen the usefulness of the novel supramolecular capsule, rupture of the capsular complex has been achieved with a strong competitive guest adamantylamine (AD), which helped in disrupting the capsule to release the dye from the complex as shown in Fig.7 and Scheme 4B [4,27]. The feasibility of a capsular molecular assembly formation and its rupture as in Scheme 4 is expected to have remarkable implications in targeted drug delivery, removal of toxins, on-off systems and have potential as building blocks for tailor made functional materials and molecular architectures displaying unique properties. Furthermore, the replacement of inert metal ion by transition metal ions with redox activity or catalytic properties could readily convert the supramolecular capsules into nano reactors or metalloenzyme models.



Scheme 4: (A) Proposed binding interactions in the ThT, CB7 and metal ion system leading to the highly fluorescent supramolecular capsule and (B) release mechanism of ThT from the metal ion bound supramolecular capsule by amantadine hydrochloride (AD) as the stimulant.

5.2. Interaction of ThT with CB8

The cucurbit[8]uril, having the larger cavity size, can co-host and stabilize two **3** molecules in a single CB8 cavity as observed in other CB8-dye complexes. On introducing CB8 to a dilute aqueous solution of **3**, significant spectral changes have been observed. Unlike CB7, with increase in CB8 concentration about $2\mu\text{M}$, the absorption band of **3** shifted from 412 nm towards 445 nm with a well-defined isosbestic point at 428 nm (Fig.8). Surprisingly, on further addition of CB8,

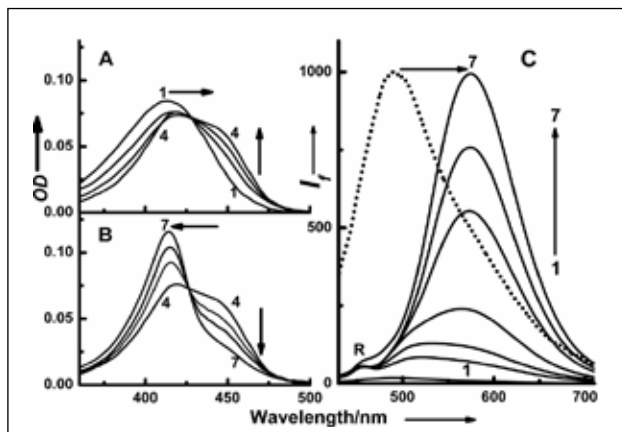


Figure 8: Absorption (A&B) and fluorescence (C) of **3** ($\sim 2\mu\text{M}$) in aqueous solution at different concentrations of CB8. [CB8]/ μM : (1) 0, (2) 0.5, (3) 1, (4) 2, (5) 4, (6) 6 and (7) 20. $\lambda_{\text{ex}} = 390\text{ nm}$. Dotted line represents spectrum 1 normalized to spectrum 7. R represents the Raman scattering.

the absorption peak retracted to 415 nm with another isosbestic point at 426 nm and the final spectrum evolved remained markedly different from the spectrum of **3** alone (Fig. 8). These changes, seen at very low concentration of CB8 ($< 20\mu\text{M}$) in contrast to $\sim 1\text{ mM}$ required with CB7, indicated strong interaction of **3** with CB8, affecting the structure and electronic distributions considerably [7]. Interestingly, the fluorescence of dye **3** in the presence of CB8 displayed striking features, a dual emission, with a distinct evolution of a hitherto unexplored intense emission band having maximum at 570 nm (Fig. 8).

Considering the cavity size and the high negative charge density at the portals, it is likely that CB8 encapsulates two **3** molecules in its cavity, forming a non-covalent dimer inclusion complex. This is more probable when the relative concentration of the dye is more. Hence, the 570 nm fluorescence band and the corresponding modulations in the absorption and emission characteristics (see Fig. 8) have been attributed due to a π -stacked excimer of **3** co-localized in the CB8 cavity in a 1:2 (CB8•**3**) stoichiometry, which subsequently transforms into a 2:2 complex (Fig.9), at higher concentration of CB8 [7,27]. Consequent to a 2:2 complex, the expected increase in the hydrodynamic volume of dye **3** has been estimated from the rotational correlation time ($\tau_r = 850\pm 30\text{ ps}$), measured at 570 nm.

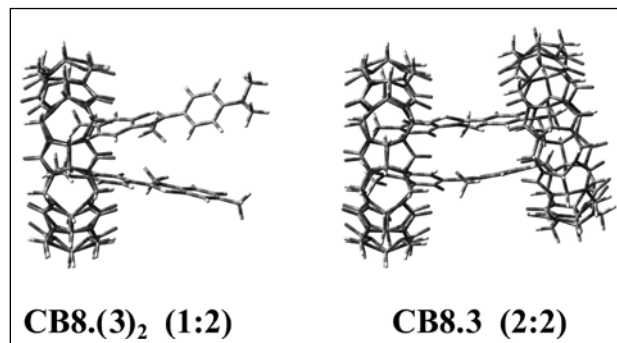
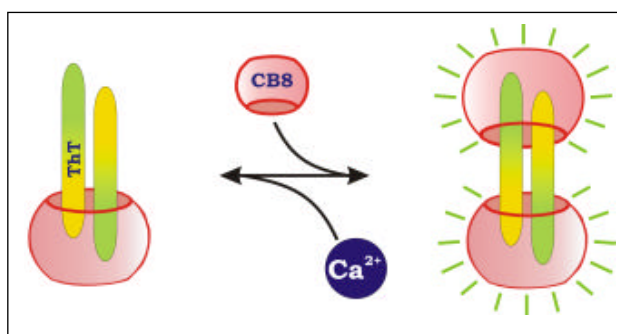


Figure 9: Geometry optimized structures for the 1:2 and 2:2 (CB8•**3**) complexes.

5.2.1 Stoichiometric control: Demonstration of On-Off mechanism

After establishing the 2:2 binding for the CB8•**3** interaction with an intense fluorescence 'turn on' at 570 nm, we have attempted to make the system 'turn off' by engaging the CB8 portals through a competitive binder, i.e. Ca^{2+} ions. Gradual addition of Ca^{2+} ions decreases the emission intensity with concurrent changes in the absorption spectrum in the reverse order, achieving the dissociation of the 2:2 complex. This Ca^{2+} induced control over the complexation equilibrium and excimer emission is projected as an on/off mechanism, as illustrated in Scheme 5 [7, 27].



Scheme 5: Schematic representation of a 2:2 CB8:3 assembly formation and dissociation, demonstrating the on/off mechanism.

6. Conclusions

In this article we have overviewed the various modulations in the physico-chemical properties of different cucurbituril and cyclodextrin-based supramolecular assemblies brought out by non-covalent interactions. These interactions enhance/change the molecular properties like

acidity constant, photostability, fluorescence behavior, excited state dynamics of the selected guests. The significant supramolecular pK_a shift is useful to stabilize the protonated form of the dye/drug molecule in the basic medium. It has also been seen that the interaction of guests having multiple binding sites with cucurbituril leads to the formation of higher order complexes which can act as scaffolds/building blocks for the construction of molecular architectures with different photofunctional behavior.

Furthermore, the salt-induced pK_a tuning of the supramolecular assemblies led to relocate the guest from cucurbituril cavity into the biomolecular pocket. Through a competitive binding strategy, precise tuning of the stoichiometry of the CB8•3 complex could be achieved by added metal ions, demonstrating molecular capsule and fluorescence *on-off* switch.

The application perspectives of the modulation in the physico-chemical properties of guest molecules through host-guest complexation and stimulus responsive chemistry are manifold. The stimulus responsive binding and release of the guest molecules may find useful applications in targeted drug delivery, considering the low toxicity of CB7 and CB8 hosts.⁵¹ Supramolecular host-guest systems also have the prospects in the development of custom-made photofunctional materials for optical sensors, on-off switches, etc. The pH dependent association and dissociation of molecular assemblies can also be used in the construction of pH sensitive molecular shuttles. Exploiting metal ion-CB interactions, synthesis of CB-functionalized/ surface-modified metal nanoparticles and modulation of their electronic and optical properties, which largely affect the catalytic, sensing and molecular recognition behaviors, have great challenges in the field of supramolecular chemistry.

Acknowledgements

We acknowledge all the co-authors and collaborators of our published papers cited in the references. We thank Dr. S. K. Sarkar, Head, RPCD and Dr. T. Mukherjee, Director, Chemistry group, BARC, India, for their encouragement and support.

Notes and references

1. J.-M. Lehn, *Science*, 1985, **227**, 849-856; A. V. Davis, R. M. Yeh and K. N. Raymond, *Proc. Natl. Acad. Sci.*, 2002, **99**, 4793-4796.
2. M. J. Frampton and H. L. Anderson, *Angew. Chem. Int. Ed.*, 2007, **46**, 1028-1064; B. D. Wagner in *Fluorescence Studies of Supramolecular Host-Guest Inclusion Complexes*, Vol. 3 (Ed. H. S. Nalwa), American Scientific Publishers, Stevenson Ranch, CA, 2003, 1-57.
3. Y. H. Ko, E. Kim, I. Hwang and K. Kim, *Chem. Commun.*, 2007, 1305-1315; K. Kim, N. Selvapalam, Y. H. Ko, K. M. Park, D. Kim and J. Kim, *Chem. Soc. Rev.*, 2007, **36**, 267-279.
4. S. Dutta Choudhury, J. Mohanty, H. Pal and A. C. Bhasikuttan, *J. Am. Chem. Soc.*, 2010, **132**, 1395-1401.
5. M. Shaikh, J. Mohanty, A. C. Bhasikuttan, V. D. Uzunova, W. M. Nau and H. Pal, *Chem. Commun.*, 2008, 3681-3683.
6. J. Mohanty, S. Dutta Choudhury, H. P. Upadhyaya, A. C. Bhasikuttan and H. Pal, *Chem. Eur. J.*, 2009, **15**, 5215-5219.
7. S. Angelos, Y.-W. Yang, K. Patel, J. F. Stoddart and J. I. Zin, *Angew. Chem. Int. Ed.*, 2008, **47**, 2222-2226.
8. J. Mohanty, A. C. Bhasikuttan, W. M. Nau and H. Pal, *J. Phys. Chem. B*, 2006, **110**, 5132-5138.
9. R. Wang, L. Yuan and D. H. Macartney, *Chem. Commun.*, 2005, 5867-5869; E. Arunkumar, C. C. Forbes and B. D. Smith, *Eur J. Org. Chem.* 2005, 4051-4059.
10. A. C. Bhasikuttan, J. Mohanty, W. M. Nau and H. Pal, *Angew. Chem. Int. Ed.*, 2007, **46**, 4120-4122.
11. J. Mohanty and W. M. Nau, *Angew. Chem. Int. Ed.*, 2005, **44**, 3750-3754; W. M. Nau and J. Mohanty, *Int. J. Photoenergy*, 2005, **7**, 133-141.
12. K. A. Connors, *Chem. Rev.* 1997, **97**, 1325-1357; M. V. Rekharsky and Y. Inoue, *Chem. Rev.*, 1998, **98**, 1875-1917.
13. L. Baldini, A. Casnati, F. Sansone and R. Ungaro, *Chem. Soc. Rev.* 2007, **36**, 254-266.
14. K. E. Krakowiak, J. S. Bradshaw, D. J. Zamecka-Krakowiak, *Chem. Rev.* 1989, **89**, 929-972.
15. A. C. Bhasikuttan, H. Pal and J. Mohanty, *Chem. Commun.*, 2011, **47**, 9959-9971.
16. J. Lagona, P. Mukhopadhyay, S. Chakrabarti and L. Isaacs, *Angew. Chem. Int. Ed.*, 2005, **44**, 4844-4870; L. Isaacs, *Chem. Commun.*, 2009, 619-629; J. W. Lee, S. Samal, N. Selvapalam, H.-J. Kim and K. Kim, *Acc. Chem. Res.*, 2003, **36**, 621-630.
17. M. Shaikh, J. Mohanty, P. K. Singh, W. M. Nau and H. Pal, *Photochem. Photobiol. Sci.*, 2008, **7**, 408-414.
18. M. Shaikh, S. Dutta Choudhury, J. Mohanty, A. C. Bhasikuttan, W. M. Nau and H. Pal, *Chem. Eur. J.*, 2009, **15**, 12362-12370.
19. J. Mohanty, A. C. Bhasikuttan, S. Dutta Choudhury and H. Pal, *J. Phys. Chem. B (Letts.)*, 2008, **112**, 10782-10785.
20. J. Mohanty, K. Jagtap, A. K. Ray, W. M. Nau and H. Pal, *ChemPhysChem*, 2010, **11**, 3333-3338; J. Mohanty, H. Pal, A. K. Ray, S. Kumar and W. M. Nau, *ChemPhysChem*, 2007, **8**, 54-56.
21. J. Kim, I. S. Jung, S. Y. Kim, E. Lee, J. K. Kang, S. Sakamoto, K. Yamaguchi and K. Kim, *J. Am. Chem. Soc.*, 2000, **122**, 540-541; A. Day, A. P. Arnold, R. J. Blanch and B. Snushall, *J. Org. Chem.*, 2001, **66**, 8094-8100; C. Marquez, F. Huang and W. M. Nau, *IEEE Trans. Nanobiosci.*, 2004, **3**, 39-45.
22. M. D. Pluth, R. G. Bergman and K. N. Raymond, *Science*, 2007, **316**, 85-88.

23. V. D. Uzunova, C. Cullinane, K. Brix, W. M. Nau and A. I. Day, *Org. Biomol. Chem.*, 2009, **8**, 2037-2042.
24. M. Shaikh, S. Dutta Choudhury, J. Mohanty, A. C. Bhasikuttan and H. Pal, *Phys. Chem. Chem. Phys.*, 2010, **12**, 7050-7055.
25. N. Kandoth, S. Dutta Choudhury, J. Mohanty, A. C. Bhasikuttan, H. Pal, *J. Phys. Chem. B*, 2010, **114** 2617-2626.
26. S. Dutta Choudhury, J. Mohanty, A. C. Bhasikuttan, H. Pal, *J. Phys. Chem. B*, 2010, **114** 10717-10727.
27. A. C. Bhasikuttan, S. Dutta Choudhury, H. Pal and J. Mohanty, *Israel J. Chem.*, 2011, **51**, 634-645; S. Dutta Choudhury, J. Mohanty, H. P. Upadhyaya, A. C. Bhasikuttan and H. Pal, *J. Phys. Chem. B*, 2009, **113**, 1891-1898.

| | |
|---|---|
|  | <p>Jyotirmayee Mohanty obtained her M. Sc. in Chemistry from Utkal University, Orissa in 1992 and joined Bhabha Atomic Research Centre, Mumbai, India, in 1994 after one year advanced orientation course conducted by the institute. After her Ph.D. from the University of Mumbai in 2002, she carried out her postdoctoral research at Max-Planck Institute for Biophysical Chemistry (MPIBPC), Göttingen and JUB, Bremen, Germany, 2002-2004. Her current research interests focus on the dynamics of noncovalent supramolecular assemblies, tuning molecular properties and exploring photofunctional activities towards various applications. She is a recipient of the Distinguished Lectureship Award-2009 from the Chemical Society of Japan, APA-Prize for Young Scientist-2010 from the Asian and Oceanian Photochemistry Association (APA) and a fellow of the Maharashtra Academy of Sciences, India.</p> |
|  | <p>Sharmistha Dutta Choudhury received her M. Sc. Degree in Chemistry with gold medal from Jadavpur University, India, in 2000. She carried out her doctoral research in the subject area of magnetic field effects on photoinduced electron transfer reactions at Saha Institute of Nuclear Physics, Kolkata and obtained her Ph.D degree from Jadavpur University in 2006. She subsequently joined Bhabha Atomic Research Centre, Mumbai, India as Dr. K. S. Krishnan Research Associate and is presently employed in the institute. The focus of her current research is the understanding of the mechanism and dynamics of photoinduced chemical processes in biomimetic and supramolecular systems. She is the recipient of the Young Scientist Award in Chemical Sciences-2009, conferred by the National Academy of Sciences, India, Young Scientist Award in Chemical Sciences-2011, conferred by the INSA and the Young Scientist Award-2010 from DAE .</p> |
|  | <p>Haridas Pal obtained his M.Sc. degree in Chemistry with gold medal from North Bengal University in 1983 and joined BARC in 1985 after one year advanced orientation course conducted by the institute. After his Ph.D. from the University of Mumbai in 1992, he joined as a JSPS postdoctoral fellow at the Institute of Molecular Sciences, Okazaki, Japan, 1994-96. His current research interests include fast and ultrafast processes, solvatochromic effects, supramolecular interactions in tuning molecular properties and single molecule spectroscopy. He is the recipient of Homi Bhabha Science & Technology Award-2008 from DAE and Bronze medal-2011 from CRSI, India and the fellow of the Maharashtra Academy of Sciences & the National Academy of sciences, India.</p> |
|  | <p>Achikanath C. Bhasikuttan obtained his M.Sc. in Chemistry from Calicut University, Kerala in 1989 and joined Bhabha Atomic Research Centre, Mumbai, India, in 1991 after one year advanced orientation course conducted by the institute. After his Ph.D. from the University of Mumbai in 1998 he joined as a JSPS postdoctoral fellow at Osaka University, Japan, 1999-2001. His research interests include the excited state molecular dynamics and to probe the intricacies of non-covalent interactions in supra-biomolecular systems. He is a recipient of the Scientific & Technical Excellence Award -2009 from DAE, India and a fellow of the Maharashtra Academy of Sciences & the National Academy of Sciences, India.</p> |

Grappling with Molecular Design: Attempts at Creating Potential Optical Probes for Targeting Zn (II)

Sabir H. Mashraqui

Department of Chemistry, University of Mumbai, Vidyaynagari, Santacruz-E, Mumbai-400098

E-mail: sh_mashraqui@yahoo.com

Abstract

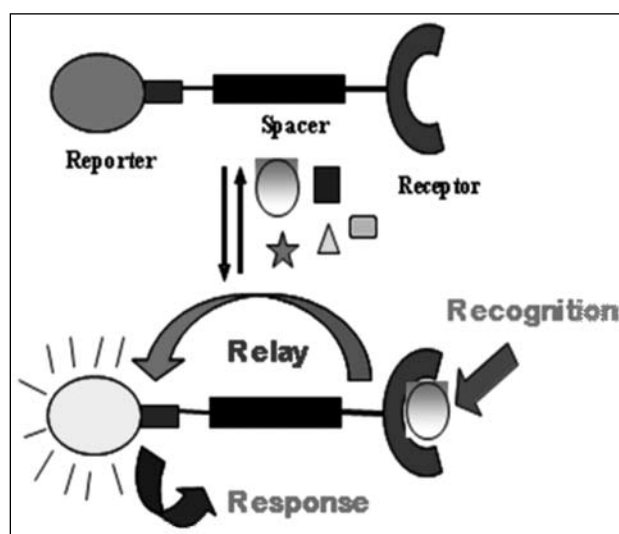
A variety of artificial photoreceptors have been designed to achieve selective recognition and quantification of biologically significant Zn^{2+} . Of the photoinduced electron transfer based probes examined, the probe **Obox** exhibited relatively pronounced selectivity towards Zn^{2+} (160 fold emission amplification) compared to biologically competing Ca^{2+} and Mg^{2+} exhibiting much truncated 24 and 4 fold emission enhancements, respectively. The probe **Benzoc**, designed on the basis of internal charge transfer, delivered selective colorimetric (yellow to pink) and fluorescence 'on-off' signaling responses, while **Isazid** induced colorimetric (yellow to red) and the more desirable fluorescence 'off-on' signaling for the discrimination of Zn^{2+} . Finally, we studied a rhodamine derived probe, **Rhoda-P**, which offered dual sensing capability, offering remarkably selective color modulation and a dramatic fluorescence amplification for the highly selective targeting of Zn^{2+} .

1. Introduction

Sensors are smart molecules that are designed to report other molecules or ions [1]. The sensing phenomena has far reaching implications in many areas, which include biological monitoring, clinical studies, material chemistry, analytical and environmental sciences, logic gates as well as in areas of security and defense [2]. During past decades, the field of molecular and ion recognition has become increasingly important in supramolecular research [3]. Though, many analytical techniques are available for analyte detection, the methods based on optical techniques seem to have a clear edge, particularly the fluorescence spectroscopy, because it offers great sensitivity, nonexpensive instrumentation, fast response and real time measurements [4].

Despite decades of work and considerable progress, challenges still remain to design ion and molecular probes exhibiting improved selectivity, detection limit and physiological measurement capabilities. Although, analytical reagents have been known for a long time, the real impetus to study sensing and recognition phenomena came

to the fore with the advent of the preorganized structures, the supramolecular systems. [5]. When endowed with requisite structural elements, these systems can participate in host-guest interactions either with ionic and neutral species, wherein the binding phenomena basically arise from electrostatic as well as one or more of the noncovalent interactions [6].



Scheme 1. General Scheme of Sensor design

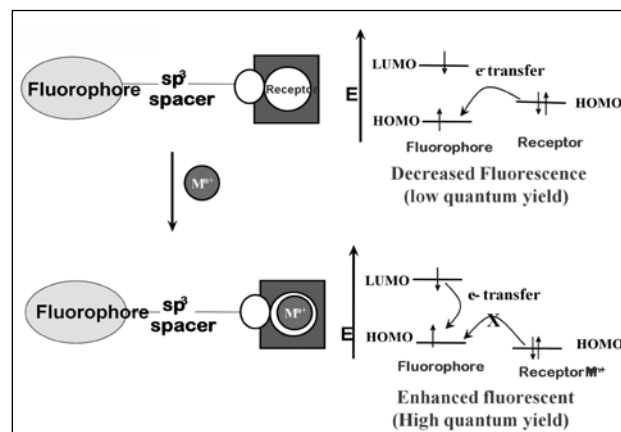
2. Design Protocol for Optical Sensors

Designing artificial ion sensors involves a basic structural paradigm, comprising of three elements, namely a receptor, signaling component and the spacer. As illustrated in Scheme 1, the sensing phenomena work on the Scheme of three Rs, Recognize, Relay and Response. The selective recognition of an analyte is electronically relayed to the signaling domain, which in turn delivers optical signals different from that of the analyte free probe, thereby allowing the detection of the interacting analyte.

Several photophysical processes, which include photoinduced electron transfer, (PET) internal charge transfer (ICT), fluorescence resonance energy transfer (FRET) and excimer/excimer formation have been widely used to design target specific chemosensors [7]. Of these protocols, the PET based chemosensors, pioneered by Prasana de Silva, have been extensively explored for designing fluorescence probes for ion recognition [8]. The design concept for the PET is illustrated in Scheme 2. Typically, the structural format for the PET based probes involves receptor- sp^3 spacer - fluorophore motif such that the presence of a saturated linker insulates any direct electronic communication between the receptor and fluorophore. In the absence of metal ion, electron transfer from the high lying HOMO of the receptor to the excited fluorophore quenches the fluorescence. However, when the receptor is engaged in metal ion binding, the HOMO of the receptor is stabilized with respect to that of the free probe. This phenomenon inhibits the electron transfer quenching and consequently, the metal ion binding event triggers fluorescence revival, giving rise to the fluorescence 'switch-on' response [9].

Factors, which play roles in the selective complexation, [10] include hard/soft nature of ligands, ionic radii, chelate ring size, extra binding sites, etc. These features need to be factored in to design an ideal sensor, which should exhibit a) high selectivity and sensitivity b) fluorescence off-on or ratiometric capability c) colorimetric (naked eye) detection d) and excitation wavelength

exceeding 360 nm, particularly for biological monitoring.



Scheme 2. Principle of Photoinduced electron transfer (PET) process

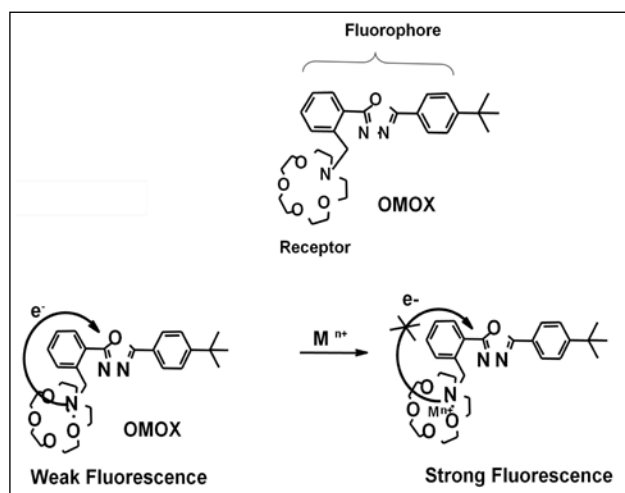
3. Designing of PET based Probes

Since, the initiation of our research in this area, we became interested in the optical targeting of zinc ion because of its topical importance in biology. Zinc is one of the essential elements for humans with approximately 300 enzymes operating directly under its control either for cellular functions or as a part of catalytic sites [11]. On the other hand, zinc metabolic disorder is implicated in neurological conditions such as Alzheimer, Parkinson's disease and epilepsy [12]. Zinc deficiency, particularly among young children in parts of Africa and Asia is believed to cause slow growth, sexual retardation, lack of appetite and frequent infections [13]. The presence of zinc in seawater is of importance for the survival of many sea organisms including the plankton.⁴ However, zinc is also a pollutant of the environment and it causes phytotoxic effects on soil bacteria and toxic to soil microbes. Not surprisingly, considerable interest exists for the development of sensitive and selective optical probes for the recognition of zinc [14].

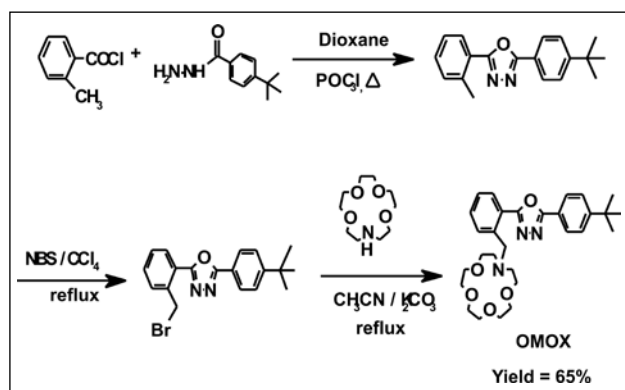
Zinc ion with its closed-shell d^{10} configuration, lacks its own optical signature, a feature which makes the optical techniques eminently suitable for its detection. Given its moderately hard character, zinc is known to bind with N and O ligands in a number of synthetic complexes [15]. In biological systems, histidine is the universal

ligand for zinc with glutamate, aspartate or cysteine occupying the remaining binding sites [16]. On these grounds, we thought that chromophores possessing N and O ligands might provide a reasonable platform to design potential zinc sensors.

To start with, one of our first probes, designated as **Omx** was investigated for its metal ion binding potential. **Omx** is characterized by the presence of a photoresponsive diaryl oxadiazole motif having a chelating monoaza-15-crown-5 placed at the *ortho* position of one of its aryl rings. As illustrated in Scheme 3, the molecule in the free state is expected to be weakly emissive due to the PET induced quenching. However, once the metal ion is engaged by the receptor, the nitrogen lone pair will no longer be available for the PET process. This phenomenon is expected to restore the fluorescence due to the native diaryloxadiazole fluorophore.



Scheme 3. Structure of the PET based probe *Omx* and the design principle



Scheme 4. Synthetic sequence for *Omx*

As outlined in Scheme 4, the synthesis of **Omx** involves condensation of 4-*t*-butylhydrazide with *o*-toluyl chloride to furnish diaryl oxadiazole. Benzylic bromination, followed by coupling with 15-monoaza-crown 5 gave the desired target, **Omx** in reasonable yield.

The photophysical sensitivity of **Omx** towards selected biologically significant metal ions was investigated both by UV-vis and fluorescence studies. **Omx** showed absorption maximum at 270 nm, which remained essentially unaltered in the company of biologically significant, Li, Na, K, Ba, Cd, Ca, Mg, and Zn ions (Figure 1). Indeed, no significant ground state perturbations were expected on account of the presence of a saturated spacer between the receptor and the fluorophore.

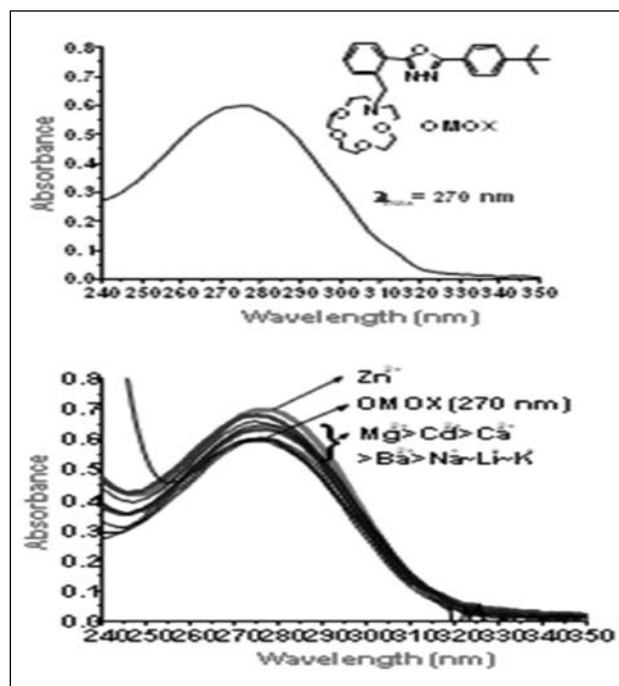


Figure 1. UV-vis of a) *Omx* and b) *Omx* + metal ions

As shown in Figure 2, **Omx** showed fluorescence maximum at 355 nm (quantum yield $\Phi_f = 0.015$), which was varyingly affected depending up on the identity of the metal ions. While alkali metal ions failed to change the probe's emission profile, Zn^{2+} , Mg^{2+} and Ca^{2+} enhanced the fluorescence by 24, 12 and 7 fold, respectively. Although, the probe, **Omx** is specific for Zn^{2+} , however it suffers from considerable interferences from Mg and Ca ions.

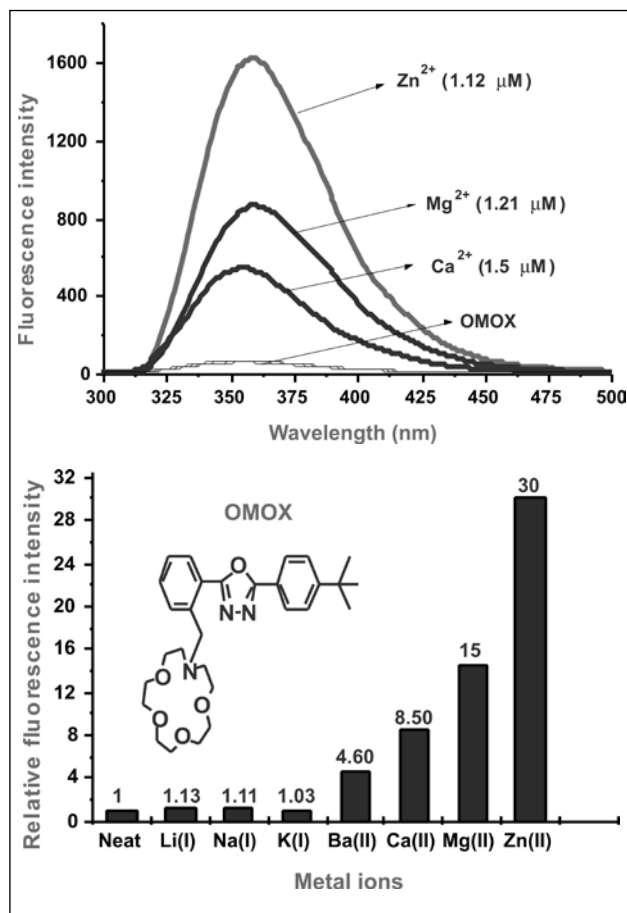
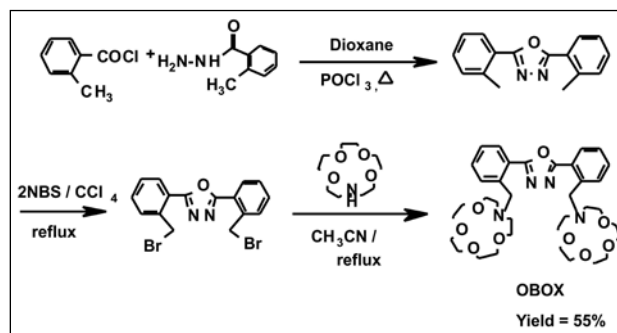


Figure 2. Fluorescence of *Omox* without and with added metal ions and relative fluorescence enhancements with metal ions.

In quest for improved optical discrimination for Zn^{2+} , the design of a new probe, **Obox** was next conceived. The probe incorporates two aza-crown receptors, and therefore it was expected to experience nearly twice as much PET quenching as observed in the mono-azacrown analog, **Omox**. Consequently, upon metal ion coordination at both the aza-crown sites, one can anticipate significantly larger fluorescence revival compared to that observed with **Omox**. The probe, **Obox** was readily assembled in a straightforward manner as outlined in Scheme 5. As expected, the UV-vis of **Obox** (not shown) was essentially invariant to the added metal ions on account of the absence of electronic communication between the diaryloxadiazoles and the metal-bound ionophore.

Excitation of **Obox** at 270 nm generated an emission at 357 nm with Φ_f of 0.006 which,



Scheme 5. Synthesis of *Obox*

as expected is nearly two fold lower than that of **Omox**. Examination of fluorescence spectra (Figure 3) revealed that alkali cations, including Ba, and Ca ions had little or no effects on

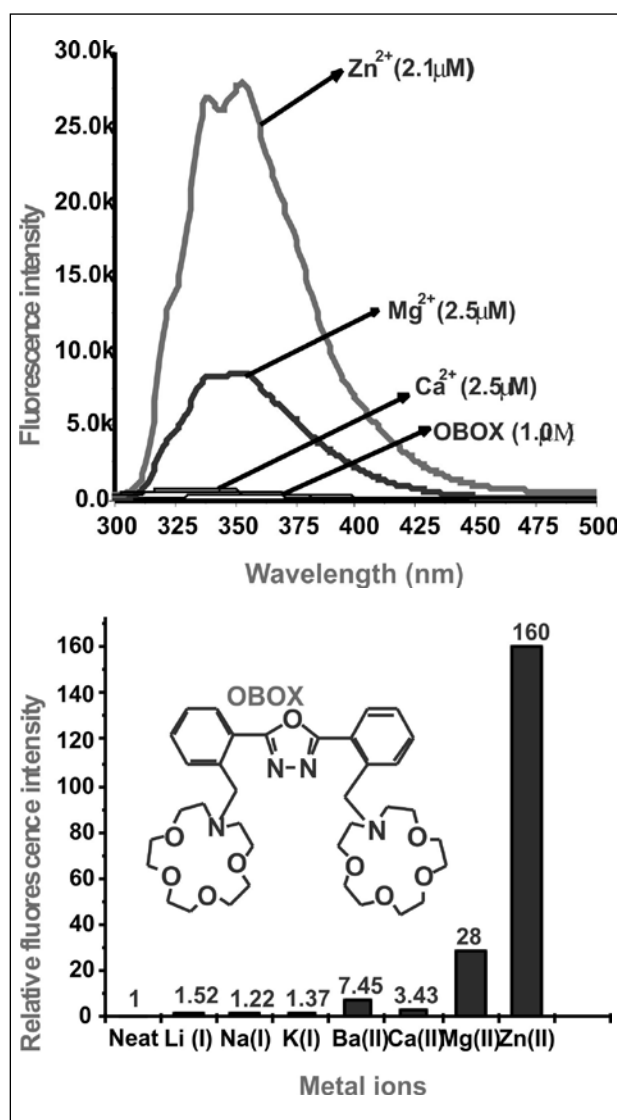
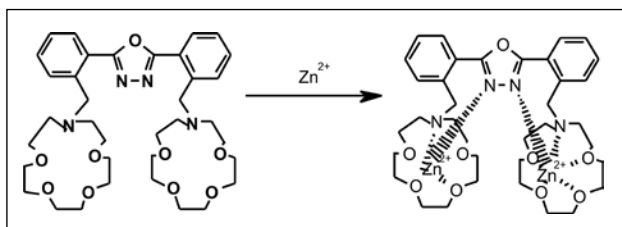


Figure 3. Fluorescence profiles of *Obox* without and with added metal ions and relative fluorescence enhancements with metal ions

fluorescence. However, to our delight, Zn^{2+} showed a dramatic fluorescence enhancement of 160 fold, whereas the coordinatively competing Mg^{2+} and Ca^{2+} induced much truncated 26 and 4 fold enhancements, respectively. Thus, **Obox** turned out to be a vastly superior probe for Zn^{2+} over biologically abundant Ca and Mg ions. The $\log K$ of 6.95 for Zn^{2+} is over an order and half greater than the next competing Mg^{2+} (5.27), implying strong binding and selectivity for Zn^{2+} [17].

Graphing the aza-crown rings at the *ortho* positions in **Obox** was not without reasons. Together with aza-crown rings, we anticipated the participation of oxadiazole nitrogens in the complexation process. As shown in Scheme 6, this extra dimension in the coordination of Zn^{2+} with oxadiazole would lock-up the conformational rotation around both the aryl-heteroaryl bonds. The resultant rigid conformation would activate the radiative channels over thermal deactivations. This conformational fixation, together with the PET blocking offer rational explanation for the observed high fluorescence enhancements of **Obox** in the company of Zn^{2+} .

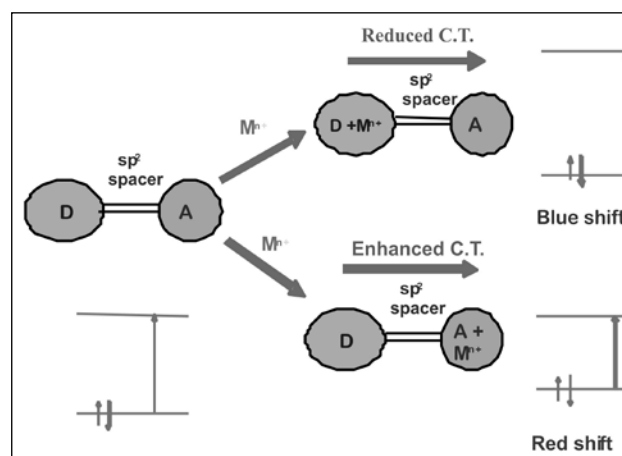


Scheme 6. Proposed Zn^{2+} binding with involving

Though, **Obox** delivers remarkably high off-on response with Zn^{2+} , however, the probe is unsatisfactory for potential sensing applications. Firstly, the probe offers signaling by way of fluorescence modulation only, and secondly the molecules absorb in the cell damaging UV region. This is a bad news because then the probe might not be user friendly to the biological community. At this point, we scouted for chromophores that could allow detection both by colorimetric as well as fluorescence modulations. For this purpose, internal charge transfer (ICT) based probes appeared eminently suitable.

4. Internal Charge transfer (ICT) Mechanism

The design and working principle of the ICT probes are illustrated in Scheme 7.

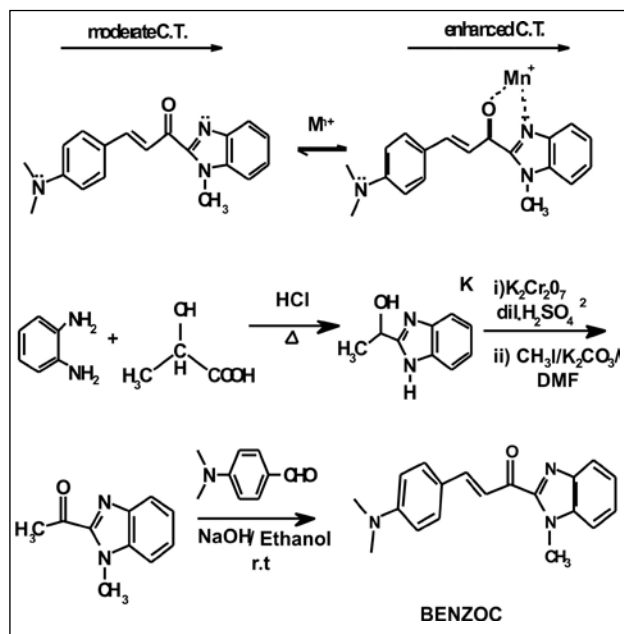


Scheme 7. Working concept of Internal Charge Transfer interaction (ICT)

In the ICT design, donor and acceptor are connected via an unsaturated spacer to allow direct through-bond electronic communication. Either acceptor (A) or donor (D) can be tailored to function as a receptor. In the event of the D being a receptor, the metal ion binding would weaken the donor character, causing higher energy separation between the ground and the excited states. In such a circumstance, one expects to see blue shift in the absorbance. On the other hand, if the A acts as the receptor, then metal ion binding would induce enhanced CT, lowering the electronic excitation energy level and giving rise to absorbance red shift. The ICT based probes are interesting since they could be tailored to exhibit absorption in the visible region [18].

5. Synthesis and Optical sensitivities of ICT based probes

Our first ICT based chromophore was a benzimidazole chalcone, designated as **Benzoc**. In this chromophore, the acceptor, keto-benzimidazole moiety is designed to serve as the chelate and according to the ICT principle, pronounced chelation-induced red shifts are expected upon metal ion complexation. Synthesis of **Benzoc** was carried out in a straightforward manner as shown in Scheme 8.



Scheme 8. Synthesis and proposed binding interaction of Benzoc with metal ions, M^{n+}

The chromophore revealed absorption maximum at 436 nm, which is attributed to a charge transfer transition. No appreciable changes in the absorbance were detected with alkali metal ions as well as with Ba and Ca ions. Though, Mg^{2+} produced a weak absorption at 540 nm, but the original band at 436 nm remaining essentially intact. However, addition of Zn^{2+} induced dramatic changes both in the shape and energy of the absorbance. The presence of Zn^{2+} caused complete bleaching of the original band at 436 nm with simultaneous emergence of a strong red shifted maximum at 550 nm. As shown in Figure 4, this phenomena induced color change from yellow to deep pink, allowing for a visual naked eye detection of Zn^{2+} . The Job plot indicated 1:1 binding stoichiometry, and a bidentate chelation of Zn^{2+} involving benzimidazole nitrogen and carbonyl oxygen of the probe is supported by the shift of 1652 cm^{-1} band to 1597 cm^{-1} in IR spectrum and downfield shifts of NMe_2 and the methyl group of benzimidazole by δ 0.25 and 0.13, respectively in the 1H NMR spectrum of **Benzoc** in the presence of Zn^{2+} .

Upon excitation at 436 nm, a structureless emission at 580 nm with Φ_f of 0.025 was observed. From the fluorescence studies, we found Zn^{2+} at $5.4 \times 10^{-3} M$ inducing a remarkably high emission

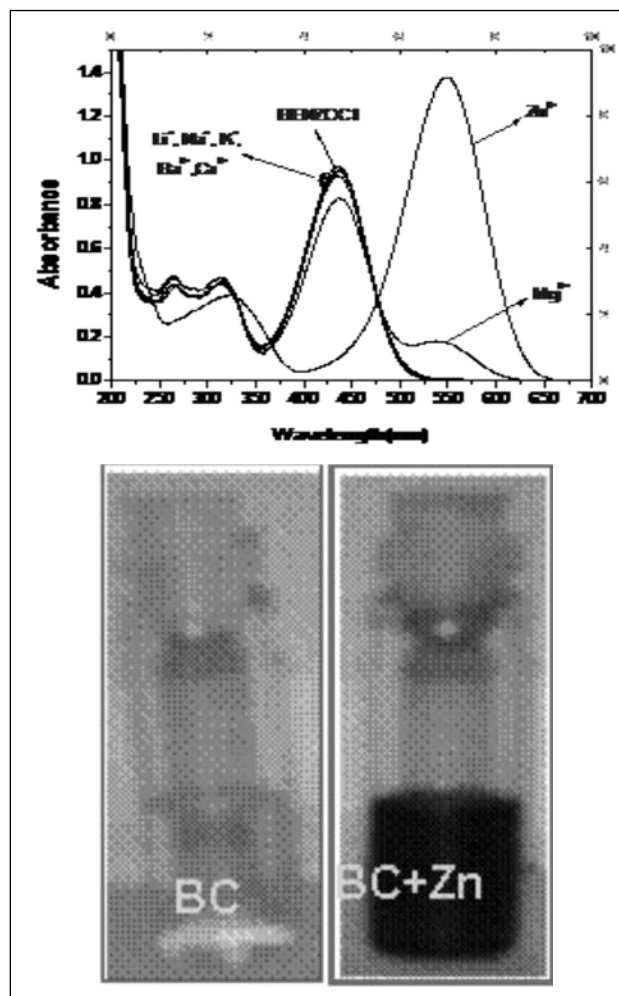


Figure 4. UV-vis of a) **Benzoc** with metal ions and b) colorimetric response with Zn^{2+} .

quenching by 92%. In addition, the λ_{em} also was red shifted from 580 to 591 nm, which is consistent with a similar shift observed in the absorbance as well. In contrast to Zn^{2+} , several other cations, Li, Na, K, Mg, and Ca ions at the same concentration as used for Zn^{2+} produced no more than 10% quenching. To give an indication of selectivity, 90% quenching by Mg^{2+} required ca. 150 fold higher concentration than Zn^{2+} [19]. The observed quenching is believed to be due to the chelation induced quenching. It is known that in many heterocyclic chromophores, the $n-\pi^*$ and $\pi-\pi^*$ states are quite close in energy. It is conceivable that Zn^{2+} complexation via cooperative 'N' and 'C=O' chelation could enhance the energy of the $n-\pi^*$, thereby rendering the $\pi-\pi^*$ as a dominant excited state. This shift in the nature of the excited state could lead to mixing of their vibronic states,

causing radiationless decay of the excited state upon metal ion coordination.

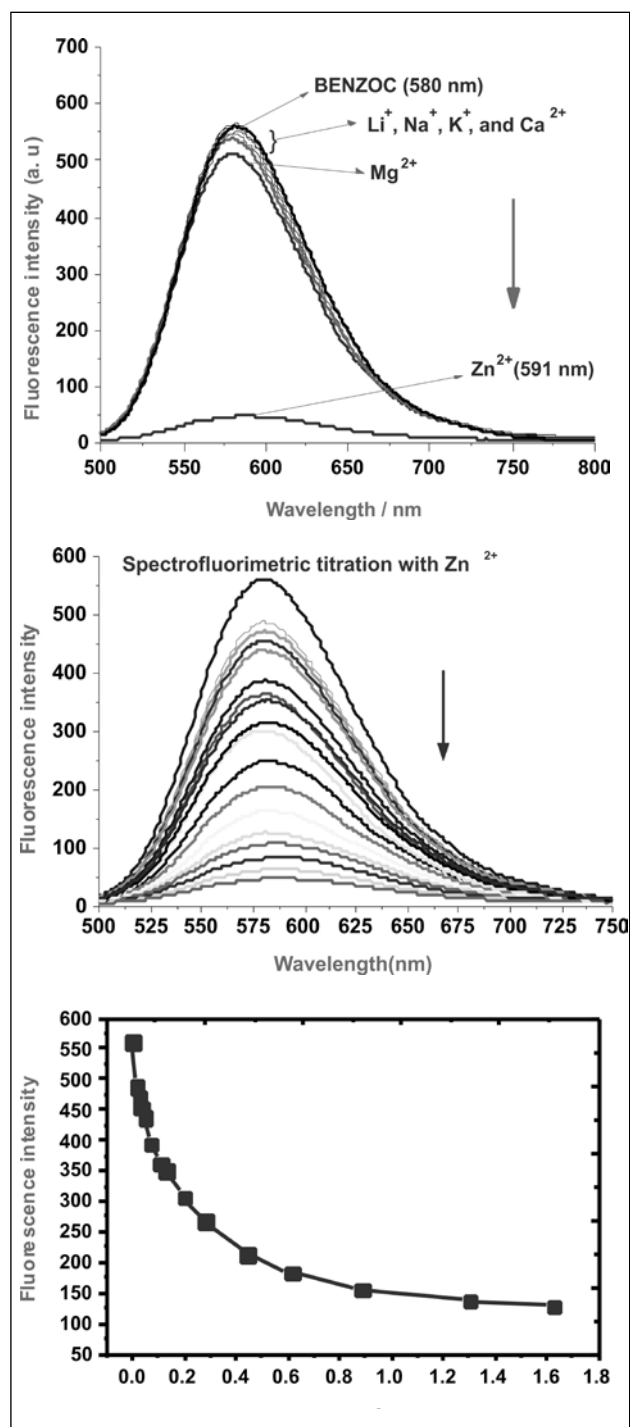
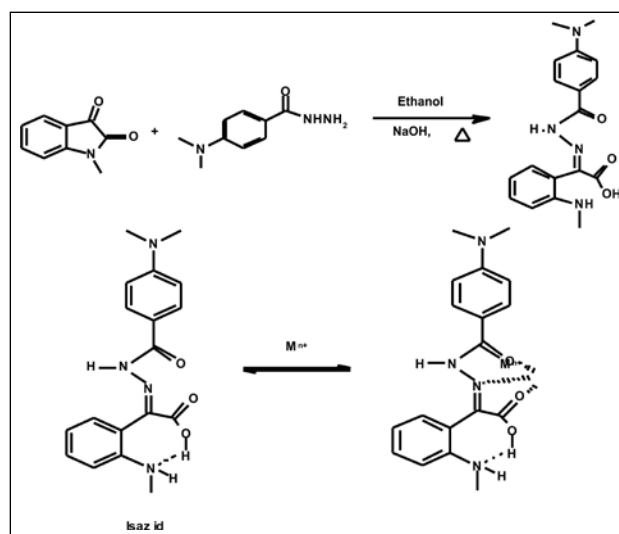


Figure 5. Emission profiles of a) **Benzoc** with metal ions, b) fluorimetric titration of **Benzoc** with Zn²⁺, and c) plot of fluorescence intensity vs Zn²⁺ conc.

Going a step further, we became interested design a sensor that would deliver not only colorimetric response, but also a more desirable, fluorescence off-on response. After synthesizing

and examining several chromophoric systems, the one that satisfied the above objective turned out to be the donor-acceptor system, designated as **Isazid**. The molecule harbors three coordination sites in the form of azomethine nitrogen, hydrazone carbonyl and carboxylic acid. In the metal binding mode, we expect enhanced ICT resulting from electron donation by the attached anilino groups. The synthesis of **Isazid** was readily accomplished in a single step as shown in Scheme 8.



Scheme 8. Synthesis of an ICT probe **Isazid** and its proposed coordination with metal ions, Mⁿ⁺

Isazid revealed a strong absorbance at 380 nm, which was scarcely perturbed by alkali metal ions as well as Ba, Ca and Mg ions. Clearly, these cations interact poorly with the probe. On the other hand, Cd²⁺ generated a new, rather weak absorption at 460 nm. However, with Zn²⁺, a very prominent red shifted band is seen at 464 nm at the expense of the original 380 nm absorption. As a result of the red shift, the addition of Zn²⁺ is accompanied by color change from yellow to pink, an event that is readily visualized by naked eye. A linear absorbance ratiometric response at two different wavelengths, namely 380 and 464 nm is possible to monitor Zn²⁺ in the presence of other cations, as shown in Figure 6.

Upon excitation at 410 nm, **Isazid** gave rise to a weak emission band ($\Phi_f = 0.0125$) at 431 nm. To our delight, the fluorescence was found to be enhanced in the presence of cations.

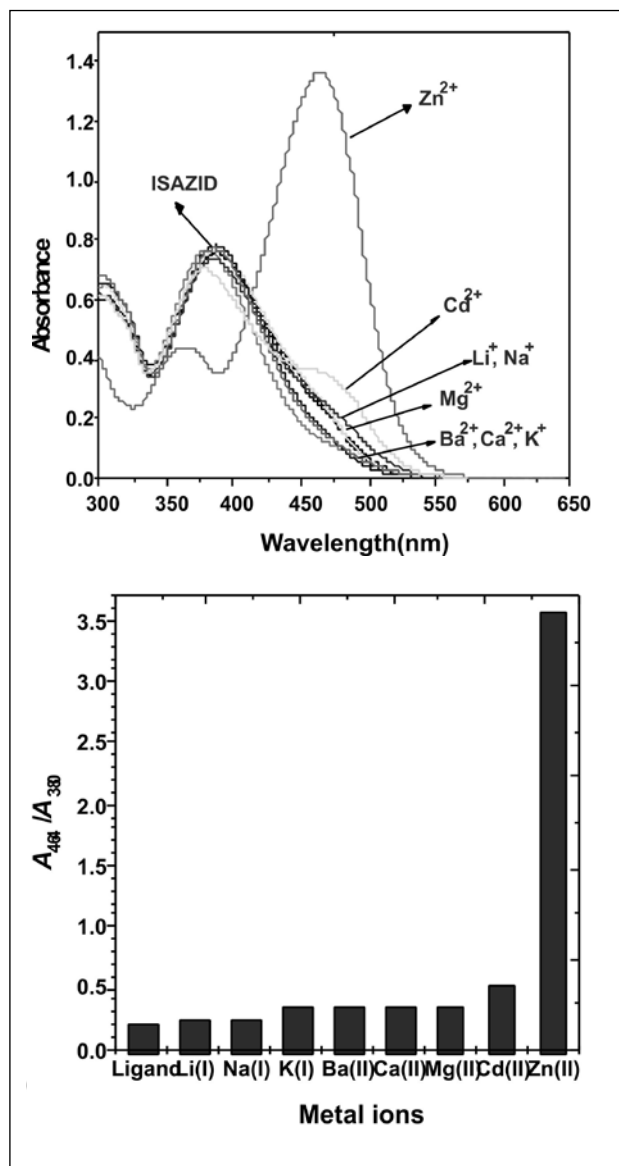


Figure 6. UV-vis profile of Isazid in the presence of metal ions and the absorbance ratiometric responses with different metal ions.

Gratifyingly, the Zn²⁺ addition resulted in the highest enhancements by 13 fold compared to less than 3.5 fold displayed by several other physiologically significant cations. The relative fluorescence enhancements induced by different metal ions are shown in Figure 7. A strong red shift in the absorbance and relatively high fluorescence enhancements clearly imply superior binding of Zn²⁺ compared to other cations [20]. The fluorescence enhancement may be attributable in part to change in the emissive state from less radiative n-π* of the free probe to the more radiative π-π* transition in the

Isazid-Zn²⁺ complex and in part to chromophore rigidification upon complexation [21].

Thus, Isazid proved to be both colorimetric as well as fluorescence off-on signaling probe for targeting of Zn²⁺ with high selectivity. With these results, we moved closer to our goal of designing a dual sensing probe.

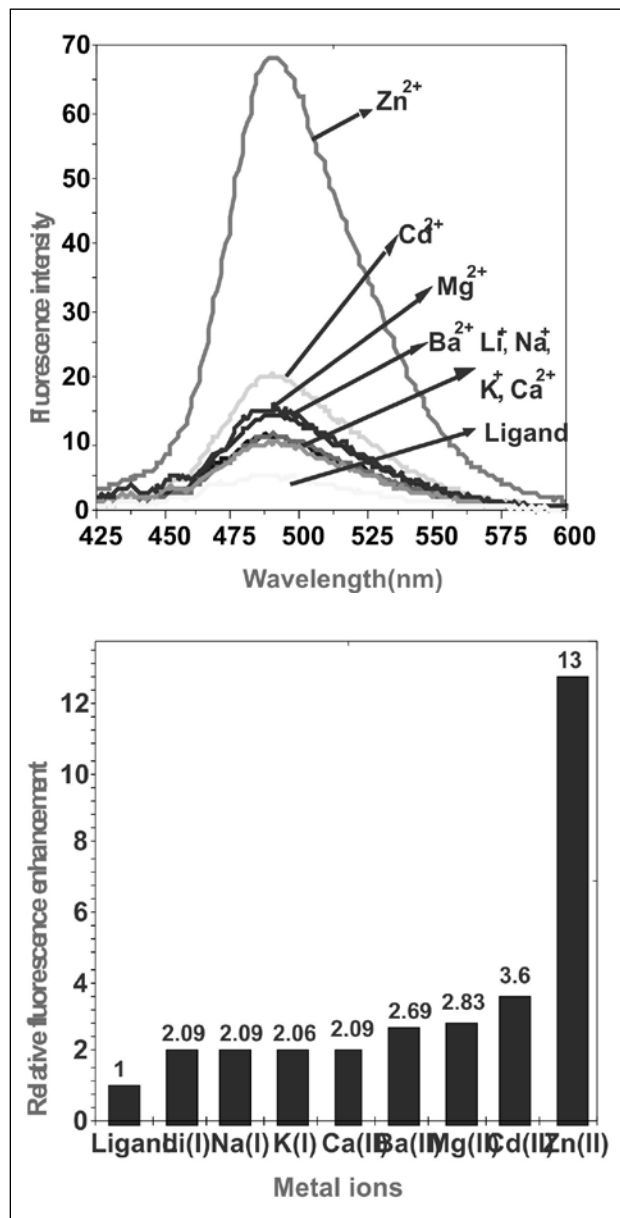
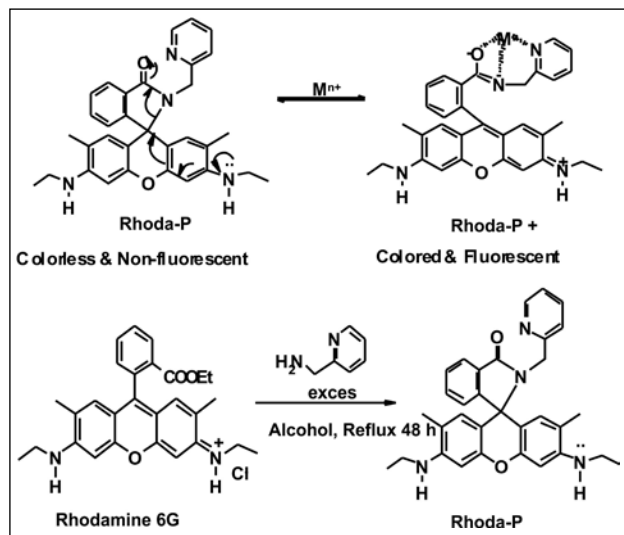


Figure 7. Emission spectral of Isazid + metal ions, and relative emission enhancements of Isazid with metal ions.

6. Rhoda-P, A highly selective sensor for Zn²⁺

In our continuing search for improved binding towards Zn²⁺, we next studied a rhodamine-based probe, designated as Rhoda-P.

Though, rhodamine platform has been used for designing Hg, Fe, and Pb ion sensors, as far as we are aware, the molecule has never been used to tailor Zn²⁺ recognition.



Scheme 9. The proposed metal ion binding and Synthesis of Rhoda-P.

As shown in Scheme 9, **Rhoda-P** was synthesized in a single step by reacting rhodamine G with 2-pyridyl methylamine. The probe has amide carbonyl and the pyridyl nitrogen as the potential bidentate chelating site. In conformity with the literature precedence [22] on related rhodamine chelates, we anticipated the complexation induced spiro-ring opening of **Rhoda-P**, assisted by participation of the anilino nitrogen. In contrast to the colorless and non-emissive **Rhoda-P**, the resultant ring-opened structure, being highly delocalized, is known to possess red shifted absorption and high fluorescence quantum yield.

The results of spectrophotometric analysis of a fixed concentration of **Rhoda-P** with the saturating metal perchlorates are depicted in Figure 8. A solution of **Rhoda-P** in acetonitrile displayed an absorption maximum at 302 nm. Addition of Zn²⁺ induced a new, intense absorption maximum at 528 nm. Clearly, the zinc binding triggers spiro ring opening, as proposed in the design concept. Noteworthy, none of the other metal ions, such as Li, Na, K, Ca, Ba, Mg, Co, Cu, Ni, and Cd ions detectably perturb the energy or shape of the absorption profile at

concentrations exceeding 300 times over that of the Zn²⁺. The color changes from colorless to pink which allows for a ready naked eye detection of Zn²⁺. This observation implies remarkably high selectivity in favor of Zn²⁺ over other cations. The log K calculated using nonlinear curve fitting is 2.41.

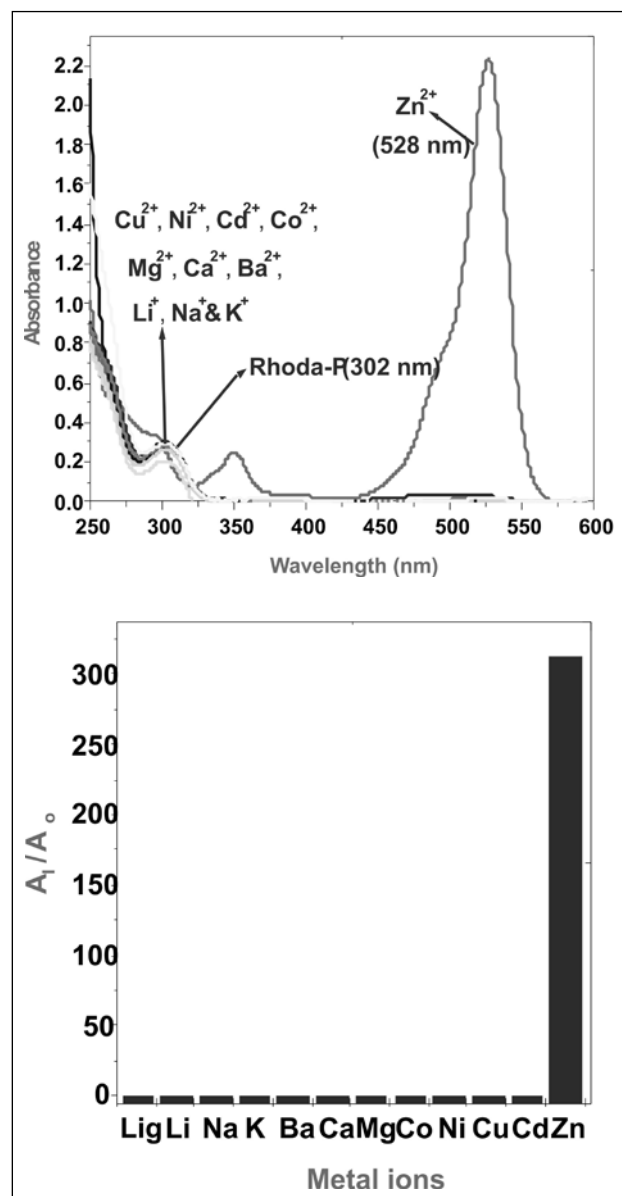


Figure 8. UV-vis of Rhoda-P + metal ions and the absorbance ratiometric responses with different metal ions.

Examination of the fluorescence profile with different metal ions revealed that only zinc binding is capable of inducing dramatically large fluorescence enhancement of 158 fold (Figure 9). Fluorescence intensity increased linearly with increasing zinc conc and the log Ks determined

spectrophotometrically and fluorimetrically were found to 2.41 and 2.39, respectively. These data imply that zinc binding is of similar magnitude both in the ground as well as excited states.

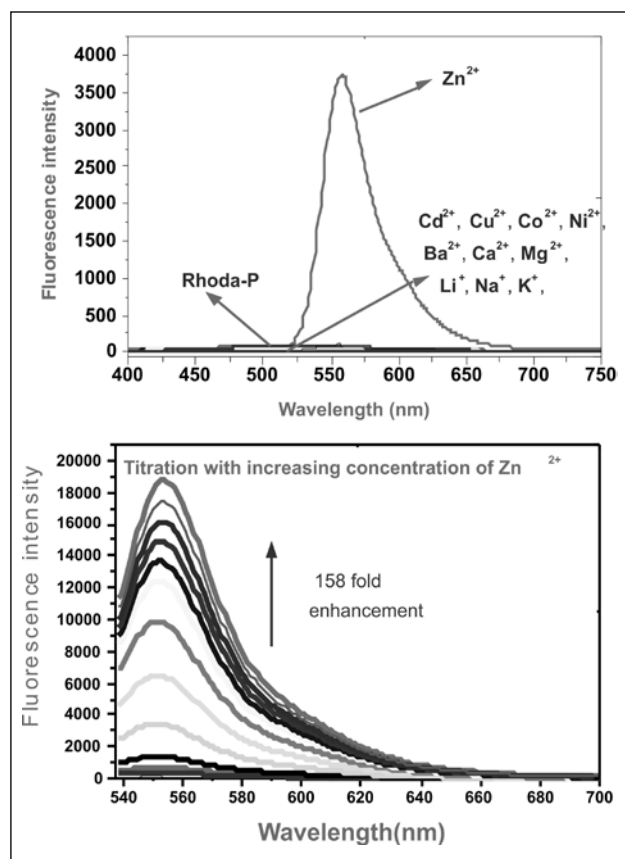


Figure 9. Emission profile of **Rhoda-P** with different metal ions and fluorimetric titration with Zn^{2+}

The detection limit, calculated on the basis of fluorescence data vs. Zn^{2+} concentration was found to be 4.8×10^{-7} M. The excited state of **Rhoda-P** without and with Zn^{2+} followed a single exponential decay with the excited state lifetime of 4.95 and 3.82 ns, respectively. On the other hand, the excited state life time of rhodamine 6G dye has been reported to be 4.21 ns. Clearly, a new excited state structure with an excited state life time intermediate between **Rhoda-P** and rhodamine 6G dye is involved as a consequence of binding interaction between **Rhoda-P** with Zn^{2+} [23]. Though, **Rhoda-P** has all the making of a good sensor, except for one serious drawback. The probe works only in the organic solvent, acetonitrile; the stability constant drops by an order of magnitude even in the presence of added 5% water. Though, **Rhoda-P** may be suitable for

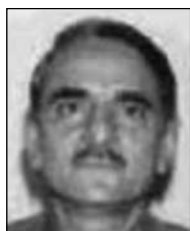
chemical analysis, however, in the present form, it is unsuited for the physiological monitoring of Zn^{2+} .

In summary, we have investigated the potential of many chemosensors for the selective recognition of biologically and environmentally significant Zn^{2+} . Of the two PET based probes, **Omx** and **Obox**, the later demonstrated vastly improved selectivity towards Zn^{2+} , while biologically abundant Ca^{2+} and Mg^{2+} displayed less pronounced fluorescence responses. Among the ICT based probes studied, the probe, **Benzoc** delivered colorimetric and fluorescence 'on-off' response. On the other hand, **Isazid** gave rise to colorimetric and the more desirable fluorescence 'off-on' signaling for the selective discrimination of Zn^{2+} . Finally, we studied a rhodamine derived probe, **Rhoda-P**, which turned out by far the best dual sensing probe for Zn^{2+} , offering remarkably selective color modulation and high fluorescence amplification. Work is ongoing to suitably modify the design strategy to make the systems compatible for aqueous measurements.

7. References

1. J. Andréasson and U. Pischel, *Chem. Soc. Rev.*, **2010**, *39*, 174-188.
2. a) Y. E. Spichiger-Keller, *U S-Sensors and Biosensors for Medical and Biological Applications*, Wiley-VCH, New York, 1998. b) Czarnik, A. W. *Act. Chem. Res.* **1994**, *27*, 302-308.
3. a) Pietraskiewicz, M in *Comprehensive Supramolecular Chemistry*, **1996**, Vol. 10, 225-266. b) J.-M. Lehn, *Supramolecular Chemistry*, VCH, Weinheim, **1995**. c) A. P. De Silva, H. Q. N. Gunaratne, T. Gunnlaugsson, A. J. Huxley, C. P. McCoy, J. T. Rademacher, T. E. Rice, *Chem. Rev.* **1997**, *97*, 1515.
4. Lakowicz, J. R. *Principles of Fluorescence Spectroscopy*, 2nd ed.; Kluwer Academic / Plenum Publishers: New York, **1999**.
5. J. W. Steed and J. L. Atwood, *'Supramolecular Chemistry'*, J. Wiley & Sons: Chichester, **2000**.
6. Y. Inoue, G. W. Gokel, "Cation binding by macrocycles: complexation of cationic species by crown ethers", M. Dekker, **1990**.
7. A. T. Wright and E. V. Anslyn, *Chem. Soc. Rev.*, **2006**, *35*, 14.
8. a) de Silva, A. P.; Gunaratne, H. Q. N.; Gunnlaugsson, T.; Huxley, A. J. M.; McCoy, C. P.; Rademacher, J. T.; Rice, T. E. *Chem. Rev.* **1997**, *97*, 1515. b) Kim, H. N.; Lee, M. H.; Kim, H. J.; Kim, J. S.; Yoon, J. *Chem. Soc. Rev.* **2008**, *37*, 1465.
9. a) C. Lodeiro, J. L. Capelo, J. C. Mejuto, E. Oliveira, H. M. Santos, B. Pedras and C. Nunez, *Chem. Soc. Rev.*, **2010**, *39*, 2948. b) T. Gunnlaugsson, M. Glynn, G. M. Tocci, P. E. Kruger and F. M. Pfeffer, *Coord. Chem. Rev.*, **2006**, *250*, 3094.
10. a) V. J. Thom, C. C. Fox, J. C. A. Boeyens, R. D. Hancock, *J. Am. Chem. Soc.* **1984**, *106*, 5947. b) Knut Rurack, *Spectrochimica Acta A*, **2001**, *57*, 2161-2195.
11. J. M. Berg, Y. Shi, *Science* **1996**, *271*, 1081-1085.

12. Frederickson C. J., Koh J.-Y., Bush A. I., *Nat Rev Neurosci.* **2005**, *6*, 449-462.
13. Walker C. F., Black R. E., *Annu Rev Nutr* **2004**, *24*, 255-275.
14. a) Jiang P, Guo Z, *Coord. Chem. Rev.* **2004**, *248*, 205-229. b) Kimura E, Aoki S., *Biometals* **2001**, *14*, 191-204. c) Kikuchi K, Komatsu K, Nagano T, *Curr Opin Chem Biol* **2004**, *8*, 182-191. d) Burdette SC, Lippard SJ., *Coord Chem Rev* **2001**, *206*, 333-361. e) Taki M, Wolford JL, O'Halloran TV. *J. Am. Chem. Soc.* **2003**, *126*, 712-717. f) Gee, K. R.; Zhou, Z. -L.; Qian, W. -J.; Kennedy, R. *J. Am. Chem. Soc.* **2002**, *124*, 776-778.
15. F. E. Jacobsen, J. A. Lewis, and S. M. Cohen, *J. Am. Chem. Soc.* **2006**, *128*, 3156-3157.
16. Vallee B. L., Auld D. S. *Biochemistry* **1990**, *29* 5647-59.
17. S. H. Mashraqui, S. Subramanian, T. Khan, A. C. Bhasikuttan, *Tetrahedron*, **2007**, *63*, 11093-11100.
18. **B. Valeur, and I. Leray**, *Coord. Chem. Rev.*, **2000**, *205*, 3-40.
19. S.H.Mashraqui, S. Subramanian, T. Khan, *Chem. Lett.* **2006**, *35*, 786-787.
20. S.H.Mashraqui, T. Khan, S. Subramanian, R. Betkar, M. Chandiramani, *Tet. Lett.* **2007**, *48*, 8487-8490.
21. a) Leray, I.; O'Reilly, F.; Habib-Jiwan, J.; Soumillion, J. P.; Valeur, B. *Chem. Commun.* **1999**, 795-796. b) Zhou, Z.; Fahrini, C. J., *J. Am. Chem. Soc.* **2004**, *126*, 8862- 8863.
22. Dujols, V.; Ford, F.; Czarnik, A. W. *J. Am. Chem. Soc.* **1997**, *119*, 7386.
23. S.H.Mashraqui, T. Khan, S. Subramanian, R. Betkar, M. Chandiramani, *Chem. Lett.* **2009**, *38*, 730-731.



Sabir H. Mashraqui is Professor of Chemistry at the the Department of Chemistry, University of Mumbai. He received Ph.D. from I.I.T., Bombay in 1978, and carried out post-doctoral work at Brandies University, U.S.A (1980-83) and University of Groningen, Holland (1983-85). His current research interest includes design and synthesis of cation and anion chemosensors, nonlinear optic materials and cyclophanes.

Molecular Recognition by Calix[4]arene Scaffolds

Jugun Prakash Chinta and Chebrolu P. Rao*

Bioinorganic Laboratory, Department of Chemistry, Indian Institute of Technology Bombay, Powai,
Mumbai – 400 076, e-mail: cprao@iitb.ac.in

Abstract

Molecular recognition is an important phenomenon that governs various biological processes. This can be seen in the form of interactions that exists between a pair of molecular systems including carbohydrates, proteins and DNA, *viz.*, carbohydrate-protein, DNA-protein, protein-protein, etc. These examples demonstrate the significance of molecular recognition of biological matter and thereby the life. Thus, all these offer vital reasons for studying how molecules interact. A molecular recognition system requires rigid molecular scaffolds, which serves the important role of positioning the functionality at specific distance and orientation. Indeed in the nature, such approaches were very common, executed by utilizing various frameworks, such as, the peptide, carbohydrate, and the nucleoside/nucleotide. However, the macromolecular structures of these is difficult to synthesize, redesign and study, which nature does easily using a variety of reactions that would in turn utilizes the phenomenon of the molecular recognition abundantly. Consequently, smaller synthetic frameworks have been developed for use as mimics for the natural processes. Several small molecule scaffolds have been developed for studying the molecular recognition properties, among those, calix[4]arene is of interest because these provide versatile platform for appropriate derivatization. Some of the general features of these recognition processes and the literature reported calix[4]arene receptors have been described and the bio-molecular (amino acid and protein binding), aromatic hydrocarbon recognition by the synthetic conjugates of calix[4]arenes have been discussed. The computational modeling of several metal ion and anion complexes of different conjugates of calix[4]arene have been established and the corresponding results were discussed.

Introduction

Molecular recognition is “the specific recognition of one molecule by another”. This process refers to the specific interaction that exists between the two or more molecules. The interactions involved are mainly through non-covalent, such as, hydrogen bonding, ion-dipole (metal coordination), hydrophobic forces, *van der Waals* forces, $\pi\cdots\pi$ interactions and/or electrostatic effects. The host and guest involved in molecular recognition should exhibit molecular complementarity.¹ Molecular recognition is an important phenomenon that governs various biological processes. This can be seen in the form of interactions that exists between a pair of molecular systems including carbohydrates, proteins and DNA, *viz.*, carbohydrate-protein, DNA-protein, protein-protein, etc.² These examples demonstrate the significance of

molecular recognition of biological matter and thereby the life.

About 100 years ago, Emil Fischer used the analogy of a lock and key to describe the host-guest interaction. Till then little has been known about “intermolecular” bonds. The field of molecular recognition began in 1967 with Pedersen’s synthesis of crown ethers. These macrocyclic receptors were able to bind alkali metals with amazing efficiency and selectivity.³ Since then, synthetic receptors such as crown ethers, calixarenes, and cyclodextrins have become commercially available and even found utility in various applications. In recent years, the field has accumulated a number of new names including: hostguest chemistry and supramolecular chemistry. In 1987, this potential multidisciplinary field was acknowledged with a Nobel Prize.⁴

Common molecular scaffolds: A molecular recognition system requires rigid molecular scaffolds, which serves the important role of positioning the functionality at specific distance and orientation. Indeed in the nature, such approaches were very common which were executed by utilizing various frameworks, such as, the peptide, carbohydrate, and the nucleoside. However, the macromolecular structures of these is difficult to synthesize, redesign and study, which nature does easily using a variety of reactions that would in turn utilize the phenomenon of the molecular recognition abundantly. Consequently, smaller synthetic receptors have been developed for mimicking these. Figure.1 shows some common molecular scaffolds utilized in molecular recognition *viz.*, (a) cyclodextrins, (b) calixarenes, (c) crown ethers, (d) porphyrins *etc.* Among all these, calixarenes are of our interest. For the past several years our group has been working on the development of calix[4]arene derivatives for molecular recognition. In general, these scaffolds share some common requirements, (a) a concave shape to focus functionality towards guest systems; (b) pre-organization of the binding core; (c) structural rigidity to preserve the binding pocket; (d) solubility in a suitable solvent in which the preferred non-covalent interactions are strong.

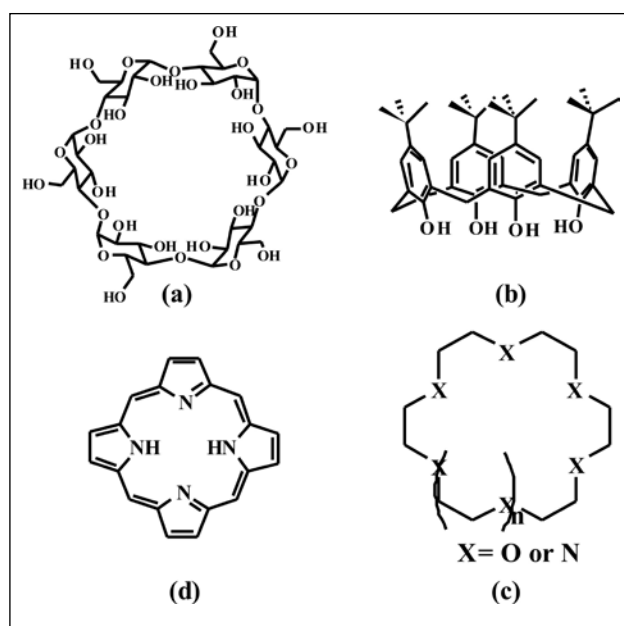


Figure 1. Common molecular scaffolds used in molecular recognition.

Interactions encountered in molecular recognition: Non-covalent interactions are the dominating ones in molecular recognition. Nature uses a collection of these non-covalent interactions in abundance in complex combinations which have made their study difficult. In contrast, most synthetic hosts utilize only one or two types of interactions and can be more easily altered, manipulated, and functionalized. Different kinds of non-covalent interactions are involved in the molecular recognition, *viz.*, hydrogen bonding, $\pi \dots \pi$ interactions, ion-dipole including metal coordination and solvation. The non-covalent interactions utilized in the course of the present work has been introduced in this paper using some examples reported in the literature.

Number of calixarene based synthetic receptors which utilize hydrogen bonding as well as $\pi \dots \pi$ interactions are reported in the literature. For example, upper rim N-linked peptido calix[4]arene (Figure 2a) acts as artificial antibiotic which is designed to bind to the peptide sequence D-ala-D-ala at bacteria cell walls, mimicking vancomycin.⁵ The calixarene has a compatible sequence at its upper rim for that purpose, consisting of two bridged pseudo peptides. The strongest binding is shown when L-ala units are a part of the bridge. The guest molecules are bound inside the cavity through hydrogen bonding between amide bonds of calix[4]arene and the peptide. On the other hand, the tetra glycoside conjugate of calix[4]arene carrying four glycosides and thiourea moiety at the upper rim are involved in the agglutination.⁶

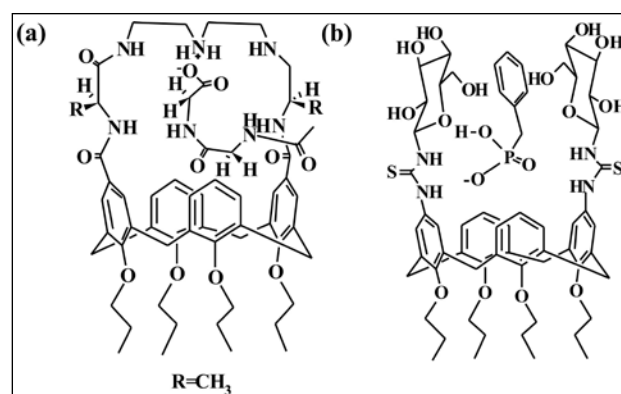


Figure 2. Synthetic receptors utilizing hydrogen bonding arrays. (a) Proposed mode of binding of N-acetyl-D-Ala-D-Ala by N-linked peptide calix[4]arene, (b) Proposed mode of binding of benzylphosphonate to thiourea-linked calix[4]arene glucose conjugate.

While the glucosyl conjugate agglutinates the receptor concanavalin A (ConA), that of the galactosyl agglutinates peanut lectin (PNA). In both the cases, the complexes of these 'calixarene-sugars' are more stable compared to those between monomeric glucose or galactose with the respective lectin. The cluster effect, caused by multivalent sugar-protein interactions was confirmed by turbidity and competitive binding experiments. These sugar-protein interactions are mainly through hydrogen bonding. Further, if two instead of four glycoside groups are present in calixarene, it effectively binds anions in DMSO- d_6 through hydrogen bonding and sugar- π interactions in the order, *viz.*, benzylphosphonate ($\log K_a = 2.2$) > benzoate (2.0) > H_2PO_4 (1.95) > NAc-L-ala (1.76) > Chloride (1.5) > acetate (1.2) (Figure 2b). The binding is accompanied by the conformational reorientation that takes place even in the solvents which are known to compete for hydrogen bonding.

Metal ion coordination also plays important role in the molecular recognition. Metal ions can either act as guests or as intermediaries to bring hosts together. Because of their charged as well as covalent bonding character, metal-ligand interactions have a tendency to be stronger than neutral non-covalent interactions. A variety of events are possible depending upon the metal ion used and the number of binding sites present on the ligand. For example, a cyclometalated palladium-azo complex (Figure 3a) has been used as a differential chromogenic probe for amino acids in aqueous solution.⁷ This complex has been chosen as the colorimetric reporting molecule because of its strong preference known for the complexation of palladium with amino acids. Palladium forms stable complexes with the N-, O-, S-donor atoms commonly present in the amino acids. The binding preference is based on the formation of stable N,O-chelating rings and also on the side chain binding groups, such as, imidazole, carboxylic, phenolic, indole, amino and thiol. The complex showed colour change in the presence of histidine (His), cysteine (Cys), alanine (Ala), lysine (Lys) and tyrosine (Tyr). Recently, calix[4]arene based silver and zinc complexes have been reported for the selective

recognition of amino acids, and inorganic as well as biological phosphates.

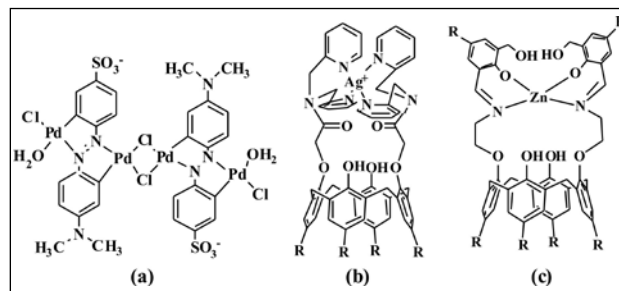


Figure 3. Molecular recognition systems utilizing metal ion coordination. R= *t*-butyl

Among these two complexes, lower rim 1,3-di{bis(2-picoly)}amide derivative of calix[4]arene Ag(I) complex (Figure 3b) showed selectivity towards Cys among the naturally occurring amino acids studied.^{8(a)} However, the zinc complex of salicylidene appended calix[4]arene derivative (Figure 3c) showed selectivity toward Cys, Asp, and His through the formation of the Zn^{2+} complex by chelating through their side chain moieties. This complex also showed selectivity towards phosphate ion among a number of other anions studied.^{8(b)}

Solvation plays an important role in determining the strengths of non-covalent interactions.⁹ Because of the exceptional nature of intermolecular bonds, solvent molecules also compete for the interactions of the host and guest. Solvents with strong attractions for either the host and/or guest will bind to these components and obstruct complexation. Because of their overwhelming stoichiometric advantage, solvent molecules do not have to interact strongly to have ominous consequences for the complex formation. Alternatively, the solvent can assist and provide the driving force for the complexation, e.g., the hydrophobicity of the host or a portion of the host (and/or guest) can actually force the complexation through repulsive forces.

Results and Discussion

Amino acid recognition: A few calix[4]arene based receptors for amino acids were reported in the literature. Novel chiral calix[4]arene derivatives bearing L-tryptophan residues

(Figure 4a) have been developed and studied their chiral recognition ability towards chiral carboxylates, two anions of the amino acids, and two amino alcohols by fluorimetric titration and ^1H NMR study. The fluorescence emission of the receptor was quenched by about 10% upon the addition of anionic L-ala, whereas no change was observed upon the addition of the anionic D-Ala. The ^1H NMR studies of the receptors with L or D-Ala anion showed the downfield shift of the -CH proton signal of the anionic Ala at $\delta = 3.834$ ppm.¹⁰ Two chiral calix[4]arene derivatives containing hydrazide and dansyl groups (Figure 4b) have been synthesized and examined their enantioselective recognition towards alanine (Ala) and phenylalanine (Phe) anions by fluorescence and ^1H NMR spectroscopic studies. These derivatives have good enantioselective recognition for the anions of L- Ala or Phe.¹¹

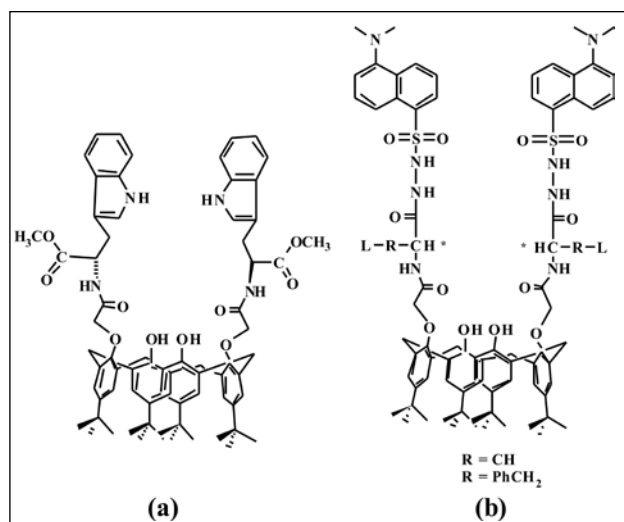


Figure 4. Structures of chiral calix[4]arene derivatives containing (a) L-Tryptophan (b) dansyl groups.

A new chiral rigid water soluble peptidocalix[4]arene (N-linked) (Figure 5a) in cone conformation was reported and investigated the inclusion properties of host with several guest molecules, especially chiral amino acids. ^1H NMR studies showed that the aromatic amino acids as their methyl esters are better complexed with the host than the aliphatic ones and the selectivity follows the order, L-Trp \approx D-Trp > L-Phe > L-Tyr > L-Ala > Gly. The highest association constant was observed for the tryptophan, with an association constant of 620 M^{-1} .¹² The upper rim modified

calix[4]arenes in cone conformation with L-alanine and phenylalanine groups (C-linked peptidocalixarenes) have been reported (Figure 5b). These are characterized by intramolecular H-bonds influencing the conformation, and by

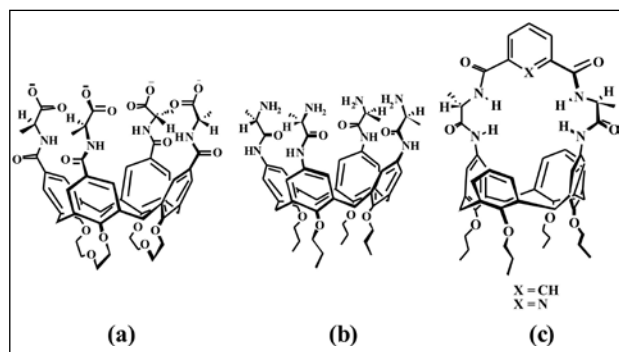


Figure 5. Structures of alanine functionalized peptidocalix[4]arene conjugates (a) N-linked (b) C-linked (c) bridged.

intermolecular aggregation. The terminal nitrogen atom in C-linked peptidocalixarenes is protonated in neutral and acidic media, rendering the molecule to be a water soluble host for anions. These derivatives were found to be complexed with anions of N-substituted amino acids, such as, alaninates, in contrast to the N-linked analogues, which complexes the ammonium cations and the carboxylic acids.¹³ The intramolecular H-bonding and self complexation have been avoided when the peptide groups are linked by a spacer such as the diacylpyridine or phthaloyl groups (Figure 5c). These molecules are rigid and their complexes with anions in organic solvents are more stable than those of unbridged calixarene conjugates with greater flexibility.¹⁴

A coumarin appended calix[4]arene conjugate recognizes L-tryptophan as 1:1 complex as studied by UV-visible and fluorescence spectroscopy (Figure 6a).¹⁵ The solid state structure of calix[4]arene dihydroxyphosphonic acid (Figure 6b) with L-lysine shows a 1-D ladder network of lysine molecules in the crystal.¹⁶ It has been found that in the asymmetric unit cell of the complex, there are four molecules of dihydroxyphosphonic acid derivatives of calix[4]arene, three molecules of lysine, and a large number of solvent molecules. Supramolecular complex formation between

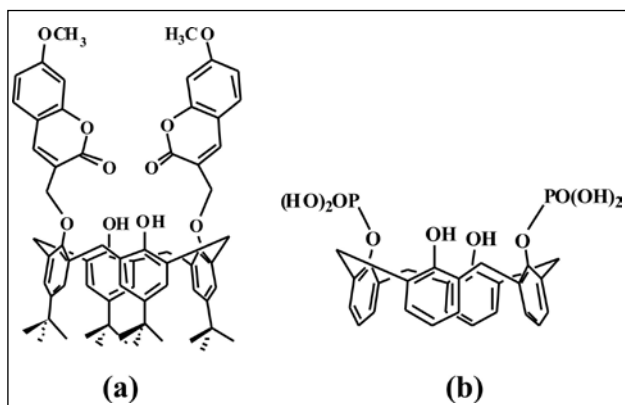


Figure 6. Structures of calix[4]arene derivatives functionalized with (a) coumarin moiety, (b) dihydroxyphosphonic acid group.

dihydroxyphosphonic acid derivative and the amino acids in the presence of metal salts have been studied by ES MS combined with ^1H NMR. They have shown that this derivative has both high affinity and strong selectivity for the formation of ternary complex between Zn^{2+} and histidine.¹⁷ Recently lower rim 1,3-diamido calix[4]arene conjugates of amino acids have been reported.¹⁸ The conjugate possessing phenylalanine moiety (Figure 7a) has been shown to exhibit recognition towards guest amino acids possessing side chain $-\text{COOH}$ moiety, *viz.*, Asp, Glu, as well as the reduced and oxidized glutathione (GSH, GSSG), by switch-on fluorescence. The nano structural features of the complexes formed between the conjugates and the amino acids have been demonstrated by Atomic Force Microscopy (AFM) and Scanning electron microscopy (SEM), which differ substantially from the features of the receptor alone. The mode of binding between amino acid and the receptor has been modeled by computational calculations (Figure 7b and c).

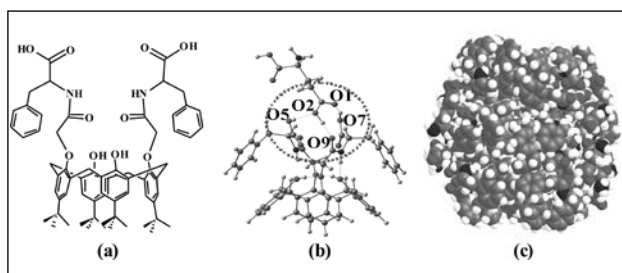


Figure 7. (a) Structures of phenylalanine functionalized calix[4]arene derivative. (b) DFT optimized glutamic acid complex of phenyl alanine derivative. (c) Space-filling model of the hexameric-aggregate of glutamic acid complex.

The *p*-sulfonato-calixarenes are important class of compounds because of their water solubility and are known to be versatile hosts for cations and amino acids. Several research groups used simple and functionalized sulfonato-calixarenes for the amino acid recognition. The interaction of *p*-sulfonato-calixarenes and their derivatives with various amino acids have been performed both by ^1H NMR, microcalorimetry and solid state investigations. Coleman and coworkers studied the interaction of sulfonato-calixarenes with the basic amino acids arginine and lysine by ^1H NMR.¹⁹ Based on these studies, it has been found that the binding occurs through strong electrostatic interactions between the sulphonato calixarene and the basic amino acids (Figure 8).

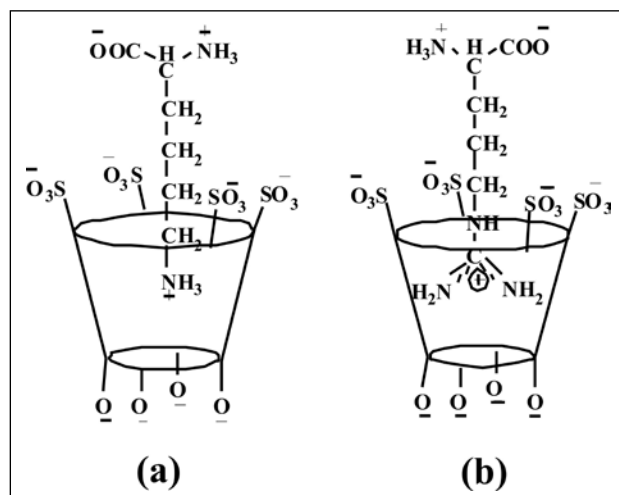


Figure 8. Schematic diagrams of the complexes between *p*-sulfonato calix[4]arene and (a) lysine and (b) arginine ($\text{pH} = 5$).

The thermodynamic data of these interactions were further investigated by microcalorimetry.²⁰ This data shows that the calix[4]arenesulfonate forms relatively strong complexes than the calix[6] and the calix[8]arenesulfonate. In all cases, the complexation is driven by a favourable enthalpy change. Further these sulfonato calixarenes were studied for the binding of dipeptides and tripeptides containing lysine or arginine by NMR and micro calorimetry.²¹ However, the functionalized sulfonato calixarenes showed strong binding with Asp, Ser and Trp as studied by ^1H NMR experiments.²² Ungaro's group synthesized various sulfonato-calix[4]arenes

having different functionalization at its lower rim and studied its inclusion properties with naturally occurring amino acids using microcalorimetry and ^1H NMR studies.²³

The complexation of amino acids by *p*-sulfonato calixarenes have been investigated by the structural characterization in their solid state. The first structure reported showed a 1:2 stoichiometry between *p*-sulfonato calix[4]arene and lysine.²⁴ Crystal structures with racemic amino-acids (alanine, phenylalanine, histidine) and chiral amino-acids (*S*-alanine, *S*-histidine and *S*-tyrosine) have been reported.²⁵ The solid state structure of *para*-sulfonato-calix[4]arene with arginine is found to have novel zigzag bilayer of calixarene molecules with six molecules of arginine each having different conformations along with an infinite water channel (Figure 9).²⁶

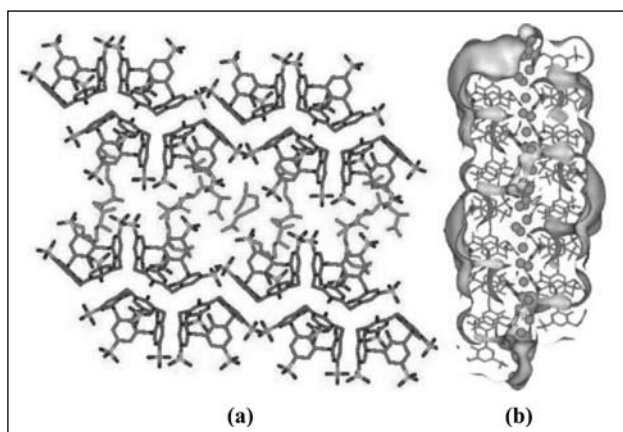


Figure 9. (a) Solid state zig-zag bilayer packing of the *p*-sulfonato calix[4]arene/arginine complex and (b) view of the water channel.²⁶

Selective sensing of tyrosine and cysteine by CdSe quantum dots with the help of *p*-sulfonatocalix[4]arene have been reported.²⁷ A novel colorimetric sensor based on *p*-sulfonatocalix[4]arene coated silver nanoparticles has been used to probe the His in water.²⁸ The metalloenzyme model properties of simple sulfonatocalix[4]arenes in aqueous solution has been explored and found to be based on the dynamic self-assembling.²⁹ Thus the amino acid recognition using calix[4]arene conjugates is an important area of current research and much needs to be explored in this direction. Attempts have been made to design and synthesize

several conjugates, *viz.*, naphthylidene appended Zn(II) complex of calix[4]arene, galactosyl and phenylalanine appended calix[4]arene derivatives. All the receptor molecules have been well characterized by ^1H NMR, ^{13}C NMR, FT-IR, ESI MS and elemental analysis, and studied for their amino acid recognition by various spectroscopy techniques, such as, absorption, emission and mass spectrometry. Schematic representations of these derivatives have been shown below (Figure 10).

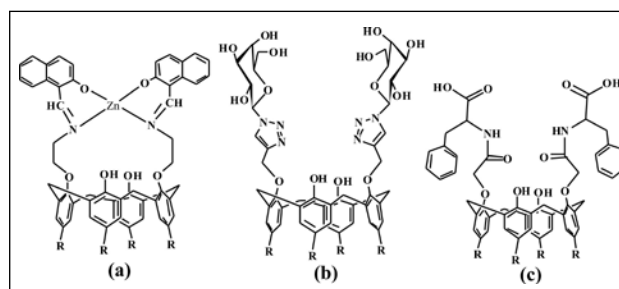


Figure 10. Schematic representation of (a) Zn(II) complex of naphthylidene conjugate of calyx[4]arene ($[\text{ZnL}_1]$) (b) galactosyl appended calix[4]arene derivative (L_2) (c) phenylalanine functionalized calix[4]arene conjugate (L_3). R= *tert*-butyl

$[\text{ZnL}_1]$ recognizes Asp, Cys, His and Glu from among the naturally occurring amino acids by exhibiting large fluorescence quenching.³⁰ The recognition of these amino acids by $[\text{ZnL}_1]$ results in the de-chelation of Zn^{2+} and re-chelation of this ion by the corresponding amino acid based on the changes observed in 340 to 450 nm region in the absorption spectra. Photoelectron transfer (PET) from the lone pair of electrons present on imine moiety of L_1 ($[\text{ZnL}_1]$ devoid of Zn^{2+}) is off in the $[\text{ZnL}_1]$ complex owing to the binding of Zn^{2+} . The trend in the fluorescence reverses to PET-on in the presence of added amino acid, suggesting the dechelation of Zn^{2+} from $[\text{ZnL}_1]$ via the possible formation of a ternary complex. The recognition features of $[\text{ZnL}_1]$ towards amino acids depends on the protonation and chelating ability (His > Phe > Asp > Cys >> Glu), $\pi \dots \pi$ interaction ability (Trp >>> Tyr > His) of the side chain with the L_1 and the de-chelation of $[\text{ZnL}_1]$ (His > Cys > Tyr > Asp ~ Trp), as demonstrated based on fluorescence, absorption and ESI MS studies, indicating that the incoming amino acid may approach the zinc center from the top, perhaps

through the formation of a ternary complex. Titration of $[\text{ZnL}_1]$ with esters of amino acids showed the involvement of side chain during the interaction. The esters of Glu, Ser, Gly, Ala, Phe exhibited large difference in the behaviour of their relative fluorescence intensity compared to their acid counter parts, those of Cys and His showed no difference at all. The behaviour of Trp and Tyr was found to be intermediate. The large difference that was observed between Glu and Glu-OEt can be explained only when both the protonation as well as chelation by the side chain carboxylate moiety towards Zn^{2+} were considered together. The relative intensity observed in case of Cys and His and their corresponding esters suggest that in both these cases the side chain plays important role. Protonation of $[\text{ZnL}_1]$ by amino acids has been further confirmed by carrying out the titrations with simple acids not possessing amino function, *viz.*, acetic acid, benzoic acid and phenylacetic acid. Thus protonation, dechelation and rechelation plays role in the amino acid recognition by $[\text{ZnL}_1]$. The re-chelation of Zn^{2+} by the amino acid has been demonstrated based on ESI MS studies carried out between L_1 and Cys to result in the formation of a $[\text{Cys} + \text{Zn} + \text{Cys} + \text{CH}_3\text{OH} - \text{H}]^+$ by exhibiting a peak at m/z of 338. All these protonation, dechelation and $\pi \dots \pi$ interaction ability of the amino acids towards $[\text{ZnL}_1]$ have been demonstrated based on the absorption studies. The band at 420 nm increases at the cost of 375 nm upon the addition of amino acids to $[\text{ZnL}_1]$ which is characteristic for L_1 , showing the de-metallation of $[\text{ZnL}_1]$. The decrease in absorbance of $[\text{ZnL}_1]$ in the region of 200-250 nm upon the addition of Trp, Tyr and His are indicative of the involvement of π - π interactions present between the aromatic side chains of these amino acids with the naphthalene moiety present in $[\text{ZnL}_1]$. $[\text{ZnL}_1]$ has also been found to be selective towards the amino acids present in GSH and GSSG. Thus $[\text{ZnL}_1]$ recognizes amino acids based on their protonation as well as chelating ability.

The galactose appended calix[4]arene derivative (L_2) showed its selectivity for aromatic amino acids by significant change in

the absorbance of L_2 whereas all other amino acids show almost no change in the absorbance. In case of Trp absorbance of both 225 nm and 280 nm bands were decreased gradually after the addition of amino acid, whereas in the case of Tyr, Phe and His, only the absorbance of 225 nm band was decreased and not the 280 nm band. The decrease in the absorbance of 225 nm band follows the order, $\text{Trp} > \text{Tyr} > \text{Phe} > \text{His}$. The changes observed in the titration of Trp with L_2 were attributed to the interaction of Trp side chain with triazole moiety of the ligand. This was further supported by $^1\text{H-NMR}$ titration carried out with Trp. $^1\text{H NMR}$ studies showed marginal change in the triazole proton of L_2 . Thus, L_2 can be used as a selective receptor for aromatic amino acids among the naturally occurring amino acids.

Lower rim 1,3-diamido calix[4]arene conjugates of phenylalanine (L_3) showed selectivity towards Asp and Glu among the 20 naturally occurring amino acids studied by fluorescence enhancement of the 312 nm band.¹⁸ The enhancement is 3.5 to 4.0 fold in methanol, and it is 5.5 to 6.0 fold in 1:1 aqueous acetonitrile. Titration of L_3 with the totally esterified Asp/Glu, *viz.*, $\text{Asp}(\text{OBz})_2$ or $\text{Glu}(\text{OMe})_2$, exhibited no change in the fluorescence intensity during the titration. These studies suggest the involvement of the side chain carboxylic group in the interaction and not the C^α bound groups. Titrations with various control molecules showed that the carboxylic groups and amide arms of the conjugates are necessary for the selective recognition of Asp and Glu among the naturally occurring amino acids. All these were further supported by several spectroscopic and microscopic studies. Thus L_3 can be used as selective receptor towards Asp and Glu among the 20 amino acids studied.

Protein recognition by the zinc complex, $[\text{ZnL}_1]$: $[\text{ZnL}_1]$ recognizes amino acids based on their protonation, chelating ability and $\pi \dots \pi$ interaction, and the present studies have been extended to proteins of α -helical (BSA, HSA) as well as β -sheet (Jacalin and PNA) structures. The titration of $[\text{ZnL}_1]$ with BSA exhibited a linear decrease in the intrinsic Trp emission observed

at ~344 nm. The emission from $[\text{ZnL}_1]$ observed at ~450 nm has also been found to be quenched.³⁰ Similar behaviour has also been observed even with lectins, *viz.*, jacalin and PNA, the extent of decrease in the intrinsic fluorescence emission of Trp of these lectins has been found to be less when compared to that of BSA. These results were suggestive of de-chelation of Zn^{2+} from $[\text{ZnL}_1]$, in addition to some changes in the conformation of the protein that brings the Trp residues more exposed. The de-chelation of Zn^{2+} was further supported by absorption studies carried out with proteins. The conformational changes occurred in the protein by the interaction of $[\text{ZnL}_1]$ have been established based on CD spectroscopy. These studies exhibited considerable changes in the ellipticity during the interaction. The secondary structural changes occurred were found to be more in the case of α -helical protein than the β -sheet ones. The aggregation of the protein when treated with $[\text{ZnL}_1]$ follows a trend, *viz.*, PNA < BSA < jacalin < HSA which is almost a trend reverse to that observed for de-metallation. Thus $[\text{ZnL}_1]$ is not only capable of recognizing the amino acids, it is also capable of interacting and recognizing the corresponding amino acid residues present in α -helical proteins, *viz.*, BSA and HSA, as well as β -sheet lectins, *viz.*, jacalin and PNA.

Aromatic moiety recognition: Aromatic hydrocarbons are widespread organic environmental pollutants and are known to be hazardous for human kind because of their carcinogenic and mutagenic properties. Owing to their lipophilic nature, their solubility in water is very poor and hence they persist in the environment for a longer period. So it is important to find effective receptors to detect these even at low concentrations. Thus, lower rim 1,3-dinaphthalimide conjugate of calix[4]arene (L_4) (Figure 11) has been synthesized and studied for the recognition of aromatic hydrocarbons by fluorescence and UV-visible spectroscopy. The fluorescence of L_4 is quenched upon the addition of the guest species. The quenching is higher in the case of the guests possessing aromatic moiety, and follows a trend, pyrenaldehyde >> Glu-2-AI \approx 9-anthraldehyde >> 2-hydroxynaphthaldehyde

> Glu-2-NI > naphthaldehyde \approx salicylaldehyde \approx Glu-2-SI \geq substituted phenyl derivatives as well some un-substituted aromatic molecules.³¹ Hence, the extent of quenching is dependent on both the ring size as well as the nature of the substituent present. Thus for the detection, at least a naphthyl moiety and a polar group are required, whereas the anthracenyl and higher aromatic hydrocarbons are recognized to almost equal extent.

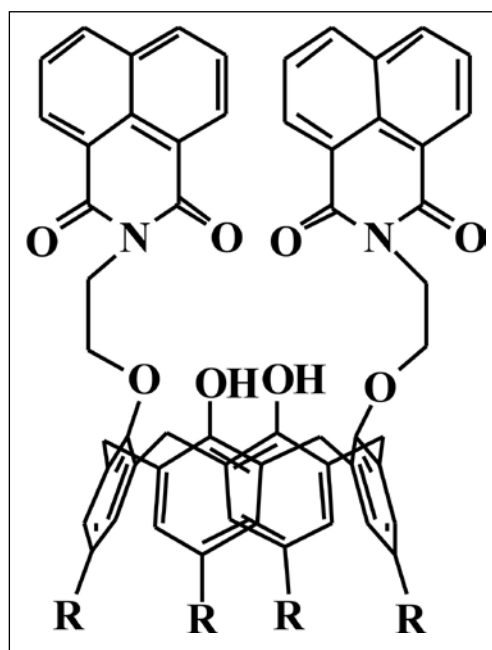


Figure 11. Lower rim 1,3-dinaphthalimide conjugate of calix[4]arene (L_4).

Modeling the receptor...guest complexes:

Several calix[4]arene derivatives have been reported in the literature and their ion and molecular recognition properties were studied. For the past several years, our group has been involved in synthesizing several lower rim modified calix[4]arene derivatives and their ion and molecular recognition properties were studied by using several spectroscopic and microscopic techniques.³² Hence, in order to show the proposed species of recognition, computational modeling has been carried out between calix[4]arene derivatives and guest the molecules (metal and anions). Computational modeling has been carried out starting from semi empirical followed by *ab initio* and then by density

functional theories. The coordination geometries around the metal centre and conformational changes in the arms have been correlated with the literature reports. The calix[4]arene derivatives used in the present course of studies are shown below. As can be seen from the figure 12, the conjugates of calix[4]arene studied were large in the size and the total number of atoms range from 150 to 200. All these derivatives, except the sulphonato calix[4]arene, possess t-butyl moieties at their upper rim as well as on the derivatized lower rim arms, while the recognition centre is quite far away from the t-butyl groups. Therefore, replacing these t-butyl groups with hydrogen atoms reduces the number of atoms to be used in the computational studies. This indeed saves the computational times and does not change any conformational features of the

arms which provide binding core. Hence, the computational calculations were carried out by using such truncated conjugates of calix[4]arene. All the receptor systems, viz., L_5 , L_6 , L_7 , L_8 and L_9 , were subjected to truncation and the resultant conjugates (L_5' , L_6' , L_7' , L_8' and L_9') were used for the modeling of metal ions and anion complexes. The calculations carried out with the truncated systems (without using any guest species) do not show any conformational changes in the arms as compared to its crystal structures and further the cone conformation is maintained throughout.

All the computations carried out and reported in this paper have adopted a cascade methodology. In this approach, the initial structures for the modeling have been obtained from the crystal structures of the receptor system. The initial structures were optimized in

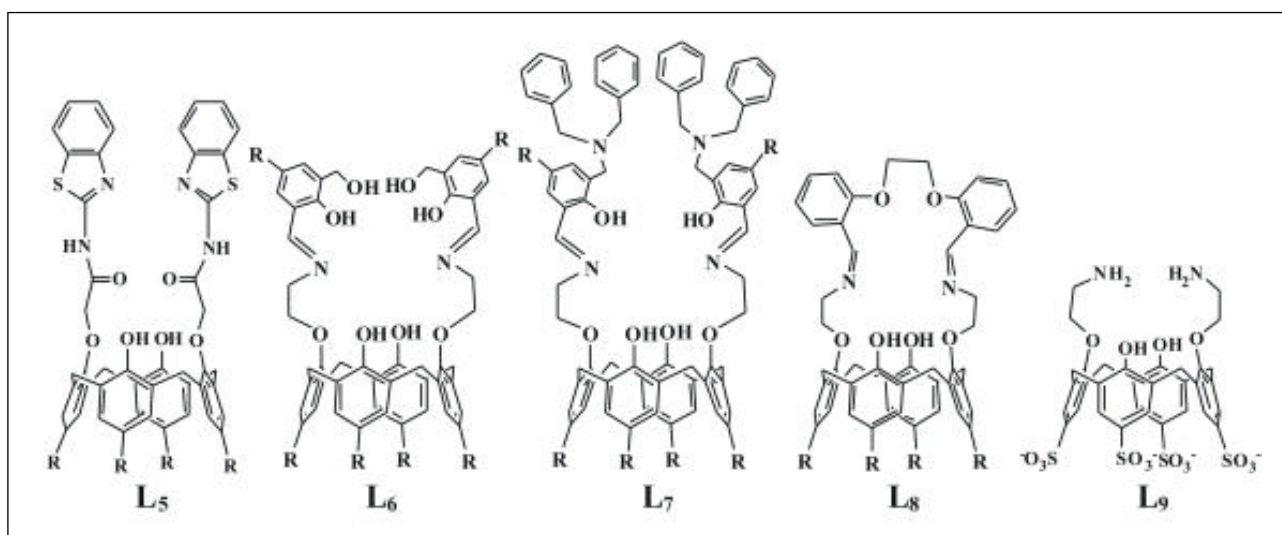


Figure 12. Schematic representation of calix[4]arene conjugates. R = tert-butyl

semi-empirical methodology, and the outcome of this has been taken to the next higher level of calculations. Such computations are carried out in a cascade manner by going through, AM1 or PM3 \rightarrow HF/STO-3G \rightarrow HF/3-21G \rightarrow HF/6-31G \rightarrow B3LYP/3-21G \rightarrow B3LYP/6-31G etc. The modeling of metal ion complexes has been carried out by using additional polarization function. All the computations carried out between the conjugates of calix[4]arene and metal ions were performed in the same fashion, unless otherwise mentioned.

Comparison of the binding cores: The species of recognition has been computationally modeled by a cascade fashion from semi-empirical to DFT level as mentioned above. Important features of the species of recognition such as the structures of the metal complexes and their coordination geometries are given in Figure 13 for appropriate comparison. As can be seen from the figure, the binding cores vary among these from N_2O_2 to NO_2S_2 , N_2O_2X , N_2O_4X , NO_4 (X = coordination site which is vacant), and the geometries vary from distorted tetrahedron (Td) to distorted square planar (SP) to

distorted trigonal bipyramidal (TBP) to distorted square pyramidal to distorted octahedral (O_h) to capped octahedral with one vacant site(s). Thus, large variations were found both in the binding cores as well as in the geometries which in turn depends on the conformational mobility of the arms.

Most of these geometries were found to be distorted owing to the presence of wide range of angles in the coordination sphere. The distorted geometries observed from the present computations match very well with some of the literature reported metal complexes. The Cu^{2+} complex of L_5 exhibits distorted trigonal bipyramidal geometry wherein each arm of L_5 acts as bidentate in filling a total of four coordinations, and the fifth coordination comes from the acetonitrile, resulting in a NO_2S_2 binding core. Even the species of recognition of L_6 with Zn^{2+}

having N_2O_2 core provides a better fit to a trigonal bipyramidal with one trigonal center being vacant. The Cd^{2+} complex of the same receptor, L_6 exhibits N_2O_4 binding core to result in a capped octahedral geometry with one vacant site. While the Zn^{2+} binds at the Schiff's base region, the Cd^{2+} binds primarily at the lower rim phenolic oxygen atoms. The mono and dinuclear Zn^{2+} complexes of L_7 exhibits N_2O_2 binding core to result in a distorted tetrahedral geometry. However, the mononuclear Fe^{2+} and Cu^{2+} complexes of the same receptor exhibited distorted square planar geometry with binding core being the same, the dinuclear complex of Cu^{2+} exhibits distorted square pyramidal geometry and the Fe^{2+} complex showed distorted octahedral geometry with one chloride as bridging ligand. All these studies seem to suggest that selective preference of one metal ion over the other depends on the binding core as well the conformational mobility of the arms attached.

Comparison of the conformational changes appeared in the arms: Comparison of the computational results obtained for the metal ion complexes with that of the original conjugate clearly indicated that there are no conformational changes observed in the arene core of the calix[4] arene moiety. Thus the conformational changes were only restricted to the arms and these changes were observed in the presence of metal ions, where as the arene core maintains a cone conformation before as well as after binding of metal ion. Hence, only the arm conformations were compared between the receptor and the corresponding metal ion complexes. Such conformational changes observed in the arms in presence of metal ions were found to be necessary to provide appropriate binding core for the incoming ion.

In L_5 , no conformational changes in the arms were observed upon binding with Cu^{2+} as compared to that of uncomplexed receptor. In the case of Zn^{2+} and Cd^{2+} complexes of L_6 , a series of conformational changes were observed in the arms. On going from $L_6' \rightarrow [Zn(L_6')] \rightarrow [Cd(L_6')]$, the conformations of the arms vary progressively to accommodate the corresponding metal ion by providing appropriate coordination. The major

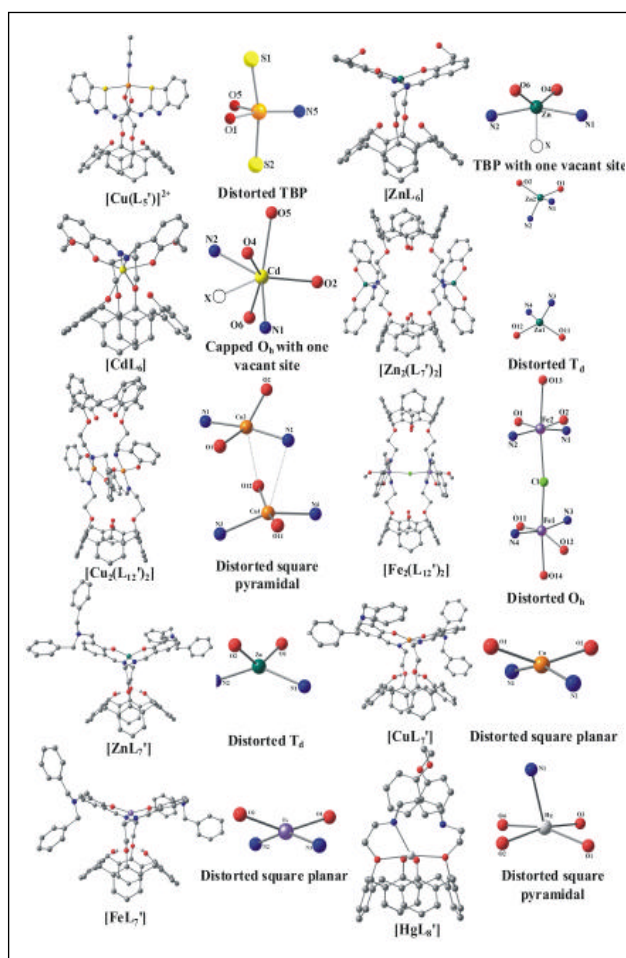


Figure 13. Species of ion recognition of calix[4]arene conjugates and the corresponding coordination geometries.

conformational change was observed with the C-N bond near the metal binding core. The dinuclear Cu^{2+} complex of L_7 , also undergone series of conformational changes in the arms, whereas in the case of Zn^{2+} and Fe^{2+} complexes, no changes were observed in the conformations of the arms. In case of mono nuclear complexes, only marginal changes were observed in the conformations of the Fe^{2+} complex. The Hg^{2+} complex of L_8 showed a series of conformational changes in the arms. The major conformational changes were observed in the arms of L_8 by bringing the two phenyl groups of the arms closer to each other. The 1:1 complex of L_9' with HSO_3^- showed two N-H...O hydrogen bond interactions between bisulfite anion and L_9' . The species of aggregation has been further modeled by taking two 1:1 complexes of $[\text{L}_9' \cdot \text{HSO}_3^-]$ and optimizing in PM3 using HYPERCHEM. The optimized structure showed the formation of dimer through the H-bond interactions between the two HSO_3^- ions of these 1:1 complexes. During the modeling of the aggregation, two of the existing hydrogen bonds were broken and a new hydrogen bond was formed between the bisulfite anions.

Conclusions

Thus, in the present paper the molecular recognition properties of several calix[4]arene conjugates have been described. The calix[4]arene has been functionalized with a number of functional moieties that would extend the binding centers. All these conjugates were extensively characterized by a variety of techniques. The molecular recognition (amino acid and protein binding) properties of all these derivatives have been explored. The recognition properties of these derivatives have been found to change abruptly upon bringing slight modification in the ligating groups. Amino acid recognition properties of several derivatives have been explored. Upon doing so, recognition of several naturally occurring amino acids have been achieved and this includes, the sensing of amino acids by metal complexes of conjugates of calix[4]arene based on their protonation and chelating ability, recognition of aromatic amino acids by $\pi \dots \pi$ interaction ability. Further the protein binding

aspects of several carbohydrate as well as metal ion complexes of calix[4]arene conjugates was studied by variety of spectroscopic techniques. Therefore, several synthetic receptors based on the calix[4]arene have been successfully designed and studied for the recognition of naturally occurring amino acids as well as proteins. Several metal ion and anion complexes of calix[4]arene conjugates have been modeled by DFT computational calculations and found that the conformational mobility and the binding core are critical for the preferential binding of one metal ion over the other. Thus, the present article provide features of importance of calix[4]arene scaffolds in the molecular recognition with several new contributions made in the field of molecular recognition and bio-inorganic chemistry. Based on all these studies, it can be said that the selectivity can be achieved by appropriately designing the molecules to have specific and effective interactions with the guest species.

Acknowledgements

CPR acknowledges the financial support by DST, CSIR and BRNS-DAE. JPC acknowledges CSIR for the research fellowship.

References

1. Samuel H. G. *Chem. Rev.* **1997**, 97, 1231.
2. (a) Sears, P.; Wong, C.-H. *Cell. Mol. Life Sci.* **1998**, 54, 223. (b) Gabius, H. J.; Andre, S.; Kaltner, H.; Siebert, H. C. *Biochim. Biophys. Acta* **2002**, 1572, 165. (c) Gustafsdottir, S. M.; Schlingemann, J.; Rada-Iglesias, A.; Schallmeiner, E.; Kamali-Moghaddam M.; Wadelius, C.; Landegren, U. *Proc. Nat. Acad. Sci. U.S.A.* **2007**, 104, 3067. (d) Stites, W. E. *Chem. Rev.* **1997**, 97, 1233.
3. (a) Pedersen, C. J. *J. Am. Chem. Soc.* **1967**, 89, 7017. (b) Pedersen, C. J. *J. Am. Chem. Soc.* **1967**, 89, 2495.
4. (a) Cram, D. J. *Angew. Chem.* **1988**, 100, 1041; (b) Lehn, J.-M. *Angew. Chem.* **1988**, 100, 91. (c) Pedersen, C. J. *Angew. Chem.* **1988**, 100, 1053.
5. (a) Casnati, A.; Fabbi, M.; Pelizzi, N.; Pochini, A.; Sansone, F.; Ungaro, R.; Modugno, E. D.; Tarzia, G. *Bioorg. & Medicinal Chem. Lett.* **1996**, 6, 2699. (b) Frish, L.; Sansone, F.; Casnati, A.; Ungaro, R.; Cohen, Y. *J. Org. Chem.* **2000**, 65, 5026.
6. (a) Casnati, A.; Sansone, F.; Ungaro, R. *Accounts Chem. Res.* **2003**, 36, 246. (b) Sansone, F.; Chierici, E.; Casnati, A.; Ungaro, R. *Org. Biomol. Chem.* **2003**, 1802.
7. Shun, H. L.; Chun, W. Y.; Jin, G. X. *Chem. Commun.* **2005**, 450.
8. (a) Joseph, R.; Ramanujam, B.; Acharya, A.; Rao, C. P. *J. Org. Chem.* **2009**, 74, 8181. (b) Joseph, R.; Chinta, J. P.; Rao, C. P. *J. Org. Chem.* **2010**, 75, 3387.
9. Diederich, F. *J. Chem. Ed.* **1990**, 67, 813.

10. Qing, G.-y.; He, Y.-b.; Wang, F.; Qin, H.-j.; Hu, C.-g.; Yang, X. *Eur. J. Org. Chem.* **2007**, 1768.
11. Liu, S., He, Y., Qing, G., Xu, K., Qin, H. *Tetrahedron: Asymmetry* **2005**, 16, 1527. Liu, S. Y.; Fang, L.; He, Y. B.; Chan, W. H.; Yeung, K. T.; Cheng, Y. K.; Yang, R. H. *Org. Lett.* **2005**, 7, 5825.
12. Sansone, F.; Barbosa, S.; Casnati, A.; Sciotto, D.; Ungaro, R. *Tetrahedron Lett.* **1999**, 40, 4741.
13. Lazzarotto, M.; Sansone, F.; Baldini, L.; Casnati, A.; Cozzini, P.; Ungaro, R. *Eur. J. Org. Chem.* **2001**, 595.
14. Sansone, F.; Baldini, L.; Casnati, A.; Lazzarotto, M.; Ugozzoli, F.; Ungaro, R. *Proc. Natl. Acad. Sci. U.S.A.* **2002**, 99, 4842.
15. Lu, J. Q.; Zhang, L.; Sun, T. Q.; Wang, G. X.; Wu, L. Y. *Chin. Chem. Lett.* **2006**, 17, 575.
16. Lazar, A. N.; Danylyuk, O.; Suwinska, K.; Coleman, A. W. *J. Mol. Str.* **2006**, 825, 20.
17. Perret, F.; Morel-Desrosiers, N.; Coleman, A. W. *J. Supramol. Chem.* **2002**, 2, 533.
18. Acharya, A.; Ramanujam, B.; Chinta, J. P.; Rao, C. P. *J. Org. Chem.* **2011**, 76, 127.
19. Douteau-Guevel, N.; Coleman, A. W.; Morel, J. -P.; Morel Desrosiers, N. *J. Phys. Org. Chem.* **1998**, 11, 693
20. Douteau-Guevel, N.; Coleman, A. W.; Morel, J. -P.; Morel Desrosiers, N. *J. Chem. Soc. Perkin Trans.2* **1999**, 3, 629.
21. Douteau-Guével, N., Perret, F., Coleman, A. W., Morel, J. -P., Morel Desrosiers, N. *J. Chem. Soc. Perkin Trans.2* **2002**, 3, 524.
22. Da Silva, E.; Coleman, A. W. *Tetrahedron* **2003**, 59, 7357.
23. (a) Arena, G.; Casnati, A.; Contino, A.; Magri, A.; Sansone, F.; Sciotto, D.; Ungaro, R. *Org. Biomol. Chem.* **2006**, 4, 243. (b) Arena, G.; Contino, A.; Gulino, F. G.; Magri, A.; Sansone, F.; Sciotto, D.; Ungaro, R. *Tetrahedron Lett.* **1999**, 40, 1597.
24. Selkti, M.; Tomas, A.; Coleman, A. W.; Douteau-Guevel, N.; Nicolis, I.; Villain, F.; de Rango, C. *Chem. Commun.* **2000**, 161.
25. (a) Atwood, J. L.; Ness, T.; Nichols, P. J.; Raston, C. L. *Cryst. Growth Des.* **2002**, 2, 171. (b) Nichols, P. J.; Raston, C. L. *Dalton Trans.* **2003**, 2923.
26. Lazar, A.; Da Silva, E.; Navaza, A.; Barbey, C.; Coleman, A. W. *Chem. Commun.* **2004**, 2162.
27. Li, H.; Wang, X. *Photochem. Photobiol. Sci.* **2008**, 7, 694.
28. Xiong, D.; Chen, M.; Li, H. *Chem. Commun.* **2008**, 880.
29. Bakrici, H.; Koner, A. L.; Dickman, M. H.; Kortz, U.; Nau, W. M. *Angew. Chem., Int. Ed.* **2006**, 45, 7400.
30. Chinta, J. P.; Acharya, A.; Kumar, A.; Rao, C. P. *J. Phys. Chem. B* **2009**, 113, 12075.
31. Bandela, A.; Chinta, J. P.; Hinge, V. K.; Dikundwar, A. G.; Guru Row, T. N.; Rao, C. P. *J. Org. Chem.* **2011**, 76, 1742.
32. Joseph, R. and Rao, C. P. *Chem. Rev.* **2011**, 111, 4658.



Jugun Prakash Chinta, born in Andhra Pradesh, India (1982), received his Bachelor's degree (2002) and Master's degree (2004) from Andhra University, Visakhapatnam, Andhra Pradesh. He received his doctoral degree from the Indian Institute of Technology Bombay in 2011 under the supervision of Prof. C. P. Rao. His graduate research has focus on the synthesis, characterization and ion and molecular recognition properties of carbohydrate, calix[4]arene conjugates and small molecular metal complexes by experimental and computational methods. Currently he is working as a research associate in the same research group. His research interests are in the area of supramolecular chemistry, molecular recognition and bioinorganic chemistry.



Chebrolu Pulla Rao obtained his Master's degree (1977) from Indian Institute of Technology Madras, and Ph.D. degree (1982) from Indian Institute of Science Bangalore under the joint supervision of Professors C.N.R. Rao and P. Balaram. After one year of Research Associateship with Prof. C.N.R. Rao, he had shifted to the research groups of Prof. R.H. Holm at Harvard University (1983-85) followed by Prof. S.J. Lippard (1986-87) at Massachusetts Institute of Technology as postdoctoral fellow. Since 1988, he has been on the Chemistry faculty at Indian Institute of Technology Bombay and has been a full Professor since 1998. His research interests are broad-based and well extend into the areas of bioinorganic chemistry including metallation of proteins, and glyco-targeting, all using small molecular model systems (viz., calixarenes & carbohydrates) as well as proteins and enzymes, where some of these resulted in the development of ion and molecular sensors as well as materials.

Role of Crown Ethers and Calixarenes in Radioactive Waste Remediation

P.K. Mohapatra

Radiochemistry Division, Bhabha Atomic Research Centre, Mumbai-400085

Abstract

Radioactive waste management involves separation of fission product nuclides such as ^{137}Cs and ^{90}Sr which contribute to major radiation and heat emanating from the high level waste. Macrocyclic reagents such as crown ethers and calix-crowns have been found to be quite efficient for the separation of these radionuclides from the complex waste matrices. This article gives a brief account of the separation chemistry of these elements using calix-crowns and crown ethers using techniques such as solvent extraction and liquid membrane.

1. Introduction

The radioactivity in the HLW is primarily from the fission products ^{137}Cs ($t_{1/2}$:30.1 y) and ^{90}Sr ($t_{1/2}$:28.5y). These radionuclides are produced by the fission of uranium or plutonium in a relatively high yield and they pose a serious radiation hazard to health and environment. Therefore, a great interest was devoted over the last decade to develop separation technologies for removal and safe disposal of ^{137}Cs and ^{90}Sr from the nuclear waste solutions. Removal of ^{137}Cs and ^{90}Sr from nuclear waste facilitates not only the safe and less expensive disposal of HLW in deep geological repositories as vitrified mass, the separated radionuclides also have potential use as alternative to ^{60}Co in irradiators (^{137}Cs) and as power sources (^{90}Sr) [1]. Several separation methods have been used for the removal of ^{137}Cs and ^{90}Sr from nuclear wastes which have been reviewed by Schulz and Bray [2]. While the solvent extraction methods of ^{137}Cs separation use crown ethers, calix-crowns and dicarbolides, the ion-exchange methods are based on the use of zeolites, AMP (ammonium molybdophosphate), CST (crystalline silicotungstate), resorcinol formaldehyde resins, hexacyanoferrates, etc. [2]. On the other hand, ^{90}Sr from acidic wastes have been mainly removed using crown ether based solvent extraction methods in addition to several precipitation methods [2]. The present review deals with the use of macrocyclic ligands such as crown ethers and calix-crowns for the removal of ^{137}Cs and ^{90}Sr from nuclear wastes.

1. Cesium extraction

Cesium extraction from acidic wastes using macrocyclic ligands have been mainly divided into two parts viz. those with crown ethers and calix-crowns. While both these ligands have been based on size selective extraction based on the matching between the cavity size of the extractant molecule and the metal ion ionic radius, calix-crown ligands have shown much higher extraction efficiency and selectivity. There have been excellent review articles on this [3,4].

1.1 Crown ethers

From size considerations, 21-membered crown ethers have been suggested to be selective for Cs^+ ion. Though Cs^+ extraction from low pH or near neutral pH solutions have been reported using 21-crown-7 with picric acid or any such high molar volume organophilic anion, benzo substituted 18-membered crown ethers have been used by Davis et al. [5] for the extraction of ^{137}Cs from acidic feeds. Subsequently, Horwitz et al., have used di-*tert*-butyl-di-benzo-18-crown-6 (DTBB18C6) for selective Cs extraction from acidic wastes [6]. However, these reagents, though show selectivity, have displayed low extraction efficiency limiting their use for large scale applications. Thus, the focus has shifted to the calix-crown-6 ligands which have shown both high extraction efficiency and selectivity.

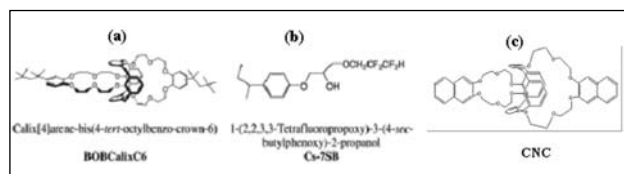


Fig. 1: Structural formulae of (a) BOBCalixC6 and (b) Cs-7SB (c) CNC

Table 1: Typical composition of the Savanna River Site waste.

| Component | Molarity | Component | Molarity |
|--------------------------------|-------------------------|-------------------------------------|----------|
| Al ³⁺ | 0.40 | F ⁻ | 0.050 |
| Na ⁺ | 7.0 | NO ₂ ⁻ | 1.0 |
| K ⁺ | 0.020 | NO ₃ ⁻ | 2.7 |
| Cs ⁺ | 7.00 × 10 ⁻⁴ | OH ⁻ (free) ^b | 1.9 |
| Cl ⁻ | 0.10 | OH ⁻ (total) | 3.5 |
| CO ₃ ²⁻ | 0.20 | SO ₄ ²⁻ | 0.22 |
| CrO ₄ ²⁻ | 0.015 | | |

2. Calix-crown Ligands:

Calix[4]-crown ligands possess high extractive strength for cesium, and their potential use in waste remediation technologies for the removal of ¹³⁷Cs from both acidic and alkaline media has been intensively investigated. One such calix-crown in particular, calix[4]arene-bis(4-*tert*-octylbenzo-crown-6) (BOBCalixC6, Fig. 1(a)) is currently being used as an effective cesium extractant in the caustic-side solvent extraction (CSSX) process developed for separating cesium from alkaline high-level nuclear wastes such as those stored at the US Department of Energy's Savannah River Site (SRS)[7]. A typical composition of the SRS waste is given in Table 1.

The CSSX solvent in its original formulation contained BOBCalixC6 at 10 mM, the alcohol modifier 1-(2,2,3,3-tetrafluoropropoxy)-3-(4-*sec*-butylphenoxy)-2-propanol (Fig. 1(b)) at 0.5 M, and tri-*n*-octylamine (TOA) at 1 mM in Isopar L diluent. The modifier plays a critical role in boosting both the extraction power of BOBCalixC6 and the solubility of BOBCalixC6 and its complexes in the diluent. Used at a low concentration, TOA stabilizes stripping performance. Whereas this concentration of BOBCalixC6 is suitable for removing cesium from a wide variety of waste streams, it is anticipated that there will be potential applications where a higher concentration of the cesium extractant would be desirable, particularly for waste streams with significantly higher concentrations of potassium that exist in the Savannah River waste (<50 mM).

Dozol et al. [8], have synthesized several calix-crown ligands viz. calix[4]arene-bis-crown-5, calix[4]arene-bis-crown-6, calix[4]arene-bis(1,2-benzo-crown-6), calix[4]arene bis(1,2-naphtho-crown-6) and calix[4]arene-bis-crown-7, etc. The calix-crowns with crown-5 and crown-7 groups were poor extractants of Cs⁺ while those with crown-6 groups had both superior extraction as well as selectivity properties (Table 2). Their work involved *ortho*-nitrophenyl hexyl ether as the organic diluent. Several calix-crown ligands were also evaluated at Radiochemistry Division, BARC for Cs uptake from feeds containing wide ranging acidities. These extracts were found to

Table 2: Distribution coefficients of Cs and Na and the separation factor (D_{Cs}/D_{Na}) values as obtained using 5x10⁻⁴ M metal nitrates in 1 M HNO₃. Organic diluent: *ortho*-nitrophenyl hexyl ether

| Extractant | D _{Na} | D _{Cs} | S.F. (D _{Cs} /D _{Na}) |
|--|----------------------|--------------------|--|
| Calix[4]arene-dipropoxy-crown-6 | 2x10 ⁻³ | 19.5 | 9750 |
| Calix[4]arene-diisopropoxy-crown-6 | <10 ⁻³ | 28.5 | >28,500 |
| Calix[4]arene-di- <i>n</i> -octyloxy-crown-6 | <10 ⁻³ | 33 | >33,000 |
| Calix[4]arene-dimethoxy-crown-7 | 4x10 ⁻³ | 7x10 ⁻³ | 1.75 |
| Calix[4]arene-bis-crown-5 | 2x10 ⁻³ | 0.5 | 250 |
| Calix[4]arene-bis-crown-6 | 1.3x10 ⁻² | 19.5 | 1500 |
| Calix[4]arene-bis-crown-7 | <10 ⁻³ | 0.3 | >300 |
| Calix[4]arene-bis-naphthyl-crown-6 | <10 ⁻³ | 29.5 | >29,500 |
| <i>n</i> -Decylbenzo-21-crown-7 | 1.2x10 ⁻³ | 0.3 | 250 |

be very efficient extractants for Cs(I) as evident from the high D values obtained with relatively low concentration ($< \text{mM}$) of the ligand [9,10]. For an aqueous phase Cs concentration of 1 g/L (in 3 M HNO_3), $>99.5\%$ extraction is possible using 3 contacts (volume ratio of 1) when the organic phase contained 0.01M calix-crown in nitrobenzene. Near quantitative extraction was also found possible from simulated HLW solutions. The results sound encouraging.

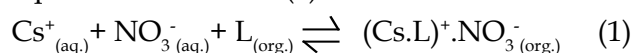
Table 3: Comparison of distribution data of Cs using calix-crowns (0.01 M) and crown ethers (0.1 M) in organic diluents at 1 M HNO_3

| Ligand | D_{Cs} | Ligand | D_{Cs} |
|--------------------------------------|---------------------------------------|--|---------------------------------------|
| Calix[4]arene-bis-crown-5 | 0.5 ^a | Calix[4]arene-bis(1,2-naphtho-crown-6) | 29.5 ^a , 27.5 ^b |
| Calix[4]arene-bis-crown-6 | 19.5 ^a , 5.5 ^b | Di-tert-butylbenzo18crown6 | 0.56 ^c |
| Calix[4]arene-bis(1,2-benzo-crown-6) | 32.5 ^a , 28.5 ^b | BOBCalixC6 | 10 ^d |

Note: ^a: diluent: *ortho*-nitrophenyl hexyl ether; ^b: $9.8 \times 10^{-3} \text{ M}$ in nitrobenzene; ^c: aq. phase: 3 M HNO_3 ; organic phase: 0.1 M ligand in nitrobenzene; ^d: diluent: Isopar L

Work initiated at Radichemistry Division, BARC is aimed at developing methods for Cs extraction using various modified diluents. Though nitrobenzene solutions of the calix[4]arene-crown-6 ligands have shown very high distribution coefficients for Cs(I) from acidic medium, their stripping was not possible using distilled water. On the other hand, 0.4% Alamine 336, when added to the organic phase, resulted in near quantitative stripping of Cs(I). Due to the toxic effects of nitrobenzene, a modified diluent system containing 50% toluene + 50% nitrobenzene was used for Cs(I) extraction from acidic feeds [10]. Alternatively, a mixture of NPOE (2-nitro-phenyloctylether) and n-dodecane was found to extract Cs(I) from acidic feeds with reasonably high distribution coefficient values.

The D_{Cs} values were determined for SHLW (simulated high level waste) feeds at different acidities by the organic phase containing $2.5 \times 10^{-3} \text{ M}$ CNC + 0.4% Alamine 336 in 1:1 NB : toluene and the results show (Fig. 2) that the D_{Cs} value increased with HNO_3 concentration reaching to a maximum at 3M HNO_3 and decreased thereafter [10]. Initial increase in the D_{Cs} value was attributed to the increase in the nitrate concentration which facilitates the ion-pair formation as described by equilibrium reaction (1).



where L is the extractant. However, decrease in the D_{Cs} value beyond 4 M HNO_3 could be due to the strong interaction of hydronium ions (H_3O^+) with calixcrown ligand to form CNC-hydronium ion complex. In the light of literature and our earlier work with CNC, it appears

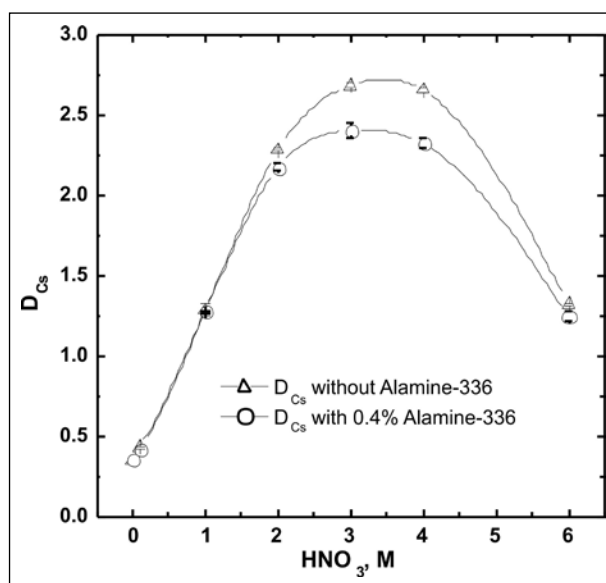


Fig. 2: Extraction profiles of Cs(I) from SHLW as a function of feed acidity using $2.5 \times 10^{-3} \text{ M}$ CNC

that at lower acidity, the extracted species was $[\text{CsL}]^+ \cdot [\text{NO}_3]^-$, while it was $[\text{HL} \cdot \text{H}_2\text{O}]^+ \cdot [\text{NO}_3]^-$ at higher acidity. On the other hand, addition of 0.4% (v/v) Alamine 336 has no significant effect on distribution of Cs(I) as D_{Cs} value at 3M HNO_3 were 2.4 and 2.6 with and without Alamine 336, respectively (Fig. 2). Higher distribution ratio of Cs(I) at moderate acidity (3-4 M HNO_3) suggested the potential application of the system for the recovery of radio cesium from HLW solutions.

Table 4: Composition of the high level waste used in the study involving diluted HLW

| Constituents | Concentration | Fission Products | Concentration (Ci/L) |
|------------------|---------------|-------------------|----------------------|
| HNO ₃ | 3.15 M | ¹⁴⁴ Ce | 22.3 |
| U | 10 g/L | ¹²⁵ Sb | 0.285 |
| Pu | 1.97 mg/L | ¹⁰⁶ Ru | 6.504 |
| Gross β | 125 Ci/L | ¹³⁷ Cs | 10.02 |
| Gross α | -- | ⁹⁵ Zr | -- |
| T.S. | 19.35 g/L | ⁹⁵ Nb | 0.018 |

Five stages were required for the quantitative extraction of Cs(I) from SHLW containing 0.32g/L Cs when O/A ratio was maintained at 0.5. Similarly, the quantitative stripping of Cs(I) could be achieved in two cycles with distilled water at O/A ratio of 2. The results demonstrated excellent potential of the solvent system for the recovery of Cs(I) from HLW. A test study carried out at FRD, BARC using actual HLW (composition given in Table 4) has indeed been shown to be quite selective for radio cesium separation. The recovered product (about 10 mCi) showed no contamination from associated gamma emitting radionuclides. The chemical and radiolytic stability of the solvent system has been studied and were found to be quite satisfactory up to 100 days and 100 MRad, respectively [11].

2. Strontium extraction

Similar to the extraction of Cs(I) by crown ethers, Sr(II) extraction by crown ethers also involved counter anions such as picrate. These reports involved the extraction of ion-pairs from alkaline or weakly acidic aqueous solutions [12]. A literature report [13] showed that substituted dicyclohexano-18-crown-6 ligands are selective extractants for Sr²⁺ ion from nitric acid medium when a complex diluent mixture of di-*n*-dodecyl naphthalene sulphonic acid (DNNS), tri-*n*-butyl phosphate (TBP), and kerosene was used. Horwitz et al. [14] have subsequently reported the extraction of radio-strontium from acidic radioactive wastes using di-*tert*-butyldicyclohexano-18-crown-6 (DTBCH18C6, Fig. 3(a)) in aliphatic alcohols such as 1-octanol

as the diluent. With decreasing alcohol alkyl chain length, the extraction of Sr(II) was found to

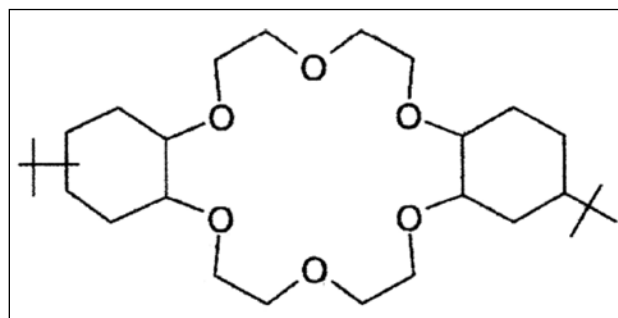
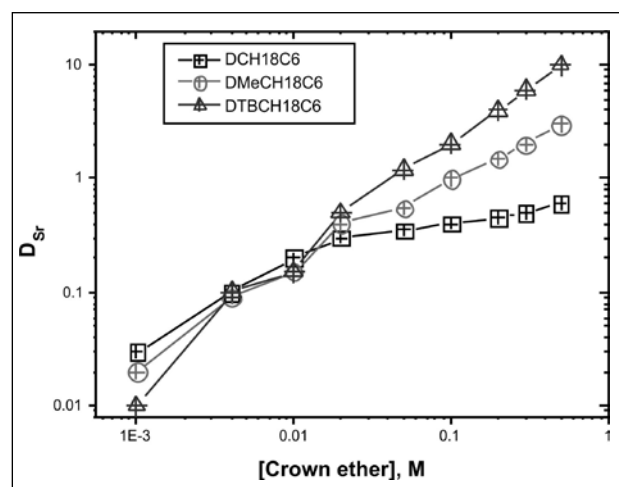


Fig. 3: (a) Structural formula of DTBCH18C6

Fig.3 (b) Extraction profiles of Sr(II) with crown ether concentration. Feed: 3 M HNO₃

increase though increasing aqueous solubility of the solvent was also seen to increase suggesting limited reusability of the solvent [14].

Table 5: Optimization of 1-octanol + toluene composition for Sr(II) extraction from HNO₃ medium (or SHLW) using 0.025 M DTBCH18C6

| Diluent composition | D _{Sr} | % Acid extraction |
|-----------------------------|-------------------|-------------------|
| 100% 1-octanol | 1.72 ^a | 21.2 ^a |
| 100% 1-octanol | 1.49 ^b | 21 ^b |
| 20% 1-octanol + 80%-toluene | 3.18 ^a | 6.4 ^a |
| 20% 1-octanol + 80%-toluene | 2.75 ^b | 5.7 ^b |

Note: ^a: studies with 3 M HNO₃; ^b: studies with SHLW

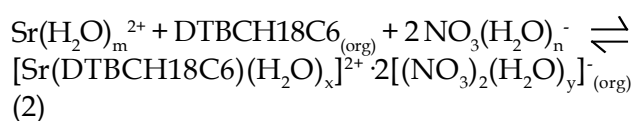
2.1 The SREX Process:

The SREX process as proposed by Horwitz et al., involved 1 M solution of DTBCH18C6 in 1-octanol. Fig. 3(b) suggests that when DCH18C6 or DMeCH18C6 were used in place of DTBCH18C6, the extraction decreases significantly at higher ligand concentrations as the deviation from the expected 'slope 1' line is attributed to aggregation of the ligands. They evaluated many aliphatic alcohols, ketones, carboxylic acids, and esters as diluents and showed a direct correlation of Sr extraction with their water uptake ability in the order: alcohol > carboxylic acid ~ ketone > ester [15]. We have reported that the extractant inventory can be drastically reduced by using a more polar diluent mixture, such as 80% 1-butanol and 20% 1-octanol [16]. All these studies have indicated that the extraction of Sr(II) is directly related with the water and acid uptake in the organic phase. This was also found to be one of the major limitations of the SREX process.

The effect of the organic diluent on Sr(II) extraction has been investigated and the results indicated that 80% toluene + 20% 1-octanol mixture gave not only higher Sr(II) extraction, but also extracted nitric acid to a much lower extent (Table 5).

It was also reported that this diluent composition was optimum as it gave higher D_{Sr}

as compared to the solvent containing 1-octanol alone. Table 5 gives the data on the extraction of Sr(II) from a simulated high level waste (SHLW). The D_{Sr} values with the diluent mixture were almost twice of those obtained with 1-octanol alone as the diluent. In all studies involving crown ethers, an increase in the D_{Sr} values with increasing crown ether concentration was observed. The dependence of Sr(II) extraction on crown ether concentration in the diluent mixture 20% 1-octanol + 80% toluene was close to 1 indicated the following extraction equilibrium was prevalent [17].



where $m > x$ and $n > y$. Fig. 4 shows the Sr(II) extraction profile as a function of varying feed acidity and the results suggested that the extraction curve of 20% toluene + 80% 1-octanol lies below that of 100% 1-octanol up to the feed acid concentration of 2.75 M HNO_3 , beyond which there was a reversal in the trend. This is of great relevance as using this solvent it is possible not only to favourably extract radio strontium from the HLW (which is usually at an acid concentration of 3-4 M), but also the stripping is more efficient when the mixed diluent solvent was used as against 1-octanol alone.

3. Liquid membrane separations

Though solvent extraction plays a pivotal role in majority of the separations involved in the nuclear fuel cycle both at the front as well as the back end, there are many drawbacks of the solvent extraction methods and with increasing concern for the environment, alternative separation methods will be employed for large scale separations in the nuclear industry as well. Two of the major drawbacks of the solvent extraction methods viz. third phase formation and phase disengagement can be overcome with the liquid membrane (LM) based separation methods as they involve non-dispersive mass transfer. LM systems also have distinct advantages over ion-exchange. Ion exchange beds are unsuitable for solutions containing large concentrations of dissolved solids as well as suspended matters whereas

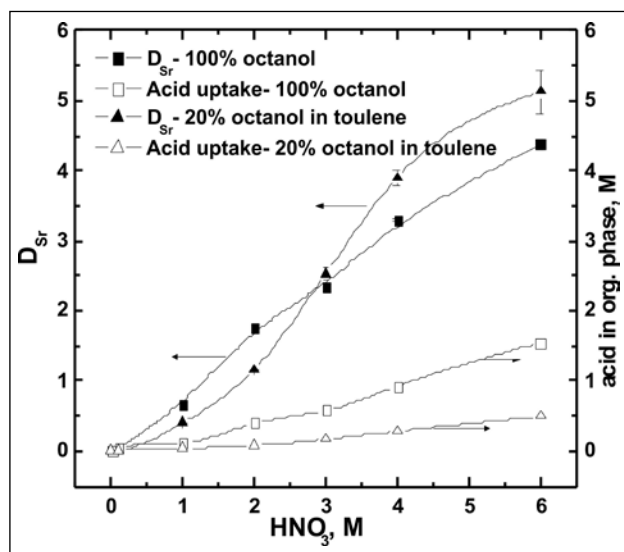


Fig. 4: Extraction profiles of Sr(II) in 100% 1-octanol and the mixed diluent solvent system as a function of feed nitric acid concentration

liquid membrane based separation methods can be quite useful for pre-concentration. Though LMs have a major disadvantage of stability, newer techniques such as polymer inclusion membrane (PIM) and Hollow Fibre Supported Liquid Membrane (HFSLM) have proved to be beneficial. Some recent studies on Cs(I) and Sr(II) separation using supported liquid membrane technique are presented below. A schematic of hollow fiber based separation system is shown in Fig. 5.

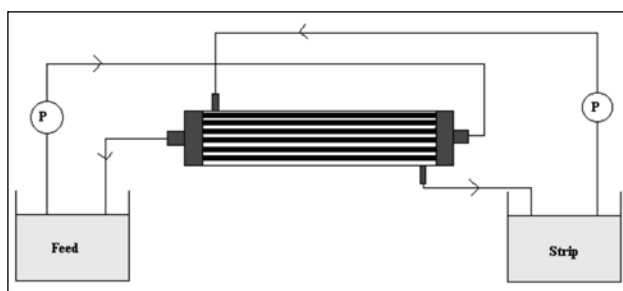


Fig. 5: Schematic presentation of the hollow fiber based liquid membrane separation system

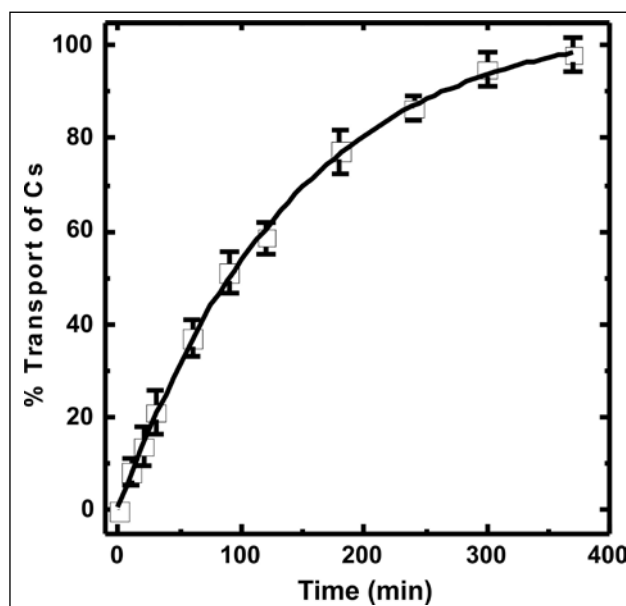


Fig. 6. Transport of Cs by HFSLM; Carrier: 1mM CNC in 80% (v/v) NPOE + 20% (v/v) *n*-dodecane + 0.4% Alamine 336; Feed: 0.5 L HNO₃ spiked with ¹³⁷Cs; Strip: Distilled water; Flow rate: 200mL/min

3.1 Recovery of Cs from high level waste

While attempting to develop alternative diluent system for Cs extraction from acidic feeds, NPOE was found to be quite good though the D_{Cs} values were somewhat lower as compared

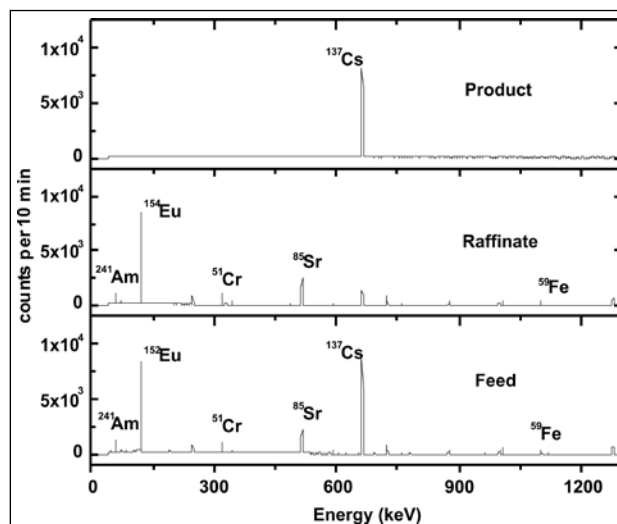


Fig. 7: Gamma ray spectra showing decontamination from other radionuclides in the product containing ¹³⁷Cs

to those obtained in nitrobenzene. On the other hand, the SLM transport studies on Cs(I) using CNC in NPOE as the carrier solvent were found to be quite efficient for the selective Cs recovery from acidic feeds. A mixture of 80% NPOE + 20% *n*-dodecane (dodecane was used to reduce viscosity) was optimized as a suitable diluent for CNC [18].

HFSLM transport of Cs(I) and other metal ions present in HLW (Cr, Fe, Sr, Am and Eu, etc.) was also investigated on 0.5 L scale using CNC from a feed solution of 3 M HNO₃ into a receiver phase of distilled water [19]. With 1 mM CNC as the carrier, quantitative transport of Cs(I) was achieved in 6 h (Fig. 6). The selectivity of Cs(I) over other radiotracers (²⁴¹Am, ¹⁵⁴Eu, ^{85,89}Sr, ⁵⁹Fe and ⁵¹Cr) was excellent with decontamination factors of ~100 with respect to various metal ions investigated in this study (Fig. 7) [19]. High decontamination factors as well as throughputs suggested possible application of the system for the recovery of radio-cesium from high level waste.

3.2 Transport of Sr(II) by di-*tert*-butyl-diyclohexano-18-crown-6

There are several studies on the transport behaviour of Sr(II) using liquid membrane based methods using various crown ether extractants. However, transport behaviour from acidic feeds,

which has relevance in HLW remediation is not studied much and those few reports are not promising enough for application. Dozol et al., have investigated the transport behaviour of Sr(II) from nitric acid medium using DCH18C6 in a number of mixed diluent systems as the carrier [20]. They have reported about 80% Sr transport using 0.5 M DCH18C6 in n-hexylbenzene containing 0.7 M isotridecanol in 24 h using a synthetic feed containing 1 M HNO₃, 3.4 M NaNO₃ and 0.6 M Mg(NO₃)₂ and reported considerable nitric acid transport. We have carried out several studies for the transport of Sr(II) from acidic feed solutions using supported liquid membranes containing DTBCH18C6 as the carrier [21]. >70% Sr(II) transport from 3 M HNO₃ was seen when 0.05 M DTBCH18C6 (Fig. 3 (a)) in 1-octanol was used as the carrier solvent which increased to >95% when the feed composition was changed to 0.5 M HNO₃ and 2 M Al(NO₃)₃. On the other hand, recent SLM study using a modified solvent system which resulted in much lower nitric acid extraction as compared to the SREX solvent, though indicated faster transport rates initially, resulted in back transport of Sr from the receiver to the feed side resulting in about 50-60% Sr transport after 3 h which remained constant thereafter even up to 24 h due to almost 50% acid transport [22]. Results from the SLM studies can be summarized as: quantitative transport of Sr from acidic feeds is a challenging task when crown ethers are used in the carrier solvent and HLW needs to be neutralized to bring down its acid strength and large concentrations of nitrate salts need to be added for any appreciable Sr(II) recovery from the waste using SLM methods. This is however, not acceptable as large volumes of secondary waste will be generated. It was thought of interest, therefore, to develop an SLM based methods which can quantitatively transport Sr(II) from acidic feed solutions without the addition of salts to the feed and at acidities comparable to the HLW (3-4 M HNO₃). In this context, our work has shown that a carrier solvent containing 0.1 M DTBCH18C6 in the diluent mixture 80% NPOE + 20% n-dodecane is capable of effecting quantitative Sr(II) transport from acidic feeds relevant from high level waste management point of view. Fig. 8 presents

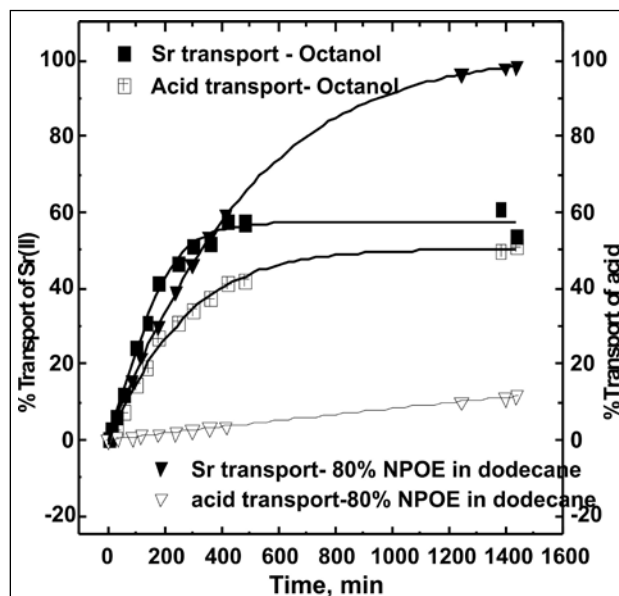


Fig. 8. Transport profiles of Sr(II) and nitric acid with the crown ether SLM system. Feed: 3M HNO₃; strip: distilled water, carrier: 0.1M DtBuCH18C6 in 80% NPOE + 20% n-dodecane

comparative transport profiles of the developed solvent system and the solvent used in a previous study which is similar to the SREX solvent.

7. Conclusions & perspectives

Macrocyclic ligands such as crown ether and calix-crowns are found to efficiently recover valuable fission product elements such as Cs and Sr from acidic wastes including HLW. SLM based methods have been found to be particularly promising as the reagent inventory could be drastically brought down. In view of the low flux in case of flat sheet supported liquid membranes, hollow fiber supported liquid membrane based separations have been found to be quite promising. One of the major obstacles, foreseen as this stage, has been the physical stability of the SLM which could be enhanced by the judicious use of diluents. Alternatively, emulsion liquid membrane (ELM) based separations can also be attempted.

Selective pre-concentration using liquid membranes may find use in the nuclear industry sooner than later. The low ligand inventory will not only reduce the cost of operation, but also can help in minimizing the secondary waste volumes. The major concern in prolonged use is

the radiation stability of the extractant / polymer. These can be alleviated by the use of grafted membranes and radiation resistant polymers.

References

- IAEA Technical Series No. 356.
- W.W. Schulz and L.A. Bray; Sep. Sci. Tech., 22 (1987) 191.
- Z. Asfari, S. Wenger and J. Vicens, 67 (1995) 1037.
- P. Thuery, M. Nierlich, V. Lamare, J.F. Dozol, Z. Asfari and J. Vicens, J. Incl. Phenom. Macrocyclic Chem., 36 (2000) 375.
- I. H. Gerow, J. E. Smith, Jr., M. W. Davis, Jr., Sep. Sci. Tech., 16(1981) 519.
- M. L. Dietz, E. P. Horwitz, S. Rhoads, R. Bartsch, J. Krzykawski, Solv. Extr. Ion. Exch., 14 (1996) 1.
- R.A. Leonard, C. Conner, M.W. Liberatore, J. Sedlet, S.B. Aase, G.F. Vandegriff, L.H. Delmau, P.V. Bonnesen, B.A. Moyer, Sep. Sci. Technol., 36(2001) 743.
- J.F. Dozol, N. Simon, V. Lamare, H. Rouquette, S. Eymard, B. Tournois, D. De Marc, R.M. Macias, Sep. Sci. Technol. 34(1999) 877.
- P.K. Mohapatra, S.A. Ansari, A. Sarkar, A. Bhattacharyya, V.K. Manchanda, Anal. Chim. Acta, 517 (2006) 308.
- D.R. Raut, P.K. Mohapatra, S.A. Ansari and V.K. Manchanda; Sep. Sci. Technol. , 44 (2009) 3664.
- D. R. Raut, P. K. Mohapatra and V. K. Manchanda; Des. Water Treat., 12 (2009)52.
- Y. Takeda, Bull. Chem. Soc. Japan, 52 (1979) 2501.
- I.H. Gerow, J.E. Smith, Jr., M.W. Davis, Jr., Sep. Sci. Tech., 16 (1981) 519.
- E.P. Horwitz, M.L. Dietz, M.L. and D.E. Fisher, Solv. Extr. Ion Exch., 8 (1990) 557.
- E.P. Horwitz, M.L. Dietz, and D.E. Fisher, Solv. Extr. Ion Exch., 9 (1991) 1.
- A. Kumar, P.K. Mohapatra, P.N. Pathak, V.K. Manchanda, Talanta, 45 (1997) 387.
- D.R. Raut, P.K. Mohapatra and V.K. Manchanda, Sep. Sci. Technol., 45(2010) 204.
- D.R. Raut, P.K. Mohapatra, S.A. Ansari and V.K. Manchanda, J. Membr. Sci., 310(2008)229.
- P. Kandwal, P.K. Mohapatra, S.A. Ansari and V.K. Manchanda, Radiochim. Acta, 98(2010)493.
- J.F. Dozol, J. Casa ans A.M. Sastre, Sep. Sci. Technol., 28 (1993) 2007.
- N. Rawat, P.K. Mohapatra, D.S. Lakshmi, A. Bhattacharyya and V.K. Manchanda, J. Membr. Sci., 275(2006)82.
- D.R. Raut, P.K. Mohapatra and V.K. Manchanda, Radiochim. Acta, 97(2009)565.



Dr. P. K. Mohapatra joined the Radiochemistry Division, B.A.R.C. in 1987 after completing his M.Sc. in Inorganic Chemistry from Utkal University and graduating from the 30th batch of the BARC Training School. He was awarded Ph.D. by Bombay University in 1994. Dr. Mohapatra carried out Post-Doctoral research work at University of Liege, Belgium under BOYSCAST Fellowship, DST (1998 - 1999) and University of Mainz, Germany, under Humboldt Fellowship (1999 - 2000) on MRI contrast agents and chemistry of transactinide elements, respectively. His research interests include separation studies of actinides and fission products using exotic reagents and novel separation techniques such as liquid membranes and supercritical fluid extraction. Dr. Mohapatra has to his credit over 160 publications in peer reviewed international journals and over 250 papers in Conferences / Symposia.

Functionalized Boron-dipyrrromethenes and their Applications in the Synthesis of New BODIPY Systems

Tamanna K. Khan and M. Ravikanth*

Department of Chemistry, Indian Institute of Technology, Powai, Mumbai 400076
Phone: 91-022-2576-7176; Fax: 91-022-2576-7152; E-mail: ravikanth@chem.iitb.ac.in

Abstract

4,4-Difluoro-boradiaza-s-indacenes (BODIPYs) are attractive fluorescent dyes because of their remarkable photophysical properties, such as high quantum yields, large absorption coefficients, narrow emission lines and high environmental stability. Therefore, they have widely used in almost every research field ranging from biology to materials chemistry. This has been stimulated tremendous interest in synthesis of new varieties of BODIPY and testing their potential for various applications. Recently our group is involved in the synthesis of functionalized BODIPYs and their use in the synthesis of new substituted BODIPYs for various applications. We have synthesized brominated BODIPYs by selectively introducing 1 to 6 bromines on borondipyrrromethene core and used them extensively for the synthesis of covalently and noncovalently linked BODIPY-chromophore conjugates. We developed BODIPY based systems which can act as a fluorescent anion sensors, redox switches and useful for energy transfer studies. We synthesized diformyl BODIPYs which can be used as a pH sensor. A simple route is developed to synthesize 3-pyrrolyl BODIPYs which has tremendous commercial potential since biologists use this type of compounds as a marker. Multi-BODIPY assemblies have been synthesized using cyclotriphosphazene ring as a scaffold. BF_2 complexes and $\text{B}(\text{OR})_2$ complexes of smaragdyrin, an expanded porphyrin were synthesized and showed that $\text{B}(\text{OH})_2$ smaragdyrin can be used as a exclusive fluoride ion sensor. We also synthesized BF_2 smaragdyrin-thiasapphyrin and BF_2 -smaragdyrin-thiarubyrin dyads and used them for fluorescent anion sensing applications. In this article, we summarized all these results on BODIPY chemistry originated in our laboratory in last two years.

1. Introduction

Among the large variety of known fluorescent dyes, the difluoro-boradiaza-s-indacene family (BODIPY) has gained recognition as being one of the most versatile fluorophore and has found great popularity with chemists, biochemists and physicists (Figure 1).¹⁻⁴ BODIPY dyes exhibit

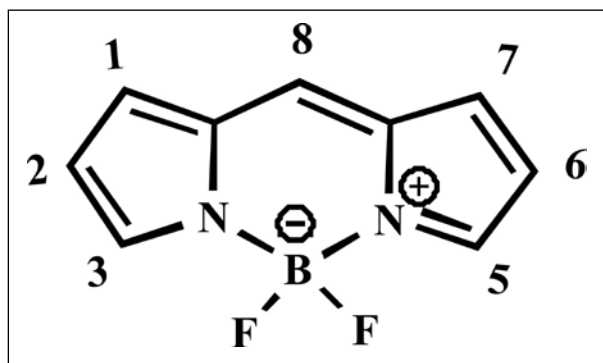


Figure 1: Basic structure of 4,4-difluoro-4-bora-3a,4a-diaza-s-indacene.

optical properties that are often superior to other long wavelength absorbing dyes such as fluorescein, tetramethylrhodamine, texas red etc.

Since their discovery by Treibs and co-workers in 1968,⁵ the number and range of applications of BODIPYs have blossomed and include such diverse uses as biomolecular labels,⁶ chromogenic probes and cation sensors,⁷⁻¹² drug delivery agents,¹³ fluorescent switches,¹⁴ electroluminescent films,¹⁵⁻¹⁷ laser dyes,^{18,19} light-harvesters²⁰⁻²³ and sensitizers for solar cells.^{24,25} The synthesis and spectroscopic properties of variety of BODIPY dyes and their derivatives have been recently reviewed by Burgess et al,¹ and Ziessel et. al.² The sudden interest in the BODIPY-based probes can be attributed to their useful photophysical characteristics such as their high molar absorption coefficients, high

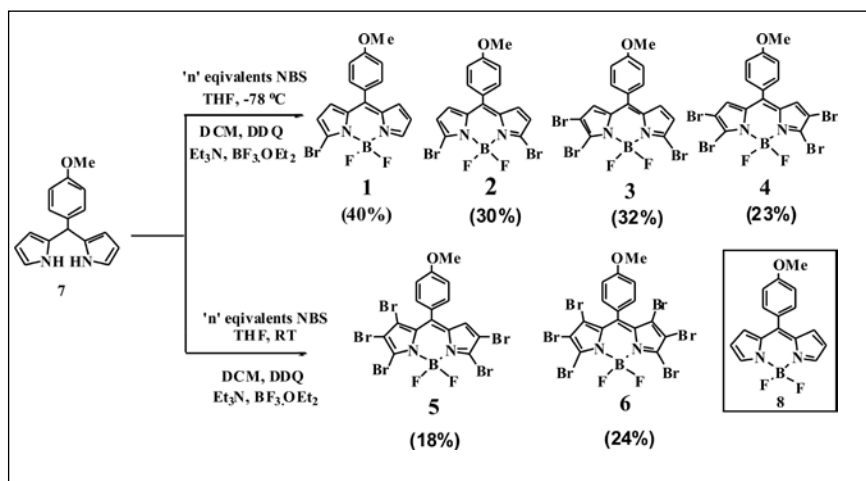


Figure 2: Synthesis of brominated compounds 1-6. The structure of reference BODIPY 8 is also included.

fluorescence quantum yields ($\Phi_F \approx 1.0$, even in water), good photostability, and narrow emission band widths (important in multicolour applications).¹⁻⁴ Additional advantages are their lack of a net ionic charge and the general insensitivity of their fluorescence to solvent or pH. Recently, our group is involved in the design and synthesis of several new BODIPY dyes using the functionalized BODIPYs and showed their applications as chemodosimeter,²⁶ fluorescent sensors,²⁷⁻³⁰ redox switches,^{31,32} pH sensors³³ and energy transfer systems.³⁴⁻³⁷ In this article, we present the highlights from our recent work on BODIPY dyes.

2. Brominated BODIPYs

BODIPYs containing halogen groups such as bromines at the pyrrole carbons are important synthons for the synthesis of variety of substituted BODIPYs. We and others synthesized halogenated BODIPYs and used for the synthesis of new interesting BODIPY based systems.^{26,31,34,38-41} We recently synthesized *meso*-anisyl BODIPYs **1-6** containing one to six bromines at the pyrrole carbons and studied the effect of bromines on the electronic properties of BODIPY.^{26,34,38,42} The brominated BODIPYs **1-6** containing one to six bromines were prepared by treating *meso*-anisyl dipyrromethane **7** with different equivalents of N-bromosuccinimide in THF either at low temperature or room temperature followed by oxidation with DDQ and complexation with BF₃·OEt₂ (Figure 2). The R_f values of mono to

hexa brominated BODIPYs are quite distinct to separate by column chromatography and isolated the compounds **1-6** in decent yields. The crystal structures solved for compounds **2-6** indicated that the boron-dipyrrromethene framework comprised of two pyrrole rings and one six membered boron containing ring is in one plane like other reported BODIPYs.⁴³ However, the dihedral angle between BODIPY core and *meso*-anisyl group is varied from 48 to 88° and the *meso*-anisyl ring is almost perpendicular in penta **5** and hexabrominated **6** BODIPYs.

The comparison of absorption spectra of brominated BODIPYs **1-6** along with unsubstituted *meso*-phenyl BODIPY⁴³ **8** recorded in toluene is shown in Figure 3. It is clear from the Figure 3 that with stepwise increase in the number of bromine groups at the pyrrole carbons of BODIPY core resulted in the bathochromic shift compared to **8** and the magnitude of red shift of absorption band depends on the number of bromines substituted at the BODIPY core. It is noted that each bromine substitution at the pyrrole carbon contributes an additional 10 nm red shift w.r.t the absorption band observed for **8**. However, this systematic red shift was observed only upto the introduction of four bromines and compounds **5** and **6** did not show any further red shift. This is also reflected in the non-linear nature of the plot of magnitude of red shift versus the number of bromines substituted which indicates that the magnitude of red shift

with each bromine substitution is non-additive (Inset in Figure 3).

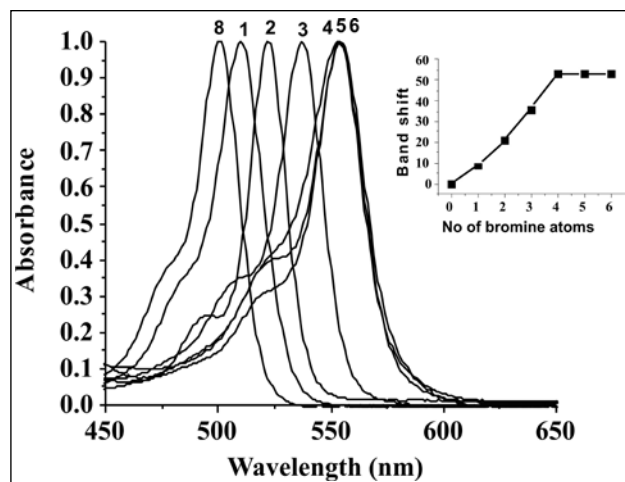


Figure 3: Comparison of absorption spectra of compounds 1-6 recorded in toluene. The concentration used was 1×10^{-6} M. The inset shows the plot of magnitude of red shift in absorption band versus the number of bromines.

The redox properties of brominated BODIPYs **1-6** also showed very interesting trend and the comparison of first reduction waves of compounds **1-6** along with **8** is shown in Figure 4. It is clear from the Figure 4 that addition of each bromine atom resulted in successive anodic shift of reduction potential compared to **8** indicating that boron-dipyrromethene dye becomes easier to reduce with the increase of number of Br groups. The positive shift in reduction potential with the increase in the number of Br groups is additive and the slope of the straight-line plot is 80 mV/

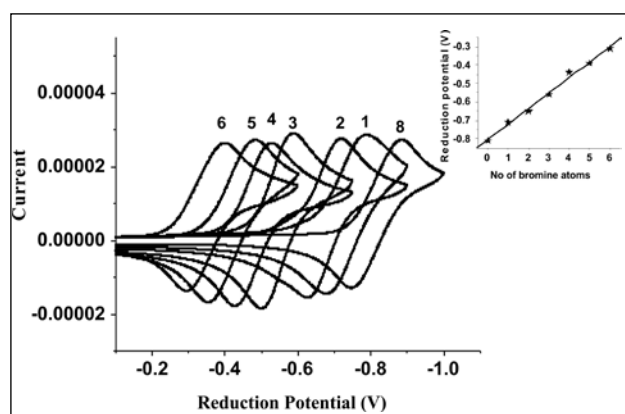


Figure 4: Comparison of first reduction waves of compounds 1-6 along with **8** in CH_2Cl_2 , measured using $n\text{-Bu}_4\text{N}^+\text{P}(\text{ClO}_4)_6^-$ (0.1 M) as supporting electrolyte at a scan rate of 50 mVs^{-1} . The inset shows the plot between the no. of bromine atoms versus reduction potential.

Br group (Inset in Figure 4). The fluorescence properties studied for **1-6** indicated that the fluorescence band also experienced red shift on addition of bromines. However, the quantum yields were reduced significantly for penta and hexabrominated BODIPYs due to heavy halogen effect which because of spin-orbit coupling enhances the non-radiative decay pathways.

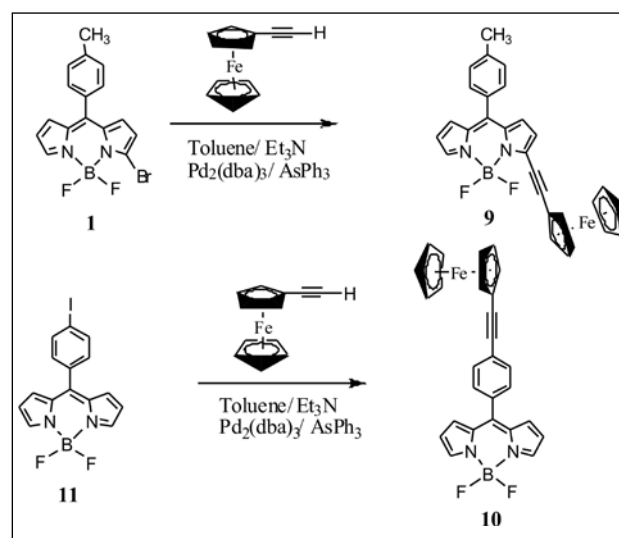


Figure 5: Synthesis of BODIPY-ferrocene conjugates **9-10**

3. BODIPY based conjugates

3.1. BODIPY-Ferrocene conjugates

3-Bromo boron dipyrromethene **1** has been used as key synthon to prepare ethynyl bridged BODIPY-ferrocene conjugate **9** by coupling **1** with α -ethynyl ferrocene in toluene/triethylamine in the presence of catalytic amount of $\text{CuI}/\text{Pd}(\text{PPh}_3)_2\text{Cl}_2$ at 50°C for 4 h (Figure 5) followed by column chromatographic purification.³¹ For comparison purpose, the reference BODIPY-ferrocene conjugate **10** in which ferrocene was linked at the *meso*-phenyl group of BODIPY was synthesized by coupling the appropriate BODIPY building block **11** with α -ethynyl ferrocene under similar reaction conditions (Figure 5).

The comparison of absorption spectra of BODIPY ferrocene conjugates **9** and **10** shown in Figure 6a clearly indicated the presence of charge transfer band in compound **9** but not in compound **10**. This indicates that in compound **9**, there is an effective conjugation

between BODIPY and ferrocenyl moieties but the communication is less effective in compound **10**. The fluorescence properties of compounds **9** and **10** indicate that the fluorescence is completely quenched in compound **9** but not in compound **10** which is attributed to an effective electron transfer from ferrocenyl moiety to BODIPY unit in compound **9**. However, upon oxidation of ferrocene to ferrocenium ion in compound **9**, the charge transfer band in absorption spectrum is

disappeared and fluorescence is restored. These observations were supported by absorption and fluorescence studies of compound **9** on titration with increasing amounts of $\text{Fe}(\text{ClO}_4)_3$ as shown in Figure 6b and 6c respectively. As clear from Figure 6b that on addition of $\text{Fe}(\text{ClO}_4)_3$, the charge transfer band at 682 nm slowly disappears whereas the fluorescence band at 612 nm was slowly restored (Figure 6c). These observations were also reflected in the colour of the solution

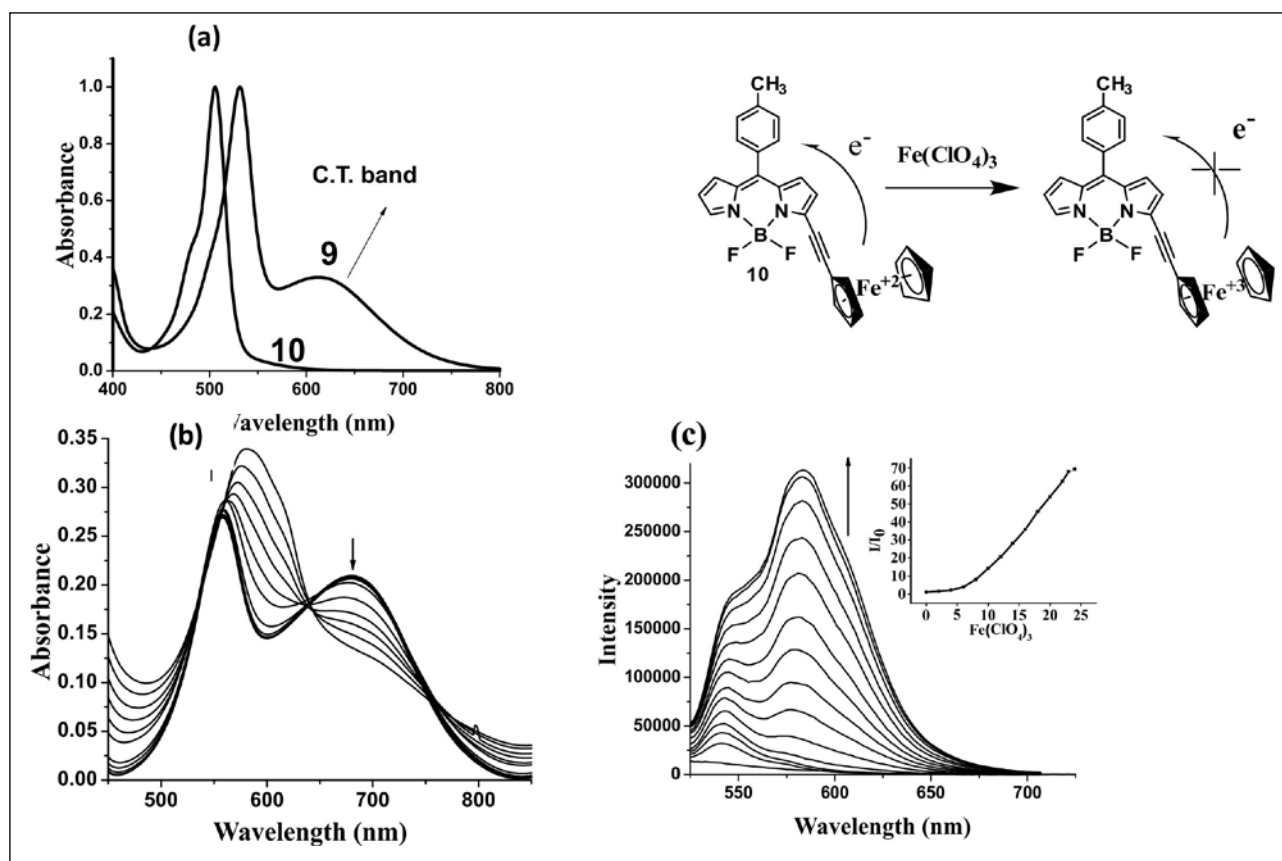


Figure 6: (a) Absorption spectra of BODIPY-ferrocene conjugates **9-10** recorded in toluene. The concentration used was 5×10^{-5} M. (b) The absorption spectral changes of **9** (10 μM) on addition of $\text{Fe}(\text{ClO}_4)_3$ in toluene. The $\text{Fe}(\text{ClO}_4)_3$ concentration was varied from 0 to 120 μM. (c) Fluorescence spectral changes of **9** (10 μM) on the addition of $\text{Fe}(\text{ClO}_4)_3$ in toluene ($\lambda_{\text{ex}} = 505$ nm). The concentration of $\text{Fe}(\text{ClO}_4)_3$ was varied from 0 to 240 μM. The inset show the plot of I/I_0 as a function of concentration of $\text{Fe}(\text{ClO}_4)_3$.

of compound **9** in toluene which changes from intense blue to fluorescent red. However, under similar experimental conditions, the compound **10** did not show any changes in absorption and fluorescence spectra as well as colour. Thus, we proved that compound **9** in which ferrocene is directly connected to BODIPY core can be used as a redox switch by controlling the oxidation of ferrocene to ferrocenium ion and vice versa.

3.2. Covalently linked BODIPY-chromophore dyads

3-Bromo boron dipyrromethene has been used further to synthesize BODIPY-chromophore conjugates **12-17** using mild Pd(0) coupling conditions (Figure 7).³⁴ The chromophores possessing very distinct features such as anthracene **18**, terpyridine **19**, porphyrin **20**, Zn(II)porphyrin, 21,23-dithiaporphyrin **21** and

thiasapphyrin **22** were connected at 3-position of boron-dipyrrromethene dye by coupling of 3-bromo BODIPY **1** with appropriate ethynyl or ethynylphenyl chromophore **18-22** in toluene/

triethylamine in the presence of catalytic amount of $\text{AsPh}_3/\text{Pd}_2(\text{dba})_3$ at 40 °C followed by column chromatographic purification. The spectral studies indicated that the interaction is

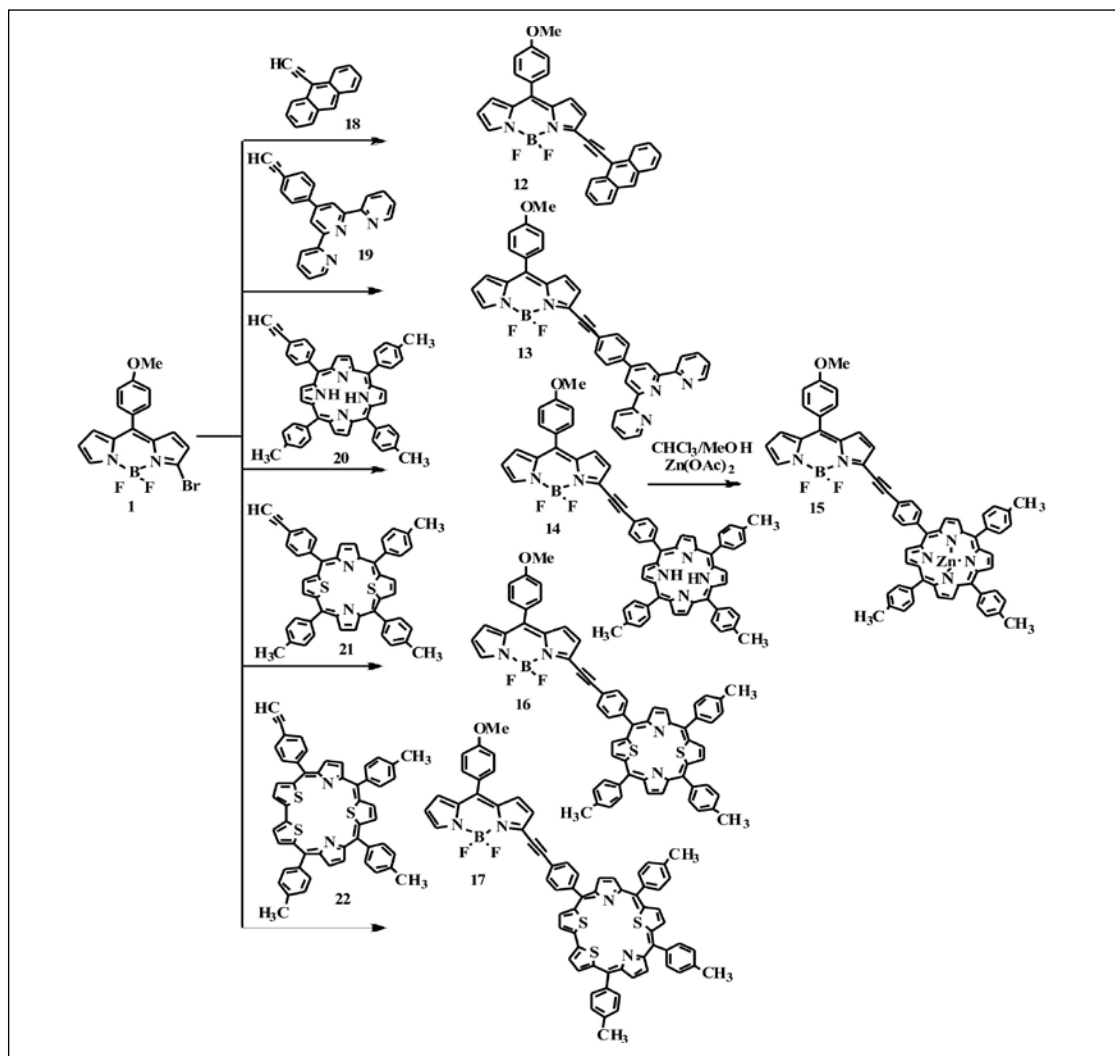


Figure 7: Synthetic scheme for the preparation of BODIPY-chromophore conjugates **12-17** Reaction conditions used were $\text{Pd}_2(\text{dba})_3/\text{AsPh}_3$, Toluene/TEA, 35-60 °C.

stronger in ethynyl bridged BODIPY-anthracene conjugate **12** compared to other ethynylphenyl bridged BODIPY-chromophore conjugates **13-17**. The steady state fluorescence indicated that in ethynyl bridged BODIPY-anthracene conjugate **12**, the BODIPY unit acts as energy acceptor and showed a possibility of energy transfer from donor anthracene unit to acceptor BODIPY unit on selective excitation of anthracene unit. However, in ethynylphenyl bridged BODIPY-porphyrin conjugates **14**, the BODIPY unit acts

as energy donor and exhibited a possibility of singlet-singlet energy transfer from BODIPY unit to other chromophore unit.

Covalently linked BODIPY-BODIPY dyad **23** was synthesized similarly by coupling of 3-bromo BODIPY **1** with 4,4-difluoro-8-(4-ethynylphenyl)-4-bora-3a,4a-diaza-s-indacene **24** under mild Pd(0) coupling conditions.³⁴ The absorption spectrum of **23** (Figure 8) showed two strong bands at 509 and 562 nm with almost equal intensity. The red shifted absorption

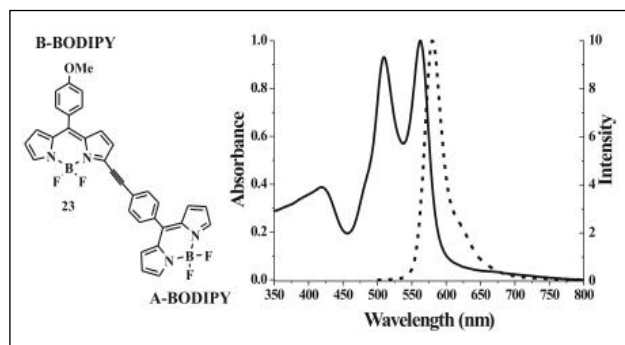


Figure 8: Normalized absorption (–) and emission spectra (....) of compound **23**.

band at 562 nm corresponds to BODIPY unit B to which ethynylphenyl group is connected at α -position and absorption band at 506 nm is due to the BODIPY unit A. This indicates that the two BODIPY units A and B exhibit quite different absorption properties and the BODIPY unit B absorbs at lower energy, whereas BODIPY unit A absorbs at higher energy. Thus, on excitation at 488 nm, the emission was exclusively observed from the BODIPY unit, which contains ethynylphenyl group at α -position (BODIPY B) and no emission was noticed from the donor BODIPY unit (BODIPY A) due to the energy transfer from BODIPY unit A to BODIPY unit B in conjugate **23** (Figure 8).

Recently, we synthesized two more covalently linked BODIPY dyads **25** and **26** containing *meso*-phenyl BODIPY and *meso*-furyl BODIPY units connected via *meso-meso* and *meso- α* positions.³⁷ Since our recent study indicated that introduction of furyl group at *meso*-position of BODIPY in place of *meso*-phenyl group alter the electronic properties significantly and *meso*-furyl BODIPY absorb at lower energy compared to *meso*-phenyl BODIPY,⁴⁴ we synthesized two BODIPY-BODIPY dyads **25** and **26** containing these two units to study the singlet-singlet energy transfer properties. In dyad **25**, on excitation at 488 nm where *meso*-aryl BODIPY unit absorbs strongly, the emission at 525 nm due to *meso*-aryl BODIPY was completely quenched and a strong emission was noted at 603 nm which is due to *meso*-furyl BODIPY (Figure 9a). Similarly, the dyad **26** which showed two clear absorption bands at 508 and 587 nm corresponding to *meso*-phenyl BODIPY and *meso*-furyl BODIPY units

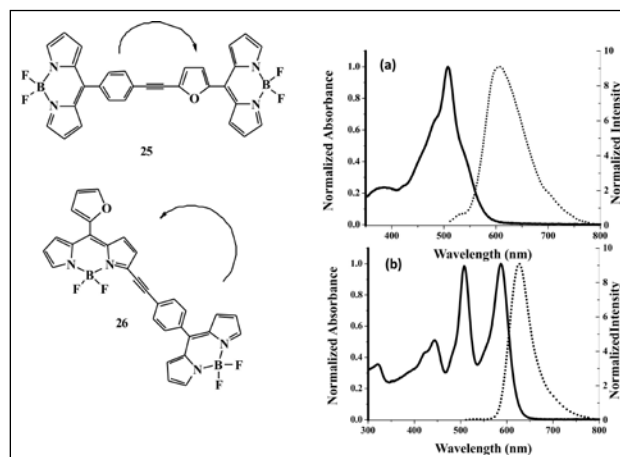


Figure 9: Normalized absorption (–) and emission spectra (....) of compounds (a) **25** and (b) **26**.

respectively, on excitation at 508 nm, the emission from *meso*-aryl BODIPY unit was quenched completely and a strong emission due to *meso*-furyl BODIPY was observed at 630 nm (Figure 9b). These observations supported a possibility of singlet-singlet energy transfer from *meso*-aryl BODIPY unit to *meso*-furyl BODIPY unit in both dyads **25** and **26**.

3.3. Chemodosimeter

3,5-Dibromo BODIPY **2** was used to synthesize BODIPY (CCTMS)₂ **27** which can be used as specific chemodosimeter for fluoride ion.²⁶ Coupling of **2** with trimethylsilylacetylene under mild Pd(0) coupling conditions followed by column chromatographic purification afforded **27** in decent yield. For comparison purpose we also synthesized the known BODIPY(CCTMS) **28** by following the reported method.⁷ We showed that compound **27** can be used as fluorescent and as well as chromogenic chemodosimeter for fluoride ion detection based on selective fluoride ion catalyzed deprotection of ethyne functional groups present at the 3- and 5-positions of the dye. It is established that if functional group is in close proximity to a fluorophore, the change in electronic properties of the functional group due to protection/deprotection may influence the photophysical properties of the dye, which should leads to an observable change in the absorption/emission profile of the dye. Since the trimethylsilyl groups, the protective groups for ethyne functional groups, are electron

donating groups and removal of trimethylsilyl groups from ethyne functional groups would alter the electronic properties of the dye, which in turn expected to result in changes in spectroscopic properties. Because of the high affinity of fluoride for silicon, the trimethylsilyl groups present at the 3,5-positions of **27** can be easily cleaved by fluoride ion but not by other anions to afford the BODIPY dye containing two ethynyl functional groups **29**, thus **27** can act as specific chemodosimeter for fluoride ion. This irreversible reaction was monitored by following changes in NMR, absorption and fluorescence spectroscopic features and also by following changes in the colour under naked eye and UV light conditions. For example, the addition of fluoride ion to a solution of **27** in CH_2Cl_2 results in clear ratiometric changes in fluorescence spectrum, which reflected in the decrease of the intensity of emission band at 584 nm corresponding to dosimeter **27** and increase in intensity of new band at 564 nm corresponding to **29** (Figure 10a).

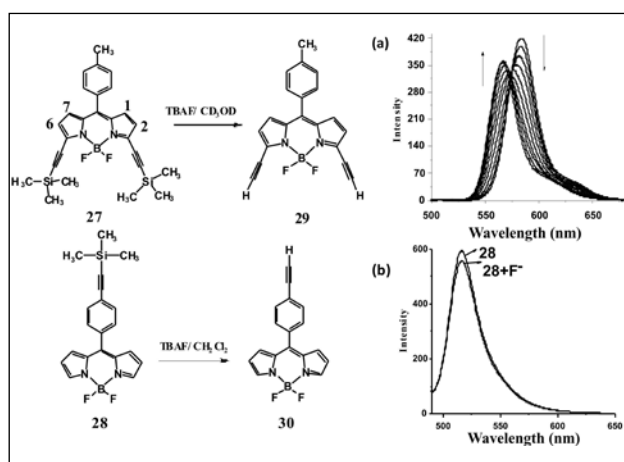


Figure 10: Fluorescence changes of (a) **27** and (b) **28** ($2\ \mu\text{M}$) upon the addition of F^- in CH_2Cl_2 ($\lambda_{\text{ex}}\ 425\ \text{nm}$).

There are no changes in absorption and fluorescence bands of **27** on addition of any other anions such as Br^- , Cl^- , I^- , $(\text{HPO}_4)_2^-$ and $(\text{ClO}_4)_2^-$. Under same conditions, the compound **28** in which the trimethylsilyl ethynyl group is present on *meso*-phenyl group, on addition of F^- ion although cleaves the trimethylsilyl group and forms compound **30**, but there are no significant changes in fluorescence bands

observed, suggesting that compound **28** cannot be used as chemodosimeter for F^- ion (Figure 10b). Thus, this study indicates that the location of functional group, such as trimethylsilyl ethynyl functional group on BODIPY plays a very important role in designing the chemodosimetric sensor.

3.4. Covalently linked trichromophore systems

3,5-Dibromo BODIPY **2** was used to synthesize four novel covalently linked trichromophore systems containing central BODIPY unit connected to two different types of porphyrin units or one porphyrin and one expanded porphyrin units at 3,5-positions **31-34** in two steps as shown in the Figure 11.³⁵ In the first step, 3-bromo-5-porphyrinyl *meso*-anisyl BODIPY **35** and 3-bromo-5-rubyrinyl *meso*-anisyl BODIPY **36** were synthesized by treating **2** with one equivalent of 5-(4-hydroxyphenyl)-10,15,20-tri(*p*-tolyl)porphyrin **37** or 5-(4-hydroxyphenyl)-10,19,24-tri(*p*-tolyl)-29,31,32,34-tetrathiarubyrin **38** in $\text{CHCl}_3/\text{CH}_3\text{CN}$ (1:1) in the presence of Cs_2CO_3 under a nitrogen atmosphere at reflux for 1 h followed by column chromatographic purification. In the second step, four covalently linked trichromophore systems **31-34** were synthesized by treating 3-bromo-5-porphyrinyl BODIPY **35** or 3-bromo-5-rubyrinyl BODIPY **36** with corresponding hydroxy porphyrin **37** or hydroxy expanded porphyrin **38** in CHCl_3 at $60\ ^\circ\text{C}$ (Scheme 5). The absorption and electrochemical studies support weak ground state interaction among the three chromophore units in trichromophore systems. In all four trichromophore systems **31-34**, the singlet state energy of the BODIPY unit is higher in energy than the other two macrocyclic units hence, the BODIPY unit acts as an energy donor and transfers energy to either one macrocyclic unit or both macrocyclic units. This observation, we illustrate by taking an example of trichromophore system **34**. A comparison of normalized emission spectra of compound **2**, bichromophoric system **35** and trichromophore system **34** recorded in CHCl_3 at 488 nm is shown in Figure 12. The bichromophore system **35**, on excitation at 488

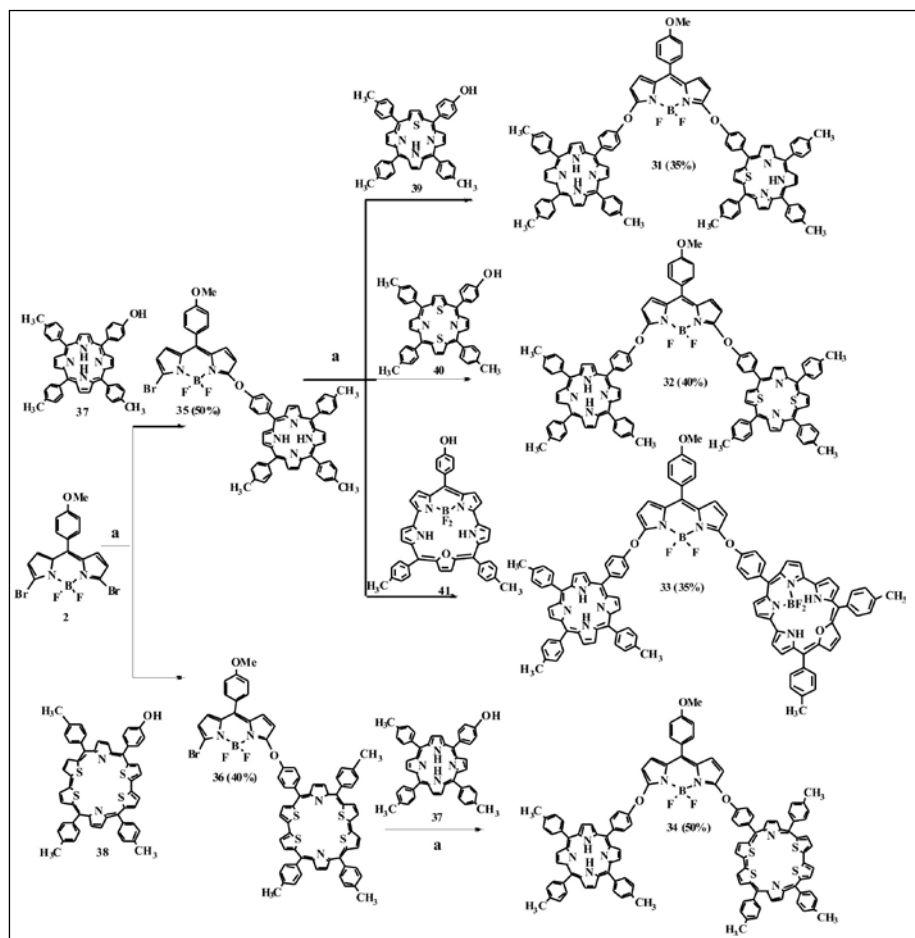


Figure 11: Synthetic scheme for bichromophore and trichromophore systems 31-36 ^aReaction conditions used were $\text{CH}_3\text{CN}/\text{CHCl}_3$ (1:1), Cs_2CO_3 , 60 °C.

nm, the wavelength at which the BODIPY unit absorbs relatively strongly, the emission from the BODIPY unit is significantly quenched and major emission was noted from the N_4 porphyrin unit. These observations suggest that there is an efficient energy transfer from the BODIPY unit to the porphyrin unit in compound 35. In trichromophore system 34, on excitation at 488 nm, the BODIPY and porphyrin emission was quenched by 99% and the major emission was noted from the BF_2 -smaragdyrin unit which indicates that there is an efficient energy transfer from BODIPY unit to the porphyrin unit as well as the BF_2 -smaragdyrin unit.

Furthermore, the study also indicates that there is a possibility of efficient energy transfer from the N_4 porphyrin unit to the BF_2 -smaragdyrin unit in 34. Thus, in compound 34, irrespective of the excitation wavelength, the

emission was noted mainly from from the BF_2 -smaragdyrin unit, the singlet state energy level of which is lower than those of the other two chromophoric units.

3.5. BODIPY-pyridone and BODIPY-oxypyridine conjugates

3,5-Dibromo BODIPY 2 was subjected to nucleophilic substitution reactions by treating one equivalent of 2 with three equivalents of 2-, 3- and 4-hydroxypyridines in CH_3CN in the presence of Cs_2CO_3 at reflux for 1 h followed by chromatographic purification yielded 3,5-bis(pyridone)BODIPYs 39 & 41 and 3,5-bis(oxypyridine)BODIPY 40 in decent yields (Figure 13).³⁸ The effect of a pyridine versus an oxypyridine substituents at 3,5-positions of BODIPY on the spectral, electrochemical and photophysical properties were studied. The compounds 39 & 41 exhibited broad, red shifted

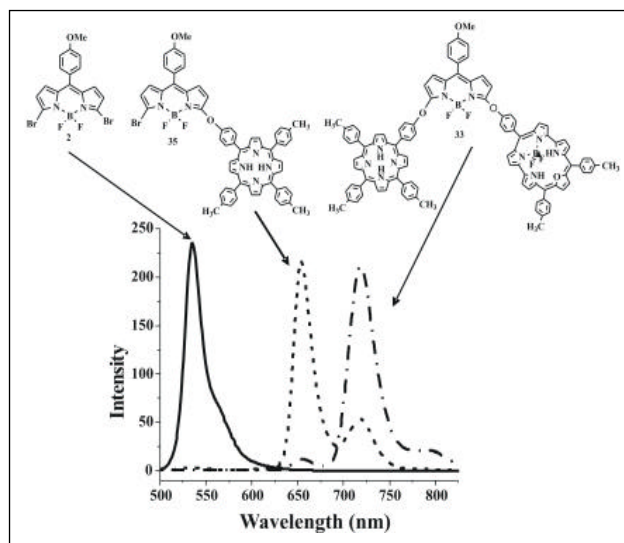


Figure 12: Comparison of normalized emission spectra of trichromophore **33** (.....) with its associated reference compounds **35** (----) and **2** (—) recorded in CHCl_3 using $\lambda_{\text{ex}} = 488 \text{ nm}$.

absorption and emission bands, decreased quantum yields and lifetimes, displayed large Stokes shifts and easier reductions than did the 3,5-bis(oxypyridine)BODIPY **40**. For example, the steady state fluorescence spectra as well as first reduction waves of compounds of **39–41** presented in Figure 13 clearly supports that the pyridine moieties alter the electronic properties of BODIPY more significantly compared to oxypyridine substituents at 3,5-positions of BODIPY. The compounds **39** and **41** exhibited emission band at higher wavelength than compound **40** (Figure 13a). Similarly, the compounds **39** and **41** are easier to reduce compared to compound **40** (Figure 13b). The differences in the properties of these two classes of BODIPY dyes are attributed to the extension of *p*-delocalization associated with the electron deficient nature of the pyridine groups.

3.6. Non-covalently linked BODIPY metalloporphyrin conjugates

Boron-dipyrromethene containing oxypyridine substituents at 3,5-positions **40** was used further to synthesize non-covalent BODIPY-metalloporphyrin triads **42** and **43** by using metal-pyridine "N" interaction (Chart 7.1).³⁶ The compound **40** was treated with two equivalents of ZnTPP and RuTPP(CO) to form non-covalent

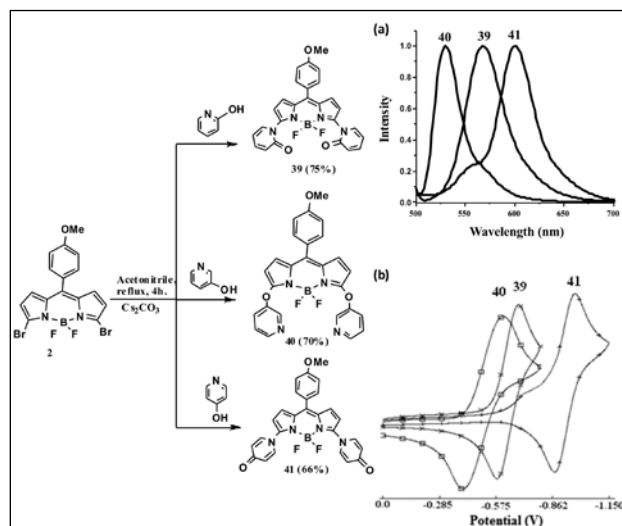


Figure 13: Synthetic scheme for compounds **39–41**; (a) Comparison of normalized emission spectra of compounds **39–41** recorded in toluene using $\lambda_{\text{ex}} = 488 \text{ nm}$. (b) Comparison of reduction waves of cyclic voltammograms of **39–41**.

BODIPY-metalloporphyrin triads **42** and **43** respectively. The formation of BODIPY-metalloporphyrin triads **42** and **43** was confirmed by 1D and 2D NMR studies. The comparison of ^1H NMR spectra of **40**, **42** and **43** is shown in Figure 14. In ^1H NMR, the signals of oxypyridine group(s) of BODIPY unit (type e and f protons) showed significant upfield shifts supporting the coordination of oxypyridine group of BODIPY unit to metalloporphyrin unit. The NMR study also indicated that Zn(II) porphyrin forms relatively weak BODIPY-Zn(II) porphyrin conjugate **42** whereas Ru(II) porphyrin forms strong BODIPY-Ru(II) porphyrin conjugate **43** (Figure 14) The absorption and electrochemical studies indicated that the conjugates exhibit features of both the constituted monomeric units and retain their individual characteristic features in conjugates.

3.7. Polyarylated BODIPYs

After successful synthesis of hexabrominated BODIPY **6** in our laboratory, we used it as a synthon for the synthesis of polyarylated BODIPYs (Figure 15).⁴⁵ The polyarylated BODIPYs **44–47** were synthesized by coupling of compound **6** with corresponding aryl boronic acids such as phenylboronic acid, 4-fluorophenylboronic acid, 4-methylphenylboronic acid and 4-methoxyphenylboronic acid in a THF/toluene/

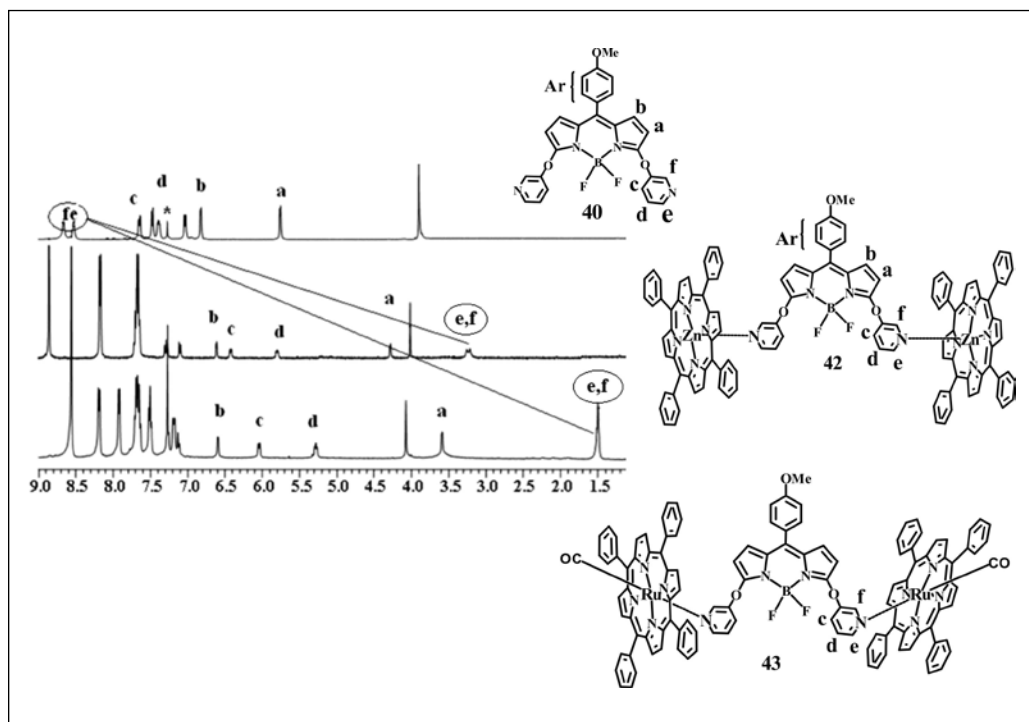


Figure 14: Comparison of $^1\text{H-NMR}$ spectra for compounds 40, 42 and 43 recorded in CDCl_3 .

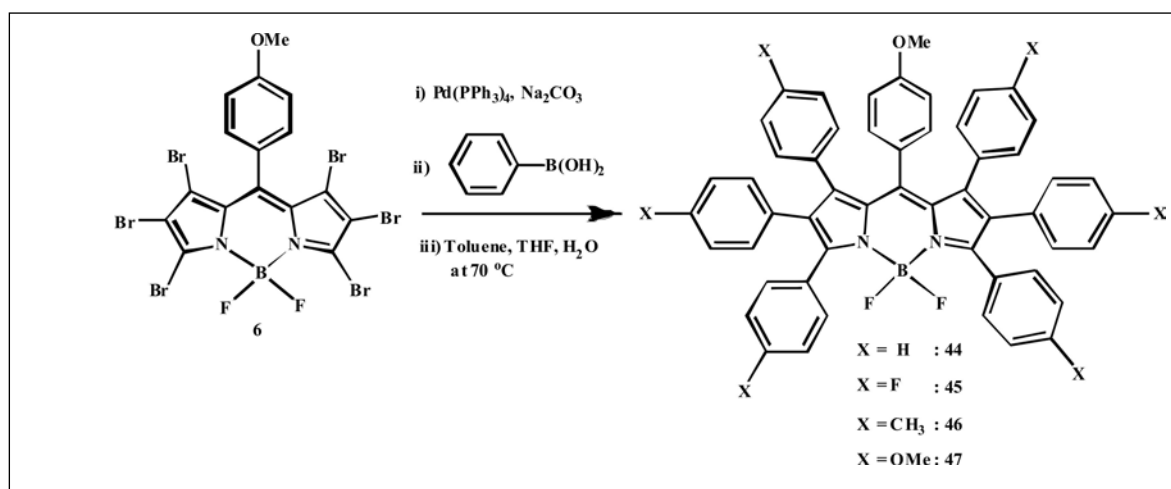


Figure 15: Synthesis of polyarylated BODIPY compounds 44-47.

H_2O (1:1:1) mixture in the presence of a catalytic amount of $\text{Pd}(\text{PPh}_3)_4/\text{Na}_2\text{CO}_3$ overnight at 80°C followed by simple column chromatographic purification. The crystal structure solved for compound **44** displayed distorted "propeller-like" conformation. The highly distorted structure of compound **44** was ascribed to the steric hindrance caused by the six phenyl groups on the BODIPY core. These polyarylated BODIPYs showed red shifts in its absorption and emission maxima

compared to **8** and hexabrominated BODIPY **6** (Figure 16a and 16b).

These are highly fluorescent in solution as well as in solid state (Figure 16c). They exhibit reversible oxidation and reduction waves compared to unsubstituted BODIPY **8**. Comparison of first reduction wave of **6** and **44** is shown in Figure 16d. The compound **8** is very easy to reduce because of its electron deficient nature whereas compound **44** is very

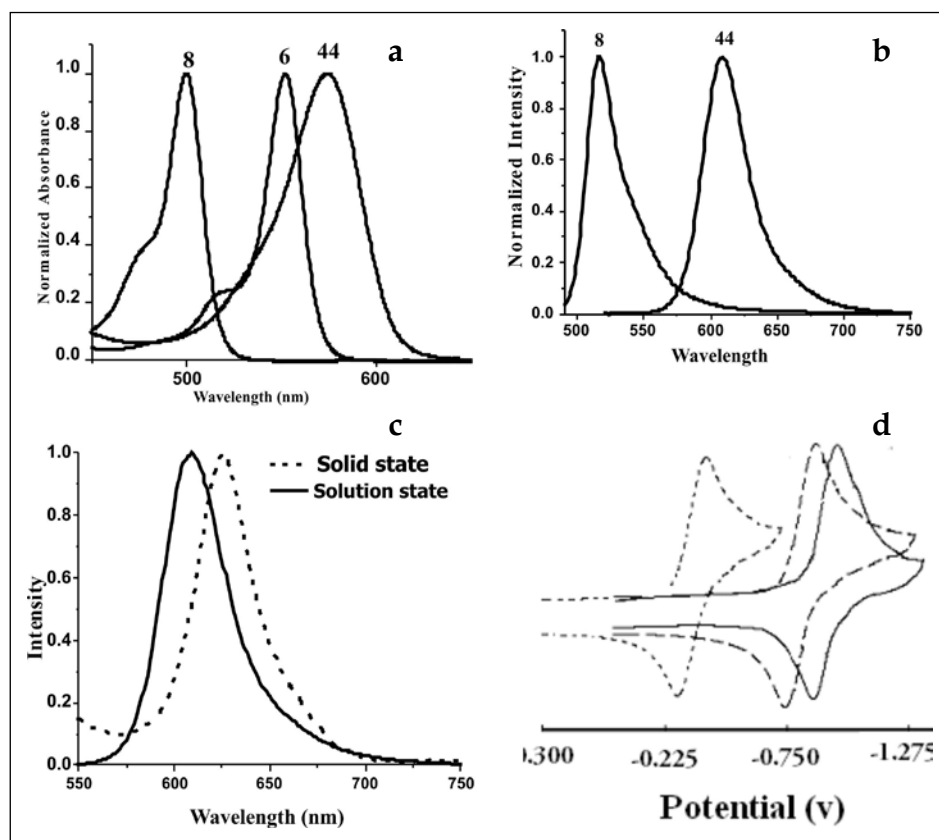


Figure 16: (a) Comparison of normalized absorption spectra of compounds 44, 8 and 6 recorded in CHCl_3 . (b) The comparison of absorption and emission spectra of compounds 44 and 8. (c) The comparison of solid state and solution state emission spectra of compound 44. (d) Comparison of reduction waves of cyclic voltammograms of compounds 6, 8 and 44 recorded in CH_2Cl_2 containing 0.1 M TBAP as supporting electrolyte recorded at 50 mV s^{-1} scan speed.

difficult to reduce because of electron rich nature.

4. 3,5-Diformylboron dipyrromethenes

A series of BODIPY dyes containing two aldehyde functional groups (**48-51**) at the 3 and 5 position have been synthesized in low-to-decent yields in two steps in our laboratory (Figure 17).³³ In the first step, the *meso*-aryl dipyrromethanes were treated with POCl_3 in *N,N*-dimethylformamide to afford 1,9-diformylated dipyrromethanes. In the second step, the diformylated dipyrromethanes were first in situ oxidized with DDQ and then reacted with $\text{BF}_3 \cdot \text{OEt}_2$ to afford 3,5-diformylboron dipyrromethenes (Scheme 17). The X-ray structural analysis indicated that the aldehyde groups are involved in intramolecular hydrogen bonding with fluoride atoms, which may be responsible for the stability of the diformylated BODIPY compounds. The presence of two formyl

groups significantly alters the electronic properties, which is clearly evident in downfield shifts in the ^1H and ^{19}F NMR spectra, bathochromic shifts in the absorption and fluorescence spectra, better quantum yields, and increased lifetimes compared to 3,5-unsubstituted BODIPYs.

Furthermore, 3,5-diformylboron dipyrromethenes are highly electron-deficient and undergo facile reductions compared to unsubstituted BODIPYs. These compounds exhibit pH dependent on/off fluorescence and thus act as fluorescent pH sensors which we demonstrated by taking 3,5-diformyl BODIPY **48**. The systematic titration of pH effect on the fluorescence spectra of compound **48** over the pH range of 4.0-9.0 is shown in Figure 18. The emission peak maxima of **48** remain unaltered in different pH solutions, but its intensity was significantly altered. It was observed that compound **48** showed some emission at pH 7, but the emission intensity

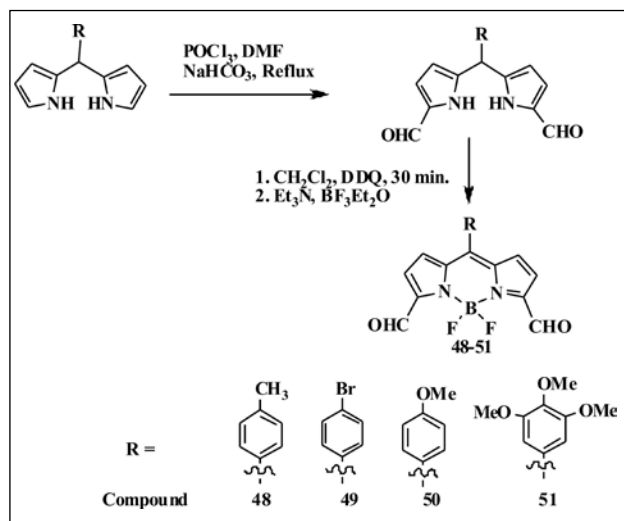


Figure 17: Synthetic scheme for 3,5 diformylated BODIPYs 48-51.

decreased as the pH of the alkaline medium was increased and compound **48** became completely non-fluorescent at pH 9. However, the decrease in the emission intensity is not very substantial as we move toward alkaline pH 7, indicating that compound **48** is less fluorescent even at neutral pH. Upon a decrease from pH 7 to acidic pH (pH = 4), the emission intensity was enhanced by 17 times and a maximum change was found within the pH range of 6.5-4.0. This is also clearly evident in the sigmoidal response observed in the plot of I/I_{\max} vs pH (Inset in Figure 18), where I_{\max} is the maximum fluorescence intensity of compound **48** and I is the fluorescence intensity at a particular pH. Thus, compound **48** can be used as ON/OFF fluorescent pH sensor.

5. 3-Pyrrolyl BODIPYs

Very recently, we developed a simple facile route for the synthesis of BF_2 complexes of Prodigiosin type oligopyrroles **52-58** and their cholesterol conjugates **59-60**.³⁰ This route gives an access to synthesis of any desired *meso*-aryl substituted 3-pyrrolyl BODIPYs. These type of compounds although available commercially in small quantities but very expensive to afford for academic research. The compounds **52-58** were prepared by adopting a three step, one pot reaction method (Figure 19). In the first step, the *meso*-aryl dipyrromethane in CHCl_3 was oxidized with 1.5 equiv of DDQ at room temperature for

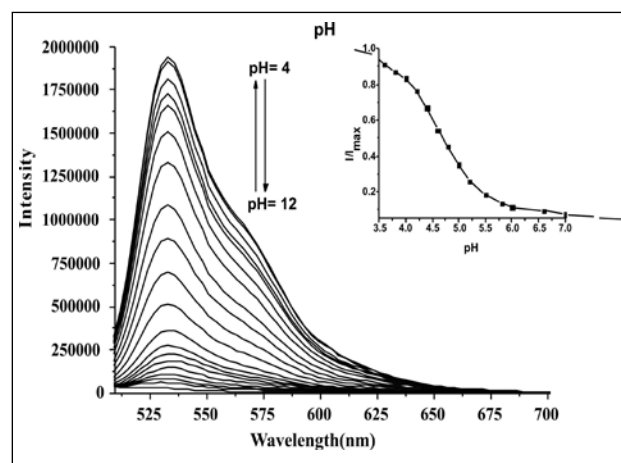


Figure 18: Fluorescence spectra of compound **48** (5 μM) in acetate buffer solution (0.1 M) as a function of pH. Excitation wavelength used was 488nm. The inset shows the plot of I/I_{\max} versus pH.

30 min. The resultant *meso*-aryl dipyrromethane without isolation was treated with 1 equiv of pyrrole at room temperature for 15 min to form the prodigiosin type of 1-pyrrolyl *meso*-aryl dipyrromethane. However, without isolation of this intermediate, the reaction mixture was treated further with triethylamine and $\text{BF}_3 \cdot \text{OEt}_2$ at room temp for 30 min. The crude compounds were purified by column chromatography and afforded pure 3-pyrrolyl BODIPYs **52-58** in decent yields. The presence of pyrrole group at 3-position resulted in better photophysical properties such as these compounds absorb at higher wavelength region and quantum yields were increased by four to eight times compared to unsubstituted *meso*-aryl BODIPY **8**.

The use of 3-pyrrolyl BODIPYs for the synthesis of biocompatible compounds was demonstrated by synthesizing 3-pyrrolyl BODIPY-cholesterol conjugates **59** and **60** as shown in Figure 20. We carried out preliminary biological studies with BODIPY-cholesterol conjugate **59** which possesses excellent fluorescence properties and showed that these conjugates can be used as potential markers to study sterol trafficking in cellular membranes and for live cell imaging.

6. Multi-BODIPY assemblies

Recently, we synthesized Cyclotriphosphazene appended with six boron-dipyrromethenes $\text{N}_3\text{P}_3(\text{BODIPY})_6$ **61-64** by following

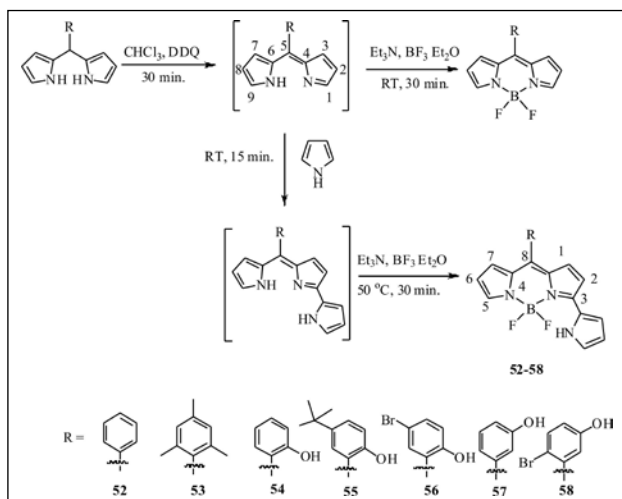


Figure 19: Synthesis of 3-pyrrolyl BODIPYs 52-58.

two different routes (Figure 21).⁴⁶ In method I, one equivalent of $N_3P_3Cl_6$ was treated with six equivalents of *meso*-(*o*- or *m*- or *p*-hydroxyphenyl) boron dipyrromethene in THF in the presence of

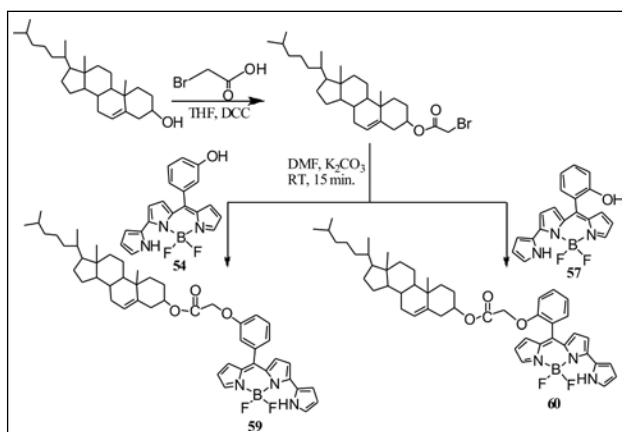


Figure 20: Synthesis of BODIPY-cholesterol conjugates 59 and 60.

cesium carbonate. This afforded $N_3P_3(BODIPY)_6$ in yields ranging from 80 to 90%. In method II, we first prepared hexakis(*p*-formylphenoxy) cyclotriphosphazene $N_3P_3(CHO)_6$ **65** by treating one equivalent of $N_3P_3Cl_6$ with six equivalents of 4-hydroxybenzaldehyde in the presence of cesium carbonate in THF. In the second step, **65** was condensed with excess of pyrrole in the presence of catalytic amount of trifluoroacetic acid in CH_2Cl_2 at room temperature and afforded hexakis(*p*-phenoxy dipyrromethane) cyclotriphosphazene **66**. In the last step, the **66** was first oxidized with six equivalents of DDQ

in CH_2Cl_2 at room temperature for 1 h followed by neutralization with triethylamine and further reaction with excess $BF_3 \cdot OEt_2$ afforded the target $N_3P_3(BODIPY)_6$ **63** in 16% yield. Although route I was straightforward to synthesize the desired compounds, the route II gives an idea about the robustness of the cyclotriphosphazene ring towards various reaction and purification conditions used here. The NMR studies indicated that the BODIPY units are interacting with each other in solution but the crystal structure solved for one of the compound showed no interaction between the BODIPY units in solid-state.

The absorption and fluorescence properties studied in different solvents indicated that the properties are sensitive to the type of BODIPY units connected to cyclophosphazene ring. The compounds exhibited large Stoke's shifts with comparable quantum yields compared to their respective reference boron-dipyrromethene

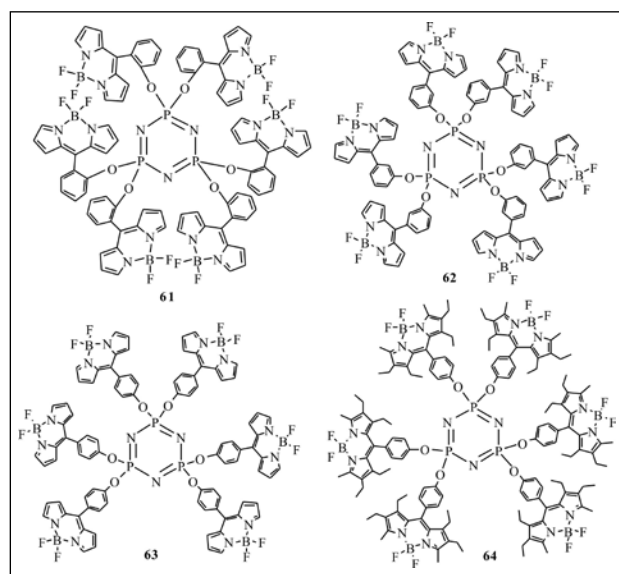


Figure 21: Hexa boron-dipyrromethenes decorated on cyclotriphosphazenes ring.

monomers. This kind of cyclophosphazene appended with fluorophores may have potential applications as organic light emitting diodes.

7. Boron complexes of oxasmaragdyrin

The extensive chemistry developed on BODIPYs now clearly indicated that BF_2 complex preferably forms with dipyrromethene

motifs containing one iminopyrrole and one aminopyrrole rings. Porphyrins are tetrapyrrolic

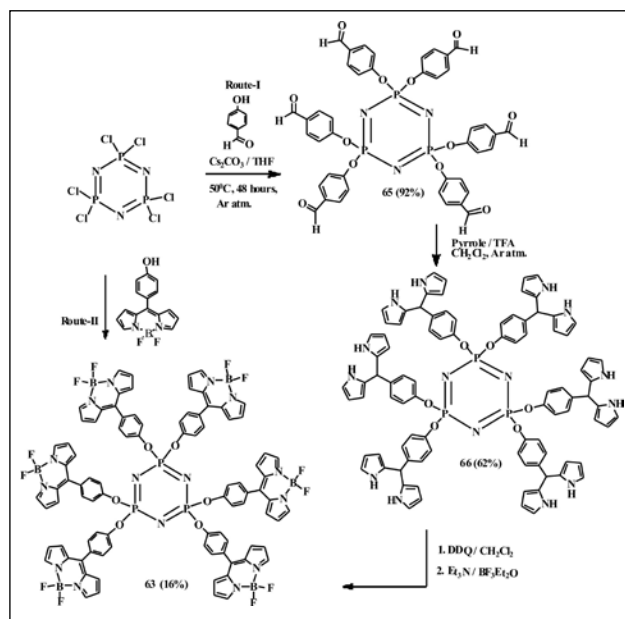


Figure 22: Synthesis of compound 63 by Route I and Route II.

macrocycles containing dipyrromethene moieties and have been explored for their complexation behaviour towards BF_2 group in recent years.⁴⁷ The porphyrin complexes with two BF_2 groups which undergoes spontaneous reductive coupling to give compounds with direct B-B bonds or undergoes hydrolysis and forms B-O-B links inside porphyrin macrocycle. This is due to the closer proximity of two boron atoms inside smaller coordination site of porphyrin leading to unusual bonds formation inside porphyrin macrocycle. The corroles which have one methine carbon less than porphyrins also exhibits the unusual chemistry of binding to two boron atoms.⁴⁸ The expanded porphyrins which contains more than four pyrrole rings⁴⁹ and having potential dipyrromethene motifs have been shown very recently that they also complex with one or two BF_2 groups.^{50,51} However, the BF_2 complexation exhibited little effect on electronic properties of expanded porphyrins. Sessler, Penelope Brothers and others^{50,52} showed that Amethyrin, a hexapyrrolic macrocycle **67** and octaphyrin **68** on reaction with $\text{BF}_3\cdot\text{OEt}_2$ gave two products containing one and two BF_2 groups which are stable and does not undergo any hydrolysis

(Figure 23).

We reported the synthesis of first examples of BF_2 -complexes **69-72** (Figure 24) and $\text{B}(\text{OR})_2$ -complexes **73-76** of oxasmaragdyrin (Figure 25), the expanded core-modified porphyrin in decent yields under very simple reaction

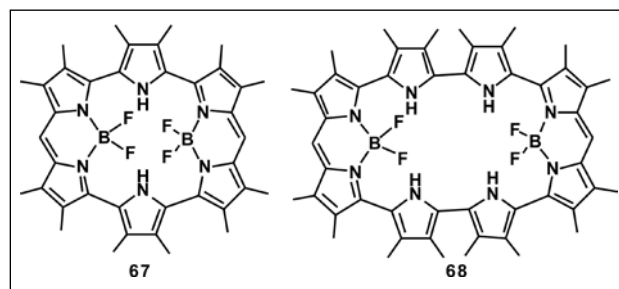


Figure 23: Structure of compounds 67 and 68.

conditions at room temperature.²⁸ The BF_2 -smaragdyrin complexes **69-72** were prepared by treating the appropriate free base smaragdyrin **77-80** with 40 equivalents of triethylamine and 50 equivalents of $\text{BF}_3\cdot\text{OEt}_2$ in CH_2Cl_2 at room temperature for 30 min. followed by column chromatographic purification. The **69-72** are stable green complexes and did not undergo any hydrolysis or decomplexation. The boron complexes of oxasmaragdyrin alter the electronic properties of the macrocycle significantly as evident by various spectroscopic techniques.

For example, these complexes **69-72** show strong band at ~ 700 nm which is three times more intense than the absorption band of their corresponding free base smaragdyrin **77-80**

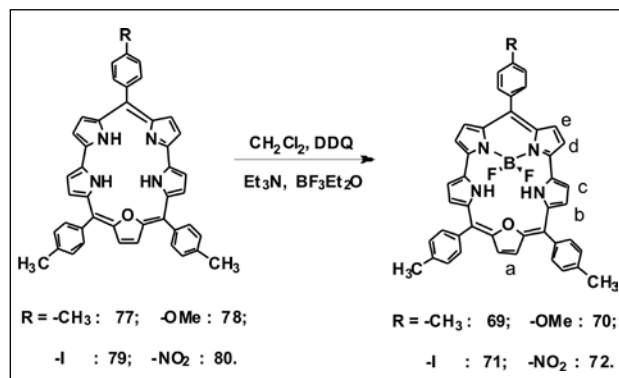


Figure 24: Synthesis of BF_2 -smaragdyrin complexes 69-72.

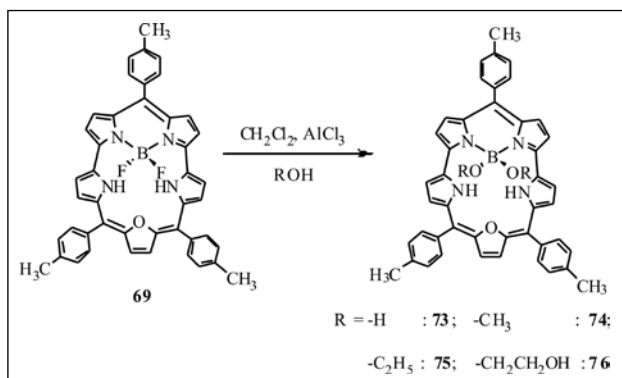


Figure 25: Synthesis of $\text{B}(\text{OR})_2$ -smaragdyrin complexes 73-76.

present in the same region. The fluorescent quantum yields of **69-72** are two times higher than those of free base smaragdyrins. The BF_2 complexation of smaragdyrins makes the resulting macrocycle more electron deficient than free base smaragdyrins. Although BF_2 -smaragdyrins **69-72** exhibited interesting spectral and electrochemical properties, these complexes cannot be used for chemical sensor applications. This is because the fluorides of the BF_2 moiety are involved in strong hydrogen bonding with the inner NH protons hence the inner NH protons are not freely accessible. To overcome this problem, we synthesized $\text{B}(\text{OR})_2$ smaragdyrin complexes **73-76** by replacing fluoride groups of BF_2 -smaragdyrin with hydroxy and alkoxy groups. The $\text{B}(\text{OH})_2$ -smaragdyrin **73** was prepared by treating **69** with AlCl_3 in CH_2Cl_2 at refluxing temperature for 5 min followed by column chromatographic purification to afford **73** as green solid in 60% yield. The alkoxy substituted $\text{B}(\text{OR})_2$ -smaragdyrin complexes **74-76** were prepared by treating **69** with AlCl_3 in the presence of an appropriate alcohol such as methanol, ethanol and glycol in excess amount under similar reaction conditions (Figure 25). The absorption and emission features of $\text{B}(\text{OR})_2$ -smaragdyrin complexes **73-76** are similar to those of BF_2 -smaragdyrins **69-72** but $\text{B}(\text{OR})_2$ -smaragdyrins are more easier to oxidize but difficult to reduce compared to BF_2 -smaragdyrin complexes because of the electron donating nature of alkoxy substituents.

We explored the anion sensing properties

of $\text{B}(\text{OH})_2$ -smaragdyrin **73** with various anions since it is a neutral expanded porphyrin with large cavity and more number of inner NH/OH protons. Our studies indicated that **73** act as an exclusive fluoride ion sensor. The fluoride anion binding to **73** was monitored by ^1H NMR, absorption, fluorescence and electrochemical studies and here we discussed only absorption and electrochemical studies. The absorption spectral titration of **73** with the addition of fluoride ion is shown in Figure 26a. It is clear from Figure 26a that the intensity of the absorption bands of **73** at 446, 475, and 705 nm decreased on addition of increasing amounts of F^- ion and new bands at 455, 487 and 720 nm appeared with four isosbestic points at 451, 468, 482 and 713 nm. The expected 1:1 stoichiometry suggested by the presence of isosbestic points, was further confirmed by Job's plot analysis. Similarly, the fluoride anion binding can also be inferred from electrochemical studies. Figure 26b shows the systematic changes in the oxidation waves of receptor on increasing addition of fluoride anion. The addition of increasing amounts of fluoride anion to the solution of **73** resulted in the decrease of current intensity of the oxidation wave at 1.06 V, which gradually disappears and at the same time the appearance of new oxidation with gradual increase in current intensity at 0.30 V was observed. However, the oxidation wave at 0.70 V experienced negligible shift in the potential on increasing the addition of fluoride ion to **73**. Furthermore, no changes in the oxidation potential of **73** were observed when we added other anions. All these results indicate that **73** can be used as a specific optical and electrochemical sensor for fluoride ion.

Since BF_2 -smaragdyrin absorbs at lower energy and it is decently fluorescent, we synthesized two covalently linked diphenylethyne bridged dyads containing two different expanded porphyrin macrocycles, namely thiasapphyrin- BF_2 -smaragdyrin **74** and thiarubyryn- BF_2 -smaragdyrin **75** by coupling appropriate mono-functionalized expanded porphyrin building blocks under mild $\text{Pd}(0)$ coupling conditions as shown in the Figure 27.²⁹ The NMR, absorption and electrochemical studies indicated that

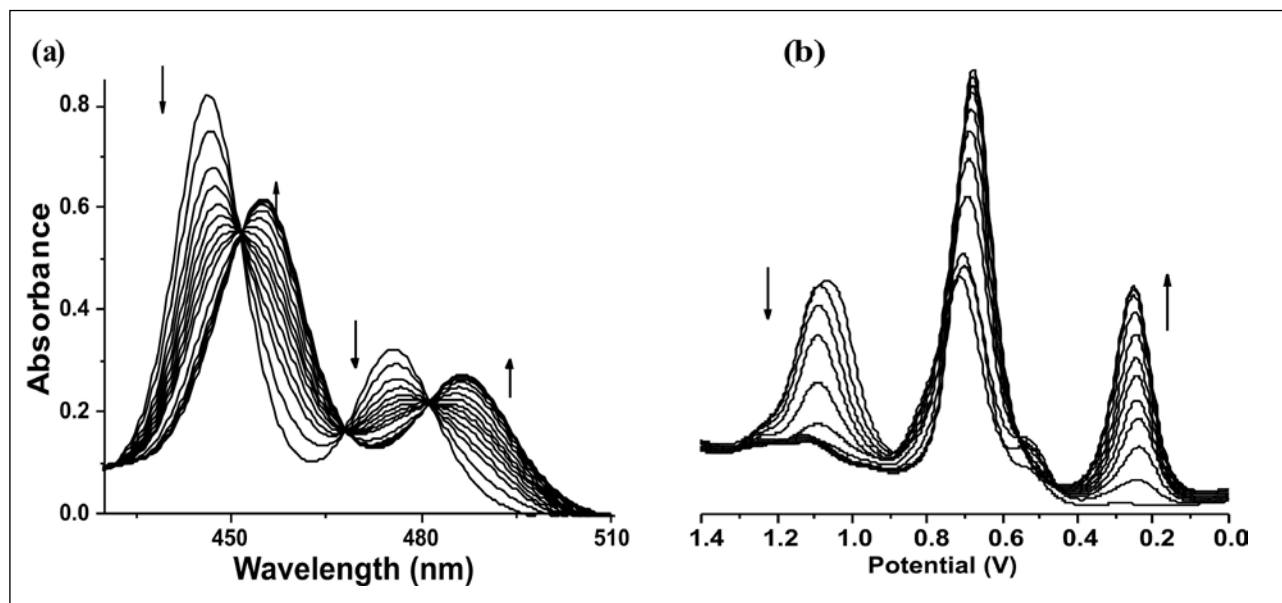


Figure 26: (a) The absorption spectra of 73 (5 μ M) in the region 400-525 nm in the presence of F^- in CH_2Cl_2 . The F^- concentration is 0, 9, 18, 27, 36, 45, 54, 63, 72, 81, 90, 99 and 108 μ M respectively. (b) Square wave voltammograms of 73 (0.59 mM) in the presence of F^- ion. The F^- concentration is 0, 0.14, 0.28, 0.42, 0.56, 0.70, 0.84, 0.98, 1.12, 1.26, 1.40 and 1.54 mM respectively

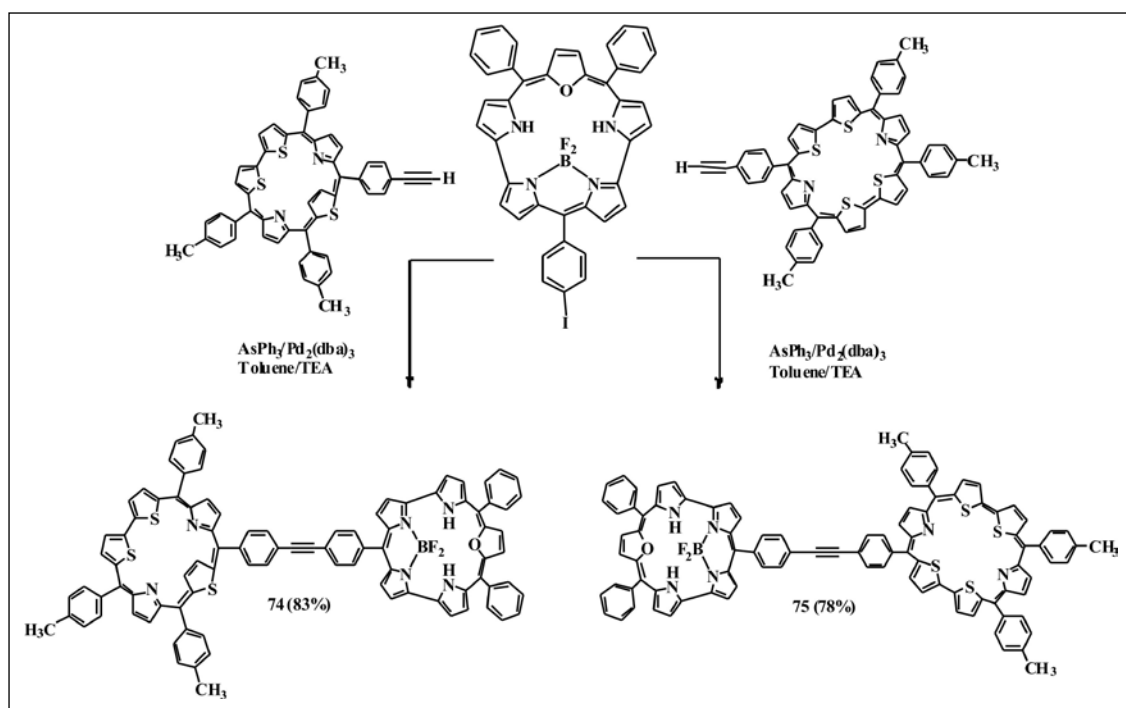


Figure 27: Synthesis of thiasapphyrin- BF_2 -smaragdyrin dyad 74 and thiarubyryrin- BF_2 -smaragdyrin dyad 75.

the two macrocycles in the dyads interact weakly with each other and maintain their independent characteristic features. The steady state fluorescence studies of the dyads showed that the thiasapphyrin unit in 74 and thiarubyryrin

unit in 75 are non-fluorescent but the BF_2 -smaragdyrin unit in both the dyads 74 and 75 are decently fluorescent. However, the quantum yield of the BF_2 -smaragdyrin unit in the dyads was less than that of monomeric BF_2 -smaragdyrin

unit because of an enhancement of nonradiative decay channels operating in the dyads. Since the thiasapphyrin and thiarubyrin units are known to bind anions in their protonated form which can be monitored by following the changes in the fluorescence spectrum of BF_2 -smaragdyrin unit, this kind of dyads can be in principle used as fluorescent sensors. Thus, we explored the potential use of these dyads as fluorescent sensors for anions.

The effects of titration of different amounts of anions on the fluorescence spectra of the BF_2 -smaragdyrin unit of the protonated dyads **74.2H⁺** and **75.2H⁺** are shown in Figure 28. As is clear from Figure 28, the addition of increasing amounts of anion to the protonated dyads **74.2H⁺** and **75.2H⁺** resulted in a gradual enhancement in the emission intensity of the BF_2 -smaragdyrin unit. Thus, in dyads **74.2H⁺** and **75.2H⁺**, the binding of anions at the protonated sapphyrin and rubyrin sites, respectively, were measured by following the changes in the fluorescence spectra of BF_2 -smaragdyrin unit, which suggests that dyads **74** and **75** should be suitable as fluorescent sensors. Thus, based on these preliminary investigations, we concluded that the dyads **74** and **75** containing the BF_2 -smaragdyrin unit can be used as fluorescent anion sensors.

8. Conclusions

In last couple of years, our group is involved in synthesis of variety of new boron-dipyromethene dyes using various functionalized BODIPYs. Although halogenated BODIPYs have been synthesized earlier and used for the synthesis of extended BODIPY derivatives, we have been successful in synthesis of brominated BODIPYs by selectively introducing 1 to 6 bromines at the pyrrole carbons of BODIPY core in decent yields. We showed the alteration of electronic properties with the addition of each bromine atom at the pyrrole carbon of BODIPY core. We used brominated BODIPYs to synthesize variety of new BODIPY derivatives ranging from covalently/noncovalently linked BODIPY-chromophore conjugates to sterically crowded polyarylated BODIPYs. Some of these systems have been used as chemodosimeter, redox

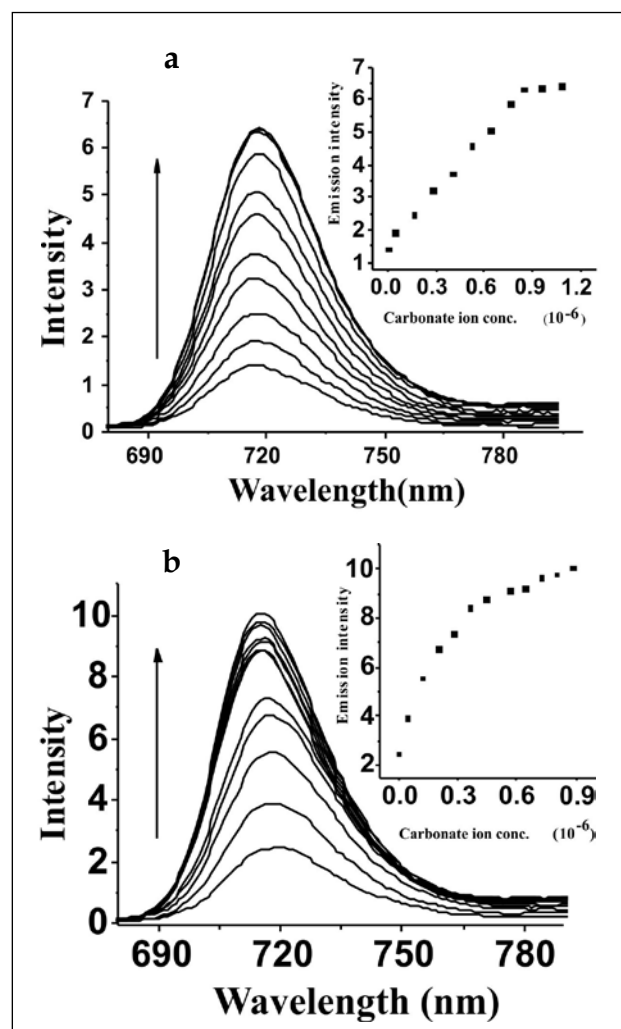


Figure 28. Fluorescence titration of (a) protonated dyad **74.2H⁺** and (b) protonated dyad **75.2H⁺** with increasing amount of carbonate ions (0 to 1.08 equivalents) in dichloromethane. Inset shows plot of the change in fluorescence intensity vs the concentration of CO_3^{2-} ions ($\lambda_{\text{ex}} = 450 \text{ nm}$).

fluorescent switches and energy transfer systems. We synthesized 3,5-diformylated BODIPYs and demonstrated their use as pH sensor. The formyl groups on BODIPY are very important functional group to synthesize variety of interesting BODIPY derivatives in future. We developed a simple route to synthesize 3-pyrrolyl BODIPYs which will have commercial use in future as these systems are very important for biological studies. We used a robust cyclotriphosphazene ring to synthesize multi-BODIPY systems. Finally, we described about the synthesis of BF_2 and $\text{B}(\text{OR})_2$ complexes of smaragdyrin, an expanded porphyrin which possess very interesting

photophysical features. We showed that B(OH)₂-smaragdyrin complex can be used as an exclusive F⁻ ion sensor. In future, we hope that the synthetic chemistry on BODIPY would grow extensively and their application in various fields ranging from biology to material science/solar cells will be explored.

9. Acknowledgements

MR thanks BRNS for financial support and TKK thanks Indian Institute of Technology for fellowship. We thank all our co-workers whose names appear in the references for their hard work and contribution for the growth of this research.

10. References

- Loudet, A.; Burgess, K. *Chem. Rev.* **2007**, *107*, 4891-4932.
- Ziessel, R.; Ulrich, G.; Harriman, A. *New J. Chem.* **2007**, *31*, 496-501.
- Ulrich, G.; Ziessel, R.; Harriman, A. *Angew. Chem. Int. Ed.* **2008**, *47*, 1184-1201.
- Benstead, M.; Mehl, G. H.; Boyle, R. W. *Tetrahedron* **2011**, *67*, 3573-3601.
- Treibs, A.; Kreuzer, F. H. *Justus Liebigs Ann. Chem.* **1968**, *718*, 208-223.
- Haugland, R. P. *Handbook of fluorescent probes and research products*; Molecular Probes, 2002.
- Wagner, R. W.; Lindsey, J. S. *Pure. Appl. Chem.* **1996**, *68*, 1373-1380.
- Beer, G.; Rurack, K.; Daub, J. *Chem. Commun.* **2001**, 1138-1139.
- Beer, G.; Niederalt, C.; Grimme, S.; Daub, J. *Angew. Chem. Int. Ed.* **2000**, *39*, 3252-3255.
- Sancenón, F.; Martínez Máñez, R.; Soto, J. *Angew. Chem. Int. Ed.* **2002**, *41*, 1416-1419.
- Gabe, Y.; Urano, Y.; Kikuchi, K.; Kojima, H.; Nagano, T. *J. Am. Chem. Soc.* **2004**, *126*, 3357-3367.
- Ueno, T.; Urano, Y.; Kojima, H.; Nagano, T. *J. Am. Chem. Soc.* **2006**, *128*, 10640-10641.
- McCusker, C.; Carroll, J. B.; Rotello, V. M. *Chem. Commun.* **2005**, 996-998.
- Golovkova, T. A.; Kozlov, D. V.; Neckers, D. C. *J. Org. Chem.* **2005**, *70*, 5545-5549.
- Lai, R. Y.; Bard, A. J. *J. Phys. Chem. B* **2003**, *107*, 5036-5042.
- Brom, J. M.; Langer, J. L. *J. Alloys Compd.* **2002**, *338*, 112-115.
- Hepp, A.; Ulrich, G.; Schmechel, R.; von Seggern, H.; Ziessel, R. *Synth. Met.* **2004**, *146*, 11-15.
- Chen, T.; Boyer, J. H.; Trudell, M. L. *Heteroat. Chem.* **1997**, *8*, 51-54.
- Sathyamoorthi, G.; Wolford, L. T.; Haag, A. M.; Boyer, J. H. *Heteroat. Chem.* **1994**, *5*, 245-249.
- Li, F.; Yang, S. I.; Ciringh, Y.; Seth, J.; Martin Iii, C. H.; Singh, D. L.; Kim, D.; Birge, R. R.; Bocian, D. F.; Holten, D. *J. Am. Chem. Soc.* **1998**, *120*, 10001-10017.
- Diring, S.; Puntoriero, F.; Nastasi, F.; Campagna, S.; Ziessel, R. *J. Am. Chem. Soc.* **2009**, *131*, 6108-6110.
- Lammi, R. K.; Ambroise, A.; Balasubramanian, T.; Wagner, R. W.; Bocian, D. F.; Holten, D.; Lindsey, J. S. *J. Am. Chem. Soc.* **2000**, *122*, 7579-7591.
- Ambroise, A.; Kirmaier, C.; Wagner, R. W.; Loewe, R. S.; Bocian, D. F.; Holten, D.; Lindsey, J. S. *J. Org. Chem.* **2002**, *67*, 3811-3826.
- Hattori, S.; Ohkubo, K.; Urano, Y.; Sunahara, H.; Nagano, T.; Wada, Y.; Tkachenko, N. V.; Lemmetyinen, H.; Fukuzumi, S. *J. Phys. Chem. B* **2005**, *109*, 15368-15375.
- Erten-Ela, S.; Yilmaz, M. D.; Icli, B.; Dede, Y.; Icli, S.; Akkaya, E. U. *Org. Lett.* **2008**, *10*, 3299-3302.
- Rajeswara Rao, M.; Mobin, S. M.; Ravikanth, M. *Tetrahedron* **2010**, *66*, 1728-1734.
- Rajeswara Rao, M.; Ravikanth, M. *Eur. J. Org. Chem.* **2011**, 1335-1345.
- Rajeswara Rao, M.; Ravikanth, M. *J. Org. Chem.* **2011**, *76*, 3582-3587.
- Pareek, Y.; Ravikanth, M. *Eur. J. Org. Chem.* **2011**, *2011*, 5390-5399.
- Rajeswara Rao, M.; Tiwari, M. D.; Bellare, J. R.; Ravikanth, M. *J. Org. Chem.* **2011**, *76*, 7263-7268.
- Rajeswara Rao, M.; Kumar, K. V. P.; Ravikanth, M. *J. Organomet. Chem.* **2010**, *695*, 863-869.
- Khan, T. K.; Pissurlenkar, RRS.; Shaikh, M. S.; Ravikanth, M. *J. Organomet. Chem.* **2012**, *697*, 65-73.
- Madhu, S.; Rao, M. R.; Shaikh, M. S.; Ravikanth, M. *Inorg. Chem.* **2011**, *50*, 4392-4400.
- Khan, T. K.; Ravikanth, M. *Tetrahedron* **2011**, *67*, 5816-5824.
- Khan, T. K.; Ravikanth, M. *Eur. J. Org. Chem.* **2011**, 7011-7022.
- Khan, T. K.; Ravikanth, M. *Tetrahedron* **2011**, (In press).
- Khan, T. K.; Ravikanth, M. *Dyes and Pigments* **2011**, (In press).
- Khan, T. K.; Rao, M. R.; Ravikanth, M. *Eur. J. Org. Chem.* **2010**, 2314-2323.
- Baruah, M.; Qin, W.; Basarić, N.; De Borggraeve, W. M.; Boens, N. *J. Org. Chem.* **2005**, *70*, 4152-4157.
- Baruah, M.; Qin, W.; Vallée, R. A. L.; Beljonne, D.; Rohand, T.; Dehaen, W.; Boens, N. *Org. Lett.* **2005**, *7*, 4377-4380.
- Rohand, T.; Baruah, M.; Qin, W.; Boens, N.; Dehaen, W. *Chem. Commun.* **2006**, 266-268.
- Lakshmi, V.; Ravikanth, M. (Unpublished work).
- Kee, H. L.; Kirmaier, C.; Yu, L.; Thamyongkit, P.; Youngblood, W. J.; Calder, M. E.; Ramos, L.; Noll, B. C.; Bocian, D. F.; Scheidt, W. R.; Birge, R. R.; Lindsey, J. S.; Holten, D. *J. Phys. Chem. B* **2005**, *109*, 20433-20443.
- Khan, T. K.; Jana, S. K.; Rajeswara Rao, M.; Shaikh, M. S.; Ravikanth, M. *Inorg. Chim. Acta* **2011**, (In press).
- Lakshmi, V.; Ravikanth, M. *J. Org. Chem.* **2011**, *76*, 8466-8471.
- Rajeswara Rao, M.; Bolligarla, R.; Butcher, R. J.; Ravikanth, M. *Inorg. Chem.* **2010**, *49*, 10606-10616.
- Belcher, W. J.; Hodgson, M. C.; Sumida, K.; Torvisco, A.; Ruhlandt-Senge, K.; Ware, D. C.; Boyd, P. D. W.; Brothers, P. J. *Dalton Trans.* **2008**, 1602-1614.
- Albrett, A. M.; Conradie, J.; Boyd, P. D. W.; Clark, G. R.; Ghosh, A.; Brothers, P. J. *J. Am. Chem. Soc.* **2008**, *130*, 2888-2889.
- Sessler, J. L.; Weighorn, S. J. *Expanded, Contracted & Isomeric Porphyrins, Tetrahedron Organic Chemistry Series*; Pergamon: New York, 1997; Vol. 15.
- Kohler, T.; Hodgson, M. C.; Seidel, D.; Veauthier, J. M.;

Meyer, S.; Lynch, V.; Boyd, P. D. W.; Brothers, P. J.; Sessler, J. L. *Chem. Commun.* **2004**, 1060-1061.

51. Brothers, P. J. *Inorg. Chem.* **2011**, (In Press).

52. Brothers, P. J. *Chem. Commun.* **2008**, 2090-2102.



M. Ravikanth was born in Andhra Pradesh, in 1966. He received his B. Sc. and M. Sc. from Osmania University, Hyderabad and Ph. D. from Indian Institute of Technology, Kanpur in 1994. After his postdoctoral stay in USA and Japan, he joined as a faculty at Indian Institute of Technology, Bombay, where he is a currently full professor. His current research interest includes porphyrin and related macrocycles and boron dipyrromethenes.



Tamanna K. Khan was born in Madhya Pradesh, in 1982. She received her B. Sc. and M. Sc. from Sant Gadge Baba Amravati University, Amravati. In 2007 she joined as a Ph. D. student in Indian Institute of Technology, Bombay under supervision of Professor M. Ravikanth, where she is a currently pursuing her research work on boron dipyrromethenes, porphyrins and expanded porphyrins.

Radiation Induced Grafting for Surface Modification of Macromolecules

N. K. Goel, Virendra Kumar, Y. K. Bhardwaj, L. Varshney

Radiation Technology Development Division

Bhabha Atomic Research Centre, Trombay, Mumbai, INDIA

(e-mail:ykbhard@barc.gov.in)

Abstract

Macromolecules because of their extraordinary range of properties are ubiquitous and are essential part of our day to day life. An emerging trend has been of combining two or more macromolecules to obtain macromolecules having properties of both parent macromolecules. Such co-macromolecules can be obtained by blending, grafting or simultaneous curing. Grafting essentially consists of covalently bonding a new macromolecule by growing it on an existing base macromolecule under suitable conditions. Radiation induced grafting results in contaminant free products and can be carried out at room temperature. In addition, because of high penetrating power of high energy radiation, uniform grafting to different depths in parent macromolecule can be achieved. Playing with machine parameters like type of high energy radiation source, total dose, dose rate, ambience during irradiation and experimental variables related to grafting mixture like monomer concentration, presence of additives, effect of solvents, effect of additives etc. can result in macromolecules with modified surfaces for target applications. Grafting can transform hydrophilic macromolecule to hydrophobic macromolecule and vice-versa by judiciously choosing monomers to be grafted. The present article covers basic and applied aspects of radiation induced grafting, including some important industrial applications, like battery separator, antibacterial surfaces and functional adsorbents for waste water treatment.

1. Introduction

Graft polymerization is an easy and efficient technique for modifying base macromolecules as it results in superposition of properties of backbone and the pendent grafted chains. Grafting can be initiated conventionally using suitable redox system [1] or using radiation [2]. Radiation grafting is an easy and highly efficient procedure for modifying the properties of macromolecules of synthetic as well as natural origin [3] and offers some unique advantages over the conventional chemical grafting method [4]. Radiation grafted macromolecules have tried for spectrum of applications like metal absorption[5,6], separation purposes [7-8], biotechnology[9-10], electrochemical applications such as electro-dialysis[11], battery separator [12], as solid macromolecular electrolyte in fuel cells [13,14] and bio-medical applications [15,16]. For separation and purification purpose chelating groups like amidoxime [17,18] have shown to form stable complex with heavy metal ions like

uranium, vanadium, cadmium, copper and ion exchange type of matrices have also been tried for the purpose [19,20].

There are many well-known chemicals, which act as germicides, e.g. halogens, alcohols, peroxygen compounds (H_2O_2 , peracetic acid), phenolic compounds, aldehydes and ionic surfactants. Among the various classes of surfactants, particularly the cationic quaternary ammonium compounds are among the most effective germicides. In recent years, trialkyl ammonium chlorides have been reported to possess germicidal effect in dilute aqueous solutions [21]. Thus with a view that radiation grafting of trialkyl ammonium chlorides (Quaternary ammonium salts) like VBT, MAETC, AETC onto finished cotton cloth may lead to incorporation of anti-bacterial into cotton, grafting of these monomers onto cotton was investigated.

Ion exchange membranes have been

investigated for their suitability as battery separator because of their durability, long life, high charge density and appreciable ion exchange capacity at optimum water content which is the most desirable property of the separator membranes [22]. The mutual radiation grafting technique has been used to graft acrylic acid onto micrometer thick polypropylene sheet to get proton exchange membranes (PEM). The grafted membranes were tested under actual battery conditions for their electrical properties.

Polytetrafluoroethylene (PTFE) commercially known as Teflon is known for its many exceptional properties [23,24]. However these exceptional properties make its disposal difficult as it does not undergo any deterioration under natural conditions. Grafting of acrylic acid onto PTFE scrap was carried out to obtain a matrix which can uptake dyes from industrial effluents and waste water. This approach would mitigate environmental pollution in two ways by utilizing the PTFE scrap and using the grafted scrap to treat industrial effluents.

2. Materials and Methods

2.1 Material

Macromolecular backbone materials non-woven thermally bonded polypropylene (NWPP) was obtained from a local supplier, micrometer thick polypropylene (PP) was provided by M/s High Energy Batteries, INDIA was a product of 3M, USA and used as received. Finished cotton cloth, procured from a local supplier, was washed by boiling in 1% sodium hydroxide solution for three hours. Treated fabric was then repeatedly washed with distilled water until neutral washings were obtained. The cotton samples thus obtained were dried at 50°C and stored in desiccator for further use. Teflon scrap in ribbon form obtained by machining of Teflon rods was procured from local supplier M/s Max Tools Co. The cleaned PTFE scrap had a bulk density=2.1 g/cc, Melting point=330°C and surface energy=22 mJ/m².

Commercial grade acrylonitrile (AN) from M/s IPCL India and dimethyl formamide (DMF) from M/s SD Fine chemicals Mumbai, were used. Hydroxylamine hydrochloride, (ar-vinylbenzyl) trimethylammonium chloride (VBT), a mixture of 3-vinyl and 4-vinyl isomers, [2-(Methacryloyloxy

ethyl] trimethylammonium chloride (MAETC), Mol wt.=207.7 in form of 75% aqueous solution, [2-(Acryloyloxy)ethyl]trimethylammonium chloride (AETC), 80 wt. % solution in water from Aldrich were used as received. 2-Hydroxyethyl methacrylate (HEMA), Mol wt. 130.14 from Aldrich chemicals (purity > 97%), was further purified by vacuum distillation at 78°C and 5 mmHg pressure. Acrylic acid (AA) purity >99% and all other chemicals used were from Aldrich. Himedia (India) nutrient broth (M244S) was used for cultivating bacterial culture and Himedia Plate count Agar (M091) was used for bacterial count experiments. *Escherichia coli* JM109, *Pseudomonas fluorescens* (lab isolate), *Staphylococcus aureus* ATCC 6538P, *Bacillus cereus* MTCC 470 cultures were maintained at 4°C. Before the start of experiment, the cultures were grown on nutrient agar for 2 days at 37°C. The isolates were subcultured twice before inoculation. The long-term storage of cultures was done in 20% glycerol (v/v) at -20°C. All the bacterial counts were done on plate count agar, (Himedia, Mumbai, India) incubated at 37°C for 24 h during the course of this work N₂ and O₂ (purity > 99%) were locally procured. Nanopure water from Millipore was used for all experiments.

2.2 Methods

2.2.1. Irradiation method and sources

Electron beam irradiation of NWPP sheets was carried out using an industrial 2 MeV, 20 kW ILU-6 accelerator (Budker Institute of Nuclear Physics, Russia) under following conditions: energy=1.8 MeV, current=10 mA and variable conveyor speed. Grafting was carried out using post irradiation technique i.e. sheets were irradiated prior to immersing them in grafting solution.

Gamma chambers having Co⁶⁰ gamma radiation source GC-5000 and GC-900, supplied by M/s BRIT, India having dose rate of 0.5-5 kGy hr⁻¹ as measured by Fricke dosimetry were used for irradiation purpose with suitable lead attenuators.

2.2.2 Radiation grafting

Post irradiation grafting technique was used to graft AN onto NWPP whereas mutual radiation grafting method was used to graft VBT, MAETC,

AETC onto cotton cellulose and to graft AA onto PP and Teflon scrap. For post irradiation grafting the NWPP was irradiated using electron beam and dipped in grafting solution of known composition for desired time. For mutual grafting experiments, the backbone macromolecule were dipped in grafting solution in glass stoppered for at least an hour prior to irradiation in gamma chamber for required doses at desired dose rates. Homopolymer was extracted from the grafted samples using suitable solvent by soxhlet extraction for 8 hours. The grafted sample was then dried and grafting yield and grafting efficiency were determined gravimetrically using relations

$$\% \text{ Grafting} = \{(\text{Weight after grafting} - \text{Initial weight}) / \text{Initial weight}\} \times 100 \quad (1)$$

$$\% \text{ Grafting Efficiency} = \text{Monomer grafted} / \text{Monomer converted to macromolecule} \times 100 \quad (2)$$

2.2.3. Antibacterial assay

To check whether grafted cotton or radiation polymerized macromolecules of VBT, MAETC & AETC were bactericidal or bacteriostatic in nature; all four bacterial cultures were inoculated to the level of 10^3 cells/ml in nutrient broth individually. Macromolecules were added (0.1% w/v) to this and incubated at 37°C for 24 h. Samples were withdrawn at regular intervals and growth was checked by measuring turbidity at 600 nm. The samples were also spread plated to count the colonies after incubation. The minimum bactericidal concentration (MBC) was found out by addition of different concentrations of polymer to 0.1 M phosphate buffered saline (PBS) (pH 7.0). The cultures were grown in nutrient broth for 18 h and centrifuged at 6000 rpm for 10 min to harvest the cells. The cells were washed twice with PBS and re-suspended in buffer containing polymers. MBC was defined as the lowest concentration at which complete elimination of cells was achieved at 37°C in 24 h. The antibacterial activity of samples grafted to different extents was assayed by colony count method. Cultures were grown; cells were harvested and suspended in similar way as described above for MBC. Aliquots of samples were withdrawn and spread plated on plate count agar to estimate the initial counts. The grafted sample as well as cotton fabric (control) was then added to this suspension and kept on rotary shaker at 37°C . Cell blank was

also included in the experiment. Samples were withdrawn after different intervals of time and spread plated.

2.2.4. Metal uptake by grafted matrix

The metal ion concentration in the aqueous solution was estimated on DIONEX-500 ion chromatograph system (DX-500, Dionex) using a column ion pack CS5 containing 2 % crosslinked micro porous divinylbenzene-styrene hydrophobic resin core agglomerated with totally permeable latex particles of polyvinylbenzyl quaternary ammonium salts that cause actual anion exchange. Oxalic acid was used as mobile phase and detection was done by absorbance method using (PAR) 4-(2-pyridylazo) resorcinol post column reagent, which has λ_{max} at 520 nm. Sample loop of 25 μL was used.

The equilibrium adsorption study was carried out for metal ions (Co^{2+} , Ni^{2+} , Mn^{2+} , Cd^{2+}) by mixing 0.3 g of AMO-g-PP adsorbent in 25 mL metal ion solution of various known concentrations in 125 mL stoppered conical flasks. The flask containing metal ion solution and adsorbent were placed in motorized thermostatic shaker bath and agitated at 25°C for 5 h until equilibrium was reached. The initial and equilibrium metal ion concentrations of different combinations were measured by ion chromatograph. These data obtained was used to calculate the adsorption capacity of the adsorbent (Q_e) using equation 5

$$Q_e = (C_0 - C_e) * V / (m * 1000) \text{ (mg / g)} \quad (3)$$

Where C_0 and C_e are the initial and equilibrium liquid phase concentration (mg/L); V is volume of metal ion solution used (mL); m is the mass of adsorbent used (g).

The kinetics of adsorption of AMO-g-PP was carried out under similar conditions for different contact time at 200 ppm ion concentration.

3. Results and Discussions

3.1. Post irradiation grafting of AN on NWPP sheet

3.1.1: Parameter standardization for grafting and amidoximation of grafted sheet

NWPP was chosen as backbone material

because of its ready availability, low cost and higher surface area for grafting of acrylonitrile. The PP backbone was characterized by DSC (endothermic peak at ~165°C corresponding to T_m of PP and by FTIR. Initial experiments indicated post irradiation method using electron beam (EB) to be more suitable for this grafting system. Effect of several experimental variables like dose & dose rate, ambience of irradiation, time of exposure after irradiation, solvent-monomer composition, temperature of grafting, optimum time for grafting and stacking were investigated. Figures 1 and 2 show effect of time spent after irradiation and dose and dose rate on grafting extent. On the basis of this investigation it was found that grafting extent of ~110 % could be achieved under following conditions [25]

- Irradiation for a dose of 200 kGy at the rate of 10kGy/pass in air
- Cooling irradiated sheets for 15 minutes in air
- Grafting solution AN-DMF mixture of position ratio 70:30 v/v
- Grafting at a temperature of 60°C

The cyano group of the grafted NWPP sheet was converted to an amidoxime group by soaking the grafted sheet in 3 % hydroxylamine hydrochloride solution (methanol:water =1:1)

at 60°C for 8 hours. The hydroxylamine hydrochloride was neutralized by adding suitable alkaline solution. After the reaction, the sheets were rinsed with water-methanol

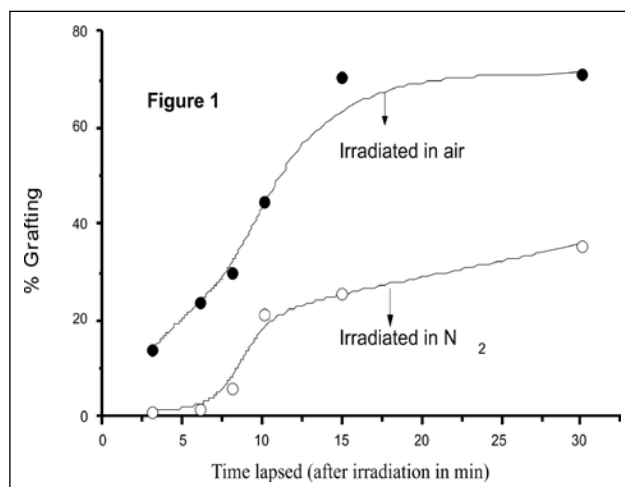


Figure 1: Effect of retention time of irradiated NWPP on grafting

mixture. ~75-80% of the grafted CN group were amidoximated $\{-C(NH_2)=NOH\}$ (AO-membrane) within three hours of treatment.

3.1.2. Metal uptake by amidoximated grafted matrix

Heavy metal ion uptake was monitored by shaking the known weight of grafted matrix with fixed volume of metal ion solution. Figure 3 shows adsorption capacity (Q_e) for metal ions as a function of initial concentration of metal ions (C_i). It can be seen that the adsorption of metal ions

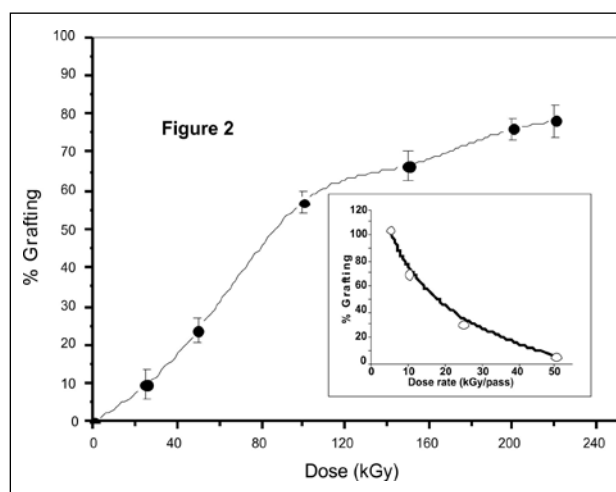


Figure 2: Effect of dose on grafting extent; Dose rate of 10 kGy/pass. Inset: Extent of grafting at different dose rates for total dose of 200 kGy.

follow the order $Cd^{2+} > Co^{2+} > Ni^{2+} > Mn^{2+}$. The adsorption was analyzed using two adsorption models namely, Langmuir [26] and Freundlich isotherms [29]. Different parameters of Langmuir isotherm (equation 4)

$$C_e/Q_e = 1/K_L + a_L C_e/K_L \quad (4)$$

where a_L = Langmuir isotherm constant constant (L/mg)

K_L = Langmuir equilibrium constant (L/g)

C_e = Equilibrium liquid phase ion concentration (mg/L)

Q_e = Equilibrium solid phase ion concentration (mg/g)

K_L/a_L = Maximum adsorption capacity of the adsorbent (mg/g) or theoretical monolayer saturation capacity (q_{max}) and of Freundlich equation obtained are tabulated in table 1 and 2

$$\log Q_e = \log K_f + (1/n) \log C_e \quad (5)$$

where K_f = Freundlich constant (L/g) is the relative indicator of adsorption capacity

n = Freundlich exponent is the indication of favorability of adsorption process.

Langmuir isotherm were good agreement with the experimental equilibrium adsorption capacities and also follow the order i.e. $Cd^{2+} > Co^{2+} > Ni^{2+} > Mn^{2+}$. On the other hand Freundlich equation treatment of sorption data for the metal ions showed deviation from linearity and instead showed a two segment relationship.

Table 1: Langmuir adsorption parameters of EB grafted AMO-g-PP adsorbent grafting extent ~115% at 25°C

| S. No. | Metal ion | K_L (L/g) | a_L (L/mg) | q_{max} (mg/g) | C.F.* |
|--------|-----------|-------------|--------------|------------------|-------|
| 1. | Cd^{2+} | 6.18 | 0.20 | 31.58 | 0.998 |
| 2. | Co^{2+} | 5.88 | 0.33 | 17.57 | 0.999 |
| 3. | Ni^{2+} | 2.72 | 0.19 | 14.24 | 0.999 |
| 4. | Mn^{2+} | 1.91 | 0.18 | 10.76 | 0.998 |

* Correlation coefficient

Table 2: Freundlich adsorption parameters of EB grafted AMO-g-PP adsorbent grafting extent ~115% at 25°C

| S. No. | Metal ion | K_f (L/g) | n | #C.R. (mg/L) | C.F.* |
|--------|-----------|-------------|------|--------------|-------|
| 1. | Cd^{2+} | 1.95 | 1.24 | 0-300 | 0.998 |
| 2. | Co^{2+} | 4.43 | 2.54 | 0-215 | 0.983 |
| 3. | Ni^{2+} | 4.38 | 3.93 | 0-250 | 0.988 |
| 4. | Mn^{2+} | 0.79 | 1.29 | 0-150 | 0.989 |

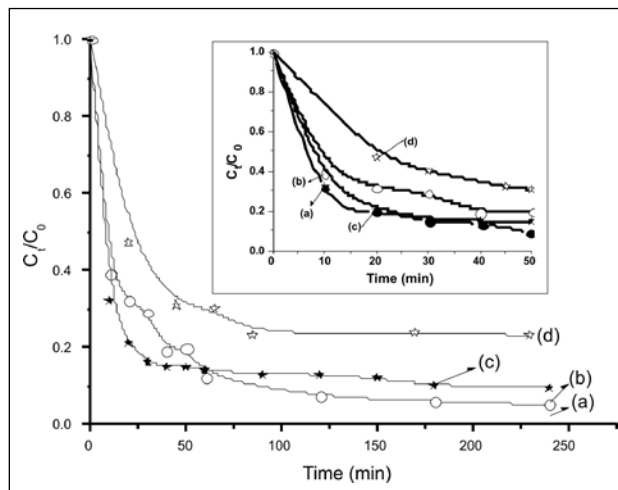


Figure 4: Kinetics of adsorption for metal ions (a) Cd^{2+} (b) Co^{2+} (c) Mn^{2+} (d) Ni^{2+} ; initial ion concentration=200 ppm. (Inset: Adsorption kinetics at lower time scale (a) Cd^{2+} (b) Co^{2+} (c) Mn^{2+} (d) Ni^{2+})

| | | | | | |
|----|-----------|------|------|-------|-------|
| 1. | Cd^{2+} | 1.95 | 1.24 | 0-300 | 0.998 |
| 2. | Co^{2+} | 4.43 | 2.54 | 0-215 | 0.983 |
| 3. | Ni^{2+} | 4.38 | 3.93 | 0-250 | 0.988 |
| 4. | Mn^{2+} | 0.79 | 1.29 | 0-150 | 0.989 |

Concentration range

* Correlation coefficient

Adsorption kinetics (figure 4) shows adsorption rate followed $Cd^{2+} > Mn^{2+} > Co^{2+} > Ni^{2+}$. Among the four ions, Cd^{2+} had the highest adsorption rate; within 1 hr more than 90% of the initial 200 ppm Cd^{2+} ions were removed. Meanwhile, Ni^{2+} had the lowest adsorption rate; within 1 hr time only upto 70% Ni^{2+} could be removed. It was interesting to see that not only the equilibrium adsorption of the Cd^{2+} ions was highest but also its rate of adsorption was fastest.

Competitive adsorption from aqueous solution containing same concentration (100 ppm) of Cd^{2+} , Co^{2+} , Ni^{2+} , and Mn^{2+} ions was carried out. The equilibrium adsorption from mixed solution followed the pattern $Cd^{2+} > Ni^{2+} > Mn^{2+} > Co^{2+}$ which was different from that obtained in the case of individual ion solution where the order was $Cd^{2+} > Co^{2+} > Ni^{2+} > Mn^{2+}$. These result showed that though uptake of ions like Cd^{2+} were not affected by presence of other metal ions but adsorption of ions like Co^{2+} was affected by presence of other metal ions in the solution [27].

3.2. Mutual radiation grafting of quaternary ammonium salts (QATS) on cotton

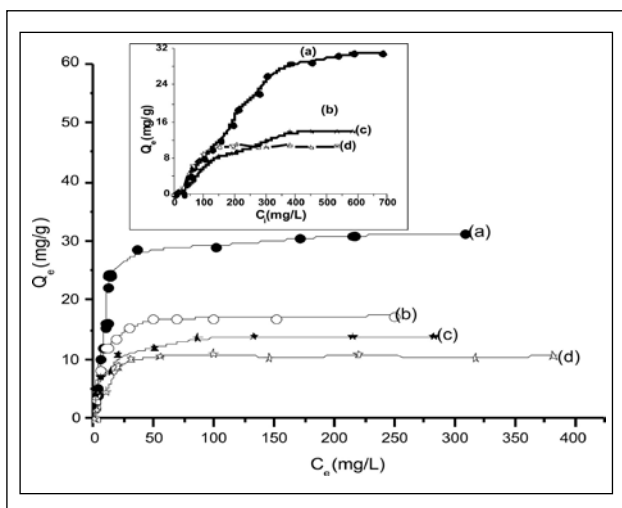


Figure 3: Adsorption isotherm for metal ions (Q_e Vs Initial metal ion concentration). (a) Cd^{2+} (b) Co^{2+} (c) Ni^{2+} (d) Mn^{2+} . Inset: Q_e Vs Metal ion concentration after adsorption. (a) Cd^{2+} (b) Co^{2+} (c) Ni^{2+} (d) Mn^{2+}

3.2.1 Antibacterial properties of quaternary ammonium salts grafted cotton

Grafting of three QATs (structures shown below) onto finished cotton cloth was carried out to introduce antibacterial property.

All three monomers underwent very fast radiation induced polymerization to yield water soluble macromolecules at appropriate radiation doses. Grafting extent increased with dose and monomer concentration for VBT and MAETC however for AETC increase in grafting extent was observed only in presence of co-monomer HEMA. Inhibitory effect on grafting extent in presence of additives like Mohr's salt, copper salt and inorganic acids was observed. Presence of O₂ hindered the grafting reaction; however de-aeration didn't enhance grafting significantly as shown in figure 5. Grafting enhanced the water uptake capacity (Figure 6) and changed the texture of pristine smooth fiber to rough.

Antibacterial activity of the grafted products was studied against gram positive bacteria *Staphylococcus aureus*, *Bacillus cereus* and gram-negative bacteria *Escherichia coli*, *Pseudomonas*

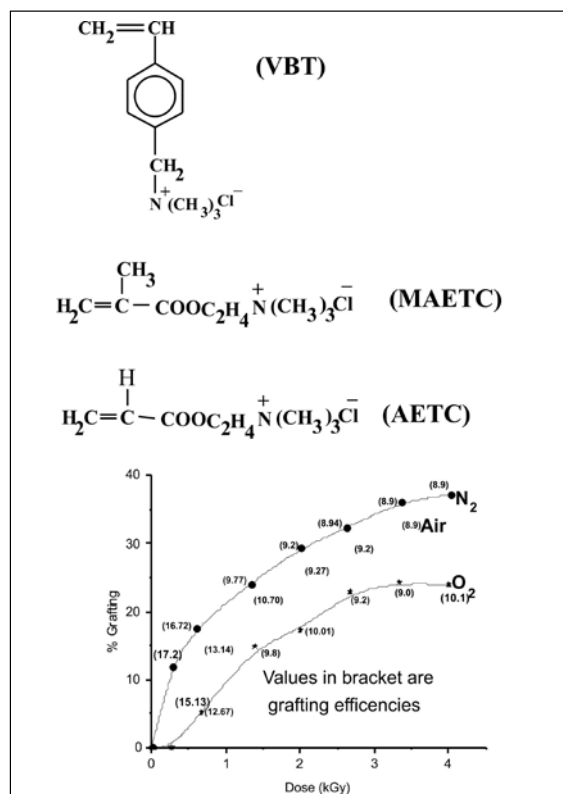


Figure 5: Effect of ambience on grafting: [VBT] = 20% (w/w) in water, Dose rate: 4.0 kGy.h⁻¹

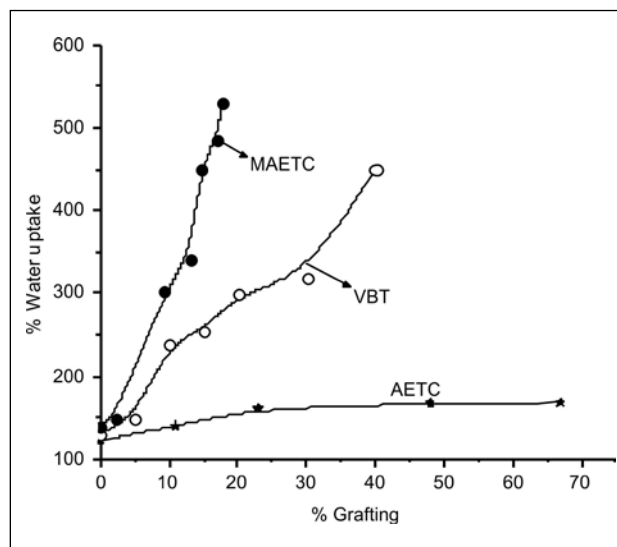


Figure 6: Water uptake by grafted cotton

fluorescens. Antibacterial activity of the grafted cotton was a function of type of monomer grafted [28, 29]. The VBT grafted cotton samples showed excellent anti-bacterial activity against strains *E. coli* and *S. aureus*. Table 3 and Table 4 show time dependent decrease in the counts of *E. coli* and *S. aureus* when VBT-grafted cotton with different extents, were tested for anti-bacterial activity.

It was observed that grafted samples showed toxicity against both these organisms at grafting levels as low as ~5 %. The toxicity increased with the grafting extent of 13 % and thereafter no significant increase in toxicity was observed. The samples grafted to the extent of ≥ 13 % showed a deduction of ~4-5 log cycles within first 2 hours and 4 hours for *E. coli* and for *S. aureus* respectively.

Table 3. Effect of grafting extent on *E. Coli* cells

| Time of exposure (hrs) | % Grafting | | |
|------------------------|---------------------|---------------------|---------------------|
| | 5 % | 13 % | 20 % |
| 0 | 1.0x10 ⁹ | 1.1x10 ⁹ | 1.0x10 ⁹ |
| 2 | 2.8x10 ⁸ | 4.0x10 ⁴ | 1.0x10 ⁵ |
| 4 | 2.0x10 ⁸ | 1.2x10 ⁴ | 4.0x10 ⁴ |
| 6 | 7.5x10 ⁸ | --- | 1.0x10 ⁴ |

Table 4: Effect of grafting extent on *S. aureus* cells

| Time of exposure (hrs) | % Grafting | | |
|------------------------|-------------------|-------------------|-------------------|
| | 5 % | 13 % | 20 % |
| | Counts (CFU/ml) | | |
| 0 | 1.0×10^9 | 1.0×10^9 | 1.1×10^9 |
| 2 | 1.0×10^9 | 6.1×10^8 | 1.0×10^9 |
| 4 | 1.0×10^9 | 1.8×10^4 | 1.7×10^4 |
| 6 | 8.0×10^6 | 3.0×10^4 | 1.6×10^4 |

The anti-bacterial activity of the grafted cotton samples was retained after several cycles of washing and drying in a commercial detergent powder.

The qualitative test for antibacterial activity of radiation synthesized PMAETC in nutrient broth showed it to be bactericidal as there was no significant increase in turbidity and number of colonies formed on solid media reduced with time. These results indicated the macromolecule is bactericidal in nature rather than bacteriostatic. The MBC of the macromolecule ranged from 0.025 to 0.075% depending on the organism used. The lowest MBC was found to be for *S. aureus*, followed by *E. coli*, *B. cereus* and *P. fluorescens*. Figure 7(a-d) shows reduction in initial load of *E. coli*, *S. aureus*, *B. cereus* and *P. fluorescens* with time for MAETC grafted samples grafted to different extents. Antibacterial assay showed variations in activity between pure PMAETC and grafted on cotton. The activity of grafted samples was less as compared to pure macromolecule, which may be due to its bound state on cotton but it was observed that grafted sample showed antibacterial activity against all these organisms at grafting levels as low as 2%. The antibacterial activity increased with extent of grafting up to 19% and thereafter there was no significant increase in activity. Maximum activity was found against *S. aureus*, as there was approximately 5-log cycle kill in 24 h (figure 7-b). This was expected as PMAETC had lowest MBC against this organism. In case of *B. cereus* (figure 7-c) and *E. coli* (figure 7-a), up to 4 log cycle was observed with 19% grafting followed by *P. fluorescens* (fig 7-d) where only 3 log cycle kill was observed.

Reduction in bacteria *E. coli* and *S. aureus* was also monitored with time for sample grafted to an extent of ~33%. It was found that reduction in initial count reaches minimum value after 6 hours itself and thereafter no significant decrease

in the number of organism is observed. These studies establish that decrease in bacterial count is less than the VBT grafted cotton as reported earlier [28] and also the decrease is not to that extent as in the earlier case. This indicated that VBT-grafted cotton inhibits the growth of *E. coli* and *S. aureus* more efficiently and effectively in comparison to MAETC grafted cotton.

For AETC-grafted-cotton anti-bacterial activity followed order: pure macromolecule > grafted cotton > co-grafted cotton > co-polymer [30]. The lower activity of the grafted matrices may be due to bound state of these polymer/co-polymer chains wherein the flexibility of the grafted chains is restricted which restricts the diffusion of hydrophobic chain into the bacteria once the bacteria held by charged interactions [31].

The AETC grafted cotton showed antibacterial activity against all these organisms at grafting levels as low as 4.7% and increased with grafting extent. The co-grafted matrices showed noticeable antibacterial activity at much higher grafting extent of ~11% which didn't improve on increase in co-grafting extent. Maximum activity was found against gram positive *S. aureus* & *B. cereus* and not so significant activity was found against gram negative *E. coli* & *P. fluorescens*. This was on expected lines as poly(AETC) had highest MBC against *E. coli* & *P. fluorescens*. This observation was important in the sense that AETC grafted matrices were effective against gram positive bacteria whereas our earlier studies show that VBT and MAETC [28,29] were more effective against gram negative organisms which are known to have lipopolysaccharide layer present over their cell walls [32].

3.3 Mutual radiation grafting of AA onto micron thick PP membrane for battery separator applications

For AA-PP grafting system grafting, presence of Mohr's salt effectively retarded the polymerization of acrylic acid but did not lead to significant grafting enhancement. Mohr's salt in presence of acids was found to be effective in enhancing the grafting yield. Figure 8 shows effect of combination of salt with acid on grafting extent.

Contact angle measurement studies of the

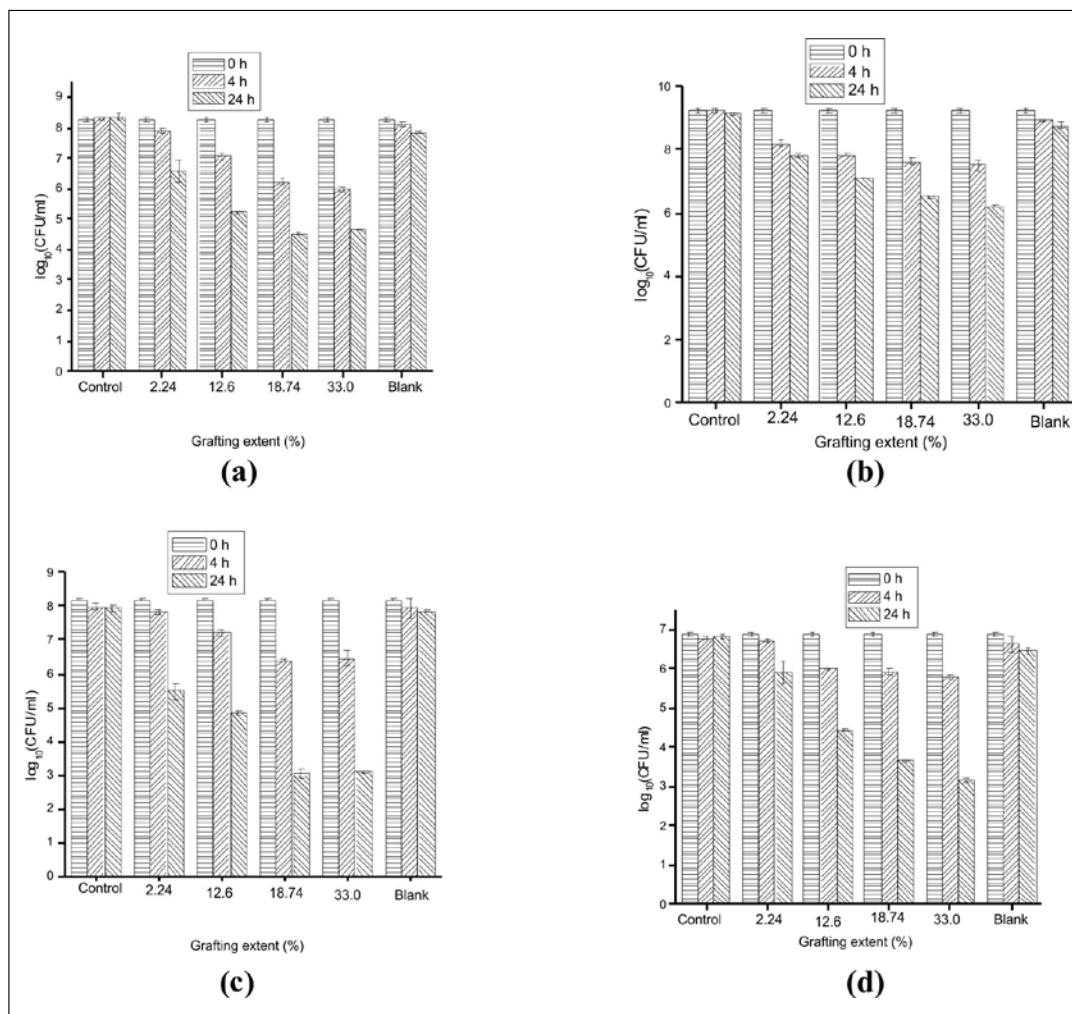


Figure 7: Anti-bacterial activity of MAETC-g-cotton against (a) *E. coli* (b) *S. aureus* (c) *B. cereus* (d) *P. fluorescens*

grafted and radiation treated polypropylene showed that initial grafting as well as radiation treatment of poly(propylene) in aqueous medium and in presence of Mohr’s salt enhances its affinity towards the grafting solution (figure 9). The surface energy measurement using solvents water and diiodomethane with Owens-Wendt method [33] indicated enhancement in the polar component of surface energy of treated polypropylene membrane is the primary cause of surface energy increase.

The developed AA grafted PP sheet was tested for its performance under actual battery conditions vis-à-vis the battery separator membrane presently used by Indian battery industry. For testing the grafted samples, the samples grafted to different extent were put in one Ni/2Cd electrode cells and soaked with KOH electrolyte. All the cells were subject to C/5

charging and 1C rate discharging. Those samples, which enabled the cells to pass 60 minutes of discharging, were considered to be working satisfactorily. Samples grafted to different extents were tested. Figures 10 and 11 show the results of some of the samples. It was seen that samples grafted to extent of 10% did not give satisfactory results. The samples grafted to extent >20% only gave satisfactory results. The sample grafted to an extent of 21% was also used for a full cell consisting of 17 Ni and 16 Cd electrodes. The performance was at par with the cell assembled using battery separator presently used by the industry. The actual testing results indicated that grafting not only converts the hydrophobic PP into battery active hydrophilic state but also helps to retain the hydrophilic state over longer storage period, which is a necessity for Ni-Cd batteries [34].

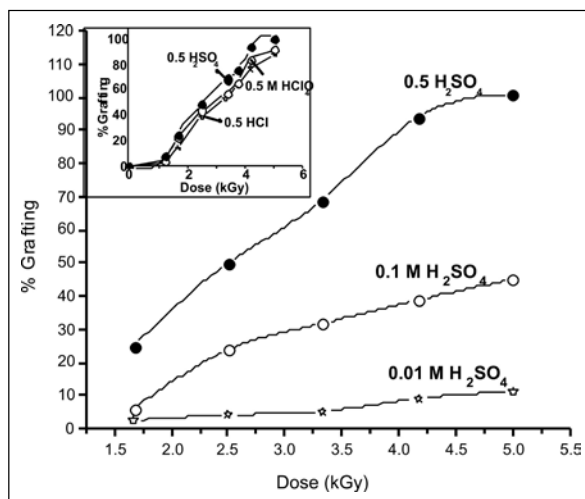


Figure 8: Effect of H_2SO_4 on grafting in 20 % AA + 4 % $FeSO_4 \cdot (NH_4)_2SO_4$ at a dose rate of $5 \text{ kGy} \cdot h^{-1}$

3.4 Teflon scrap based cation exchanger by radiation grafting

Gamma radiation from ^{60}Co -gamma radiation source was used to covalently link acrylic acid to Teflon by mutual radiation grafting technique. The grafting extent decreased with increasing dose rate and increased with monomer concentration and optimum concentration of Mohr’s salt. & sulphuric acid. As shown in figure 12 the extent and depth of grafting was strong function of the backbone thickness.

The crystallinity of the PTFE increased on irradiation (Figure 13). Probably that is why the grafting extent depends so significantly on

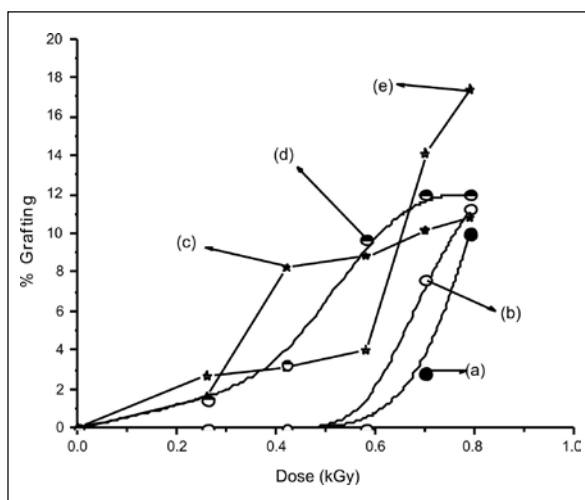


Figure 9: Grafting of treated (a) Untreated (b) Grafted to ~ 0.99 % (c) Irradiated in water (d) Irradiated in $0.5 \text{ mol} \cdot \text{dm}^{-3} H_2SO_4$ (e) Irradiated in 4 % Mohr’s salt. Dose rate= $3.2 \text{ kGy} \cdot \text{hr}^{-1}$

thickness. As during grafting the bulk of the backbone could further crystallize and hinder immediate grafting reaction.

AFM image studies and kurtosis of the AFM images (Figure 14) clearly showed that radiation grafting does not uniformly take place over whole surface.

The surface in fact showed more uniformity (less spread) only on higher grafting as reported earlier [35]. Dynamic contact angle measurement studies of the grafted and radiation treated Teflon showed that initial grafting as well as radiation treatment of Teflon enhances its hydrophilicity as shown in figure 15. In order to quantify the change in hydrophobic character of PTFE on treatment and grafting surface energy of the samples was estimated by dynamic contact angle analysis [33]. Table 5 shows results of these studies. It is clear from the values in Table 5 that irradiation of PTFE in water does not affect the surface energy significantly but presence of Mohr’s salt and acid during irradiation does enhance the surface energy when irradiated to higher doses. Probably the increase in surface energy (polar component) in presence of Mohr’s salt and acid is among the reasons which contribute to affinity enhancement of the PTFE for grafting solution which results in higher extent of grafting.

5. CONCLUSIONS

Post irradiation and mutual radiation grafting technique, both can be used for grafting of desired monomers on commercially available

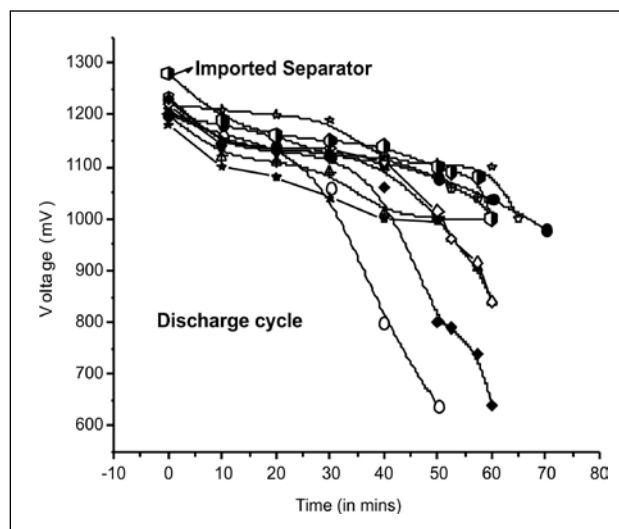


Figure 10: Profiles for charging cycle

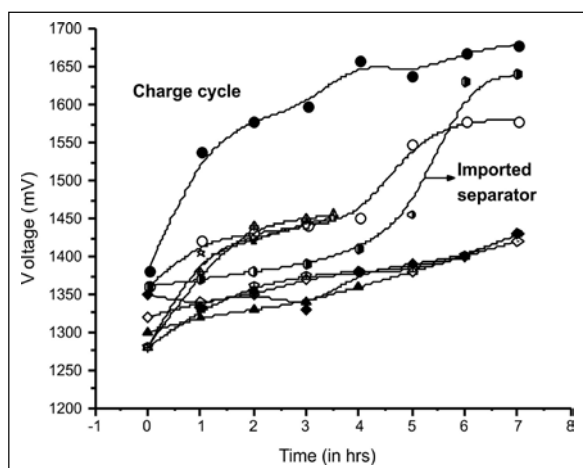


Figure 11: Profiles for discharging cycle

macromolecular backbones to get products which have applications in separation, health-care and waste water treatment industry. High energy radiation sources electron beam or gamma radiation both can be utilized for irradiation purpose depending on the backbone macromolecule. In general for all grafting systems the grafting extent is a function of dose, dose rate, homo-polymer inhibitor, additives like acid and ambience of grafting. As grafting leads to co-grafted product having properties of both the parent precursors, by judicious choice of pre-cursors and experimental conditions a macromolecule like cotton prone to bacterial and fungal attack can be made antibacterial

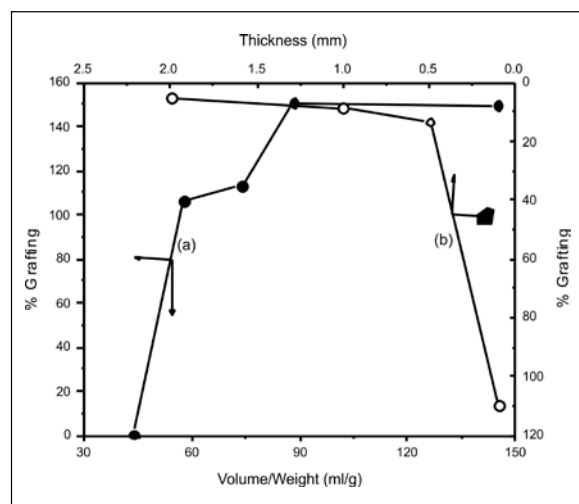


Figure 12: Grafting extent in 20% AA solution containing 4% Mohr's salt + 0.5 mol dm⁻³ H₂SO₄; Dose rate = 3 kGy.hr⁻¹; Total dose = 15 kGy (a) PTFE backbone thickness = 0.1 mm & varying Volume/Initial weight (b) Volume/Initial weight ~73.5 and varying thickness.

which will retain all properties of cotton. Highly hydrophobic macromolecules like PTFE can also be converted to a hydrophilic macromolecule easily with grafting method.

BIBLIOGRAPHY

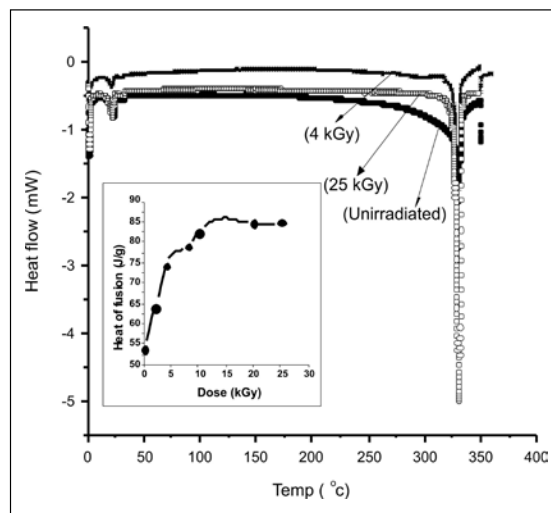


Figure 13: DSC thermograms (thickness = 0.5 mm) irradiated at dose rate of 3 kGy/hr. Inset: Heat of fusion of PTFE irradiated to different doses.

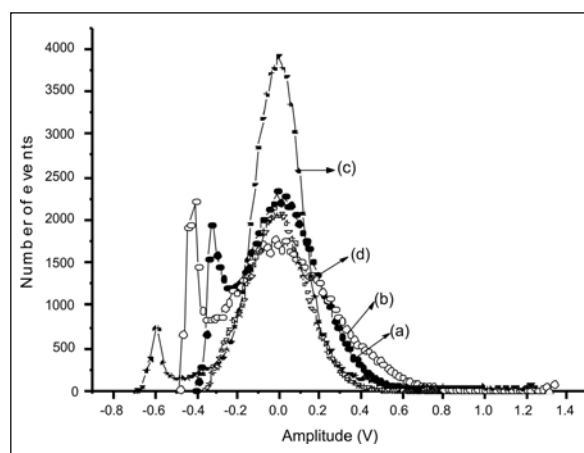


Figure 14: Surface kurtosis studies of the AFM images (a) Un-irradiated thickness = 0.5 mm, (b) Grafted 5.59%, Thick = 0.5 mm, Dose = 2.8 kGy, (c) Grafted 17.75%, Thick = 0.5 mm, Dose = 5.6 kGy, (d) PTFE irradiated in solution Thick = 0.5 mm, Dose = 20 kGy

1. Fanta, G. F., "Block And Graft Copolymerization", Vol I. Ceresa, R.J. (Ed.), Wiley London, (1973).
2. Chapiro, A., Preparation Of Graft Copolymers With The Aid Of Ionizing Radiation. In Radiation Chemistry Of Polymeric Systems. John Wiley & Sons, New York, (1962) Pp. 597-691.
3. Stanett, V., Radiat. Phys. Chem. **35**(1-3) (1990) 82-87.
4. Garnett, J. L., Radiat. Phys. Chem. **14** (1979) 79-99.

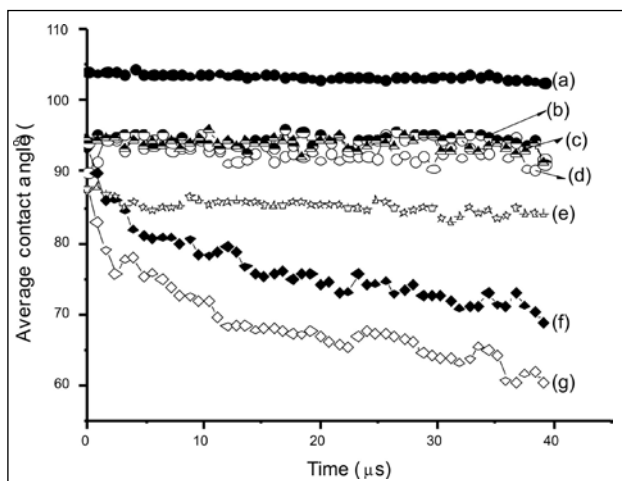


Figure 15: Change in contact angle with time against water (a) PTFE (b) PTFE irradiated in water Dose~24 kGy (c) PTFE irradiated in solution 4% $FeSO_4(NH_4)_2SO_4 \cdot 6H_2O + 0.5 \text{ moldm}^{-3} H_2SO_4$ Dose~24 kGy (d) PTFE grafted ~1.87% (e) PTFE grafted ~8.51% (f) PTFE grafted ~13.57% (g) PTFE grafted ~21.43%

5. Sahiner, A., Pekel, N., Guven, O., React. Funct. Polym. **39(2)** (1999) 139-146.
6. Zhao, D., Sengupta, A. K., Stewart, L., Ind. Eng. Chem. Res. **37** (1998) 4383-4387.
7. Katakai, A., Sugo, T., Makuuchi, K., Nippon Kagaku Kaishi **1** (1994) 68-73.
8. Roper, D. K., Lightfoot, E. N., J. Chromatogr A. **702** (1995) 3-26.
9. Kim, M., Kojima, J., Saito, K., Furusaki, S., Sugo, T., Biotechnol. Prog. **10** (1994) 114-120.
10. Hoffman, A. S., Iaea-tecdoc **486** (1988) 35-61.
11. Kostov, G. K., Turmanova, S. C., Atanassov, A. N., Electron. Electr. Eng. Res. Stud. Electron Mater. Ser. **1** (1995) 676-679.

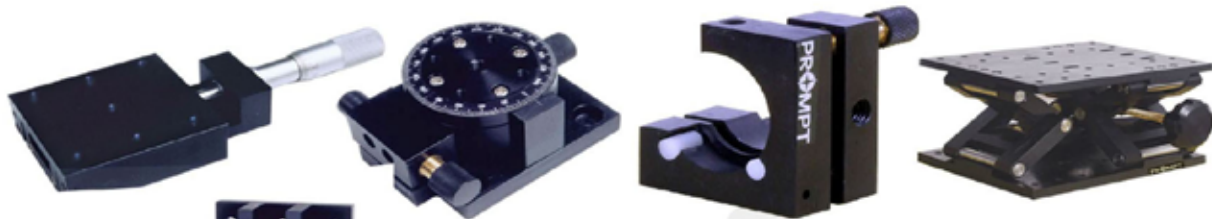
12. Chakravorty, B., Mukherjee, R. N., Basu, S., J. Membr. Sci. **41** (1989)155-161.
13. Masson, J. P., Molina, R., Roth, E., Gaussens, G., Lemaire, F., Adv. Hydrog. Ener. **2** (1981) 99-105.
14. Kabanov, V. Ya., High Energ. Chem. **38(2)** (2004) 57-65.
15. Dong, L. C., Hoffman, A. S., Radiat. Phys. Chem. **28(2)** (1986) 177-182.
16. Carezza, M., Radiat. Phys. Chem. **39(6)** (1992) 485-493.
17. Saito, K., Hori, T., Furusaki, S., Sugo, T., Okamoto, J. Ind. Eng. Chem. Res. **26** (1987) 1977-1983.
18. Sugo, T., Nippon Kaisui Gakkai-shi. **51(1)** (1997) 20-29.
19. Taher, N.h., Dessouki, A. M., Khalil, F. H., Radiat. Phys. Chem. **36(6)** (1990) 785-790.
20. Hegazy, E. S., Abd El-rehim H., Khalifa, N., Atwa, S., Shawky, H., Polym. Int. **43** (1997) 321-333.
21. Senuma, M., Iwakura, M., Ebihara, S., Shimurab, Y., Keriyama, K. Angew. Makromol. Chem., **204** (1993) 119-124.
- 22.. Gupta, B., Anjum, N., Jain, R., Revagade, N., Singh, H., J. Macromol. Sci. Part-c, Polym. Rev. **C44** (2004) 275-309.
23. Brady, Jr. R. F., Chem. Br., **26** (1990) 427-430.
24. Plunkett, R. J., High Performance Polymers: Their Origin And Development. Seymour, R. B., Kirshenbaum, G. S. (Eds.), Elsevier, New York, (1986) Pp 267-278.
25. Bhardwaj, Y. K., Virendra Kumar, Sarma, K. S. S., Khader, S. A., Sabharwal, S., Barc Technical Report No. Barc/2006/e/004 (2006)
26. Ruthven, D. M., "Principles Of Adsorption And Adsorption Process" Wiley, New York, 1984.
27. Virendra Kumar, Bhardwaj, Y. K., Tirumalesh, K., Dubey, K. A., Chaudhari, C. V., Biswal, J., Sabharwal, S., Sep. Sci & Technol. **41(14)** (2006) 3123-3140.
28. Virendra Kumar, Bhardwaj, Y. K., Rawat, K.p., Sabharwal, S., Radiat. Phys. Chem. **73** (2005) 175-182
29. Goel, N. K., Rao, M. S., Virendra Kumar, Bhardwaj, Y. K., Chaudhari, C. V., Dubey, K. A., Sabharwal, S. Radiat. Phys. Chem. **78** (2009) 399-406.
30. Goel, N. K., Rao, M. S., Virendra Kumar, Bhardwaj, Y. K., Sabharwal, S., Radiat Phys. Chem. **80** (2011) 1233-1241.
31. Suvet, G., Dupond, S., Kazmierski, K., Chojnowski, J., J.

Table 5: Surface energy of samples

| Sample | Surface energy (mJ/m ²) | | |
|---|-------------------------------------|-----------------|----------------------|
| | Total Energy | Polar component | Dispersive component |
| Ungrafted Teflon | 22.5 | 1.2 | 21.3 |
| Teflon grafted to an extent of 1.89% | 24.9 | 1.3 | 23.6 |
| Teflon grafted to an extent of 3.48% | 28.4 | 2.7 | 25.6 |
| Teflon grafted to an extent of 8.51% | 29.1 | 4.3 | 24.8 |
| Teflon grafted to an extent of 13.57% | 32.9 | 6.9 | 23.6 |
| Teflon grafted to an extent of 21.43% | 41.3 | 14.6 | 26.7 |
| Teflon irradiated in aqueous solution containing 4 % Mohr's salt+0.5 M H ₂ SO ₄ (Dose = 4 kGy) | 25.4 | 1.8 | 23.6 |
| Teflon irradiated in aqueous solution containing 4 % Mohr's salt+0.5 M H ₂ SO ₄ (Dose = 18 kGy) | 30.5 | 8.7 | 21.8 |
| Teflon irradiated in water (Dose = 4 kGy) | 22.8 | 2.5 | 20.3 |
| Teflon irradiated in water (Dose =18 kGy) | 23.1 | 2.8 | 20.4 |

- Appl. Polym. Sci. **75(8)** (2000) 1005-1012.
32. Bozja, J., Sherrill, J., Michielsen, S., Stojilkovic, I., J. Polym. Sci. Part A-polym. Chem. **41**, (2003) 2297-2303.
33. Virendra Kumar, Bhardwaj, Y. K., Jamdar, S. N., Goel, N. K., Sabharwal, S., J. Appl. Polym. Sci. **102** (2006) 5512-5521.
34. Thomas, S. P., Thomas, S., Abraham, R., Bandyopadhyay, S., Express Polym. Lett. **2(7)**, (2008) 528-538.
35. Goel, N. K., Bhardwaj, Y. K., Manoharan, R., Virendra Kumar, Dubey, K. A., Chaudhari, C. V., Sabharwal, S., Express Polym. Lett. **3(5)** (2009) 268-278.
36. Chaudhari, C. V., Paul, J., Panicker, L., Dubey, K. A., Virendra Kumar, Goel, N. K., Bhardwaj, Y. K., Sabharwal, S., Environ. Prog. & Sustain. Ener. Doi: 10.1002/ep.10533.

| | |
|---|--|
|  | <p>Mr. N. K. Goel completed his post graduation in chemistry from M. D. University, Haryana with gold medal in 2001 and joined the Radiation Technology Development Division; BARC in 2003. He is from 46th Batch (Chemistry). Since then he has been involved in developing various products like Battery separator, antibacterial and antifungal bandages ion exchange membranes etc. by using radiation technology. It involves surface modification of various synthetic and semi-synthetic macromolecules with Gamma radiation. He has number of publications in international journals and symposia/conferences to his credit.</p> |
|  | <p>After obtaining his M.Sc. degree in Chemistry from IIT Roorkee in 1998, Dr. Virendra Kumar joined Radiation Technology Development Section, BARC in 1999, through 42nd batch (1998-1999) of BARC Training school. Dr. Virendra Kumar obtained his Ph.D. degree in 2004 from University of Mumbai for his work on radiation effects on water soluble polymer systems. He did his Post-doctoral research during 2007-2009 with Prof. F. Arefi-Khonsari in LGPPTS, ENSCP, Université Pierre et Marie Curie, Paris, France on plasma processing of polymers for biomedical applications. Dr. Virendra Kumar was conferred Dr. P. K. Bhattacharya Memorial Young Scientist award for year 2006 by Indian Society for Radiation and Photochemical Science, INDIA. Dr. Virendra Kumar has more than 35 publications in peer reviewed international journals, 03 book chapters and more than 50 symposium/conference papers in his credit. His current research interest includes radiation cured high performance inorganic/organic hybrid nanocomposite coatings, metal-polymer nanocomposite, radiation induced grafting and plasma processing of polymers for various applications.</p> |
|  | <p>Dr. Y. K Bhardwaj joined Radiation Technology Development Division in 1989 and later did his Ph. D from University of Mumbai. His present research interest includes utilization of high-energy electron beam and gamma radiation for industrial applications. This includes development of grafted polymer matrices for various applications, radiation processing of elastomer blends and coatings for high performance applications. He has been actively involved in the studies on radiation polymerization/crosslinking of monomers/polymers, development of radiation processed hydrogels for medical and pharmaceutical applications, synthesis of fast stimuli-responsive hydrogels and radiation crosslinking behaviour of water soluble polymers.</p> |
|  | <p>Dr. Lalit Varshney joined Isotope Division, Bhabha Atomic Research centre in 1982 after completing 25th batch training school of BARC. He obtained Masters in Science (Chemistry) degree from University of Delhi and Ph. D. from Mumbai University. He is presently, Head Radiation Technology Development Division of Radiochemistry and Isotope Group. Dr. Varshney's contributions in the area of radiation processing of polymers and pharmaceuticals has given a lead to understanding and development of Radiation Processing applications. His work has significantly contributed to growth of pharmaceutical sectors in respect of Radiation Sterilization technology in India and developing countries. Dr. Varshney's dedicated research work on Hydrogels resulted in the development of technology of 'Hydrogel Dressing' which has already been transferred to four companies. Dr. Varshney is currently engaged in the development of advanced materials for medical and environmental applications using radiation technology. Dr. Varshney has about 50 publications, two patents and 4 technology transfers to his credit. Dr. Varshney is recipient of prestigious INS award 2004 and BARC technical excellence award-2003. He can be contacted at 022-25593745, email: lalito@barc.gov.in</p> |



WE MANUFACTURE -
Motorised & Manual translation stages,
Rotary stages, Mounts for lenses, Mirror
prism, Polarisers, Filter etc. Optical Bread
boards, Optical Rails, Optical table
Connectivity Study Cells, Equipments
for various research activities..

We are regular suppliers to The Centre for
Advanced Technology - Indore, National
Atmospheric Research Laboratory - Gadanki,
IIT's, NIT's, CSEZ and various Colleges and
Universities...

PROMPT ENGINEERING WORKS
34/2387-B, Thampuratti Parambu Road,
Palarivattom P.O,
Cochin - 682 025
email - prismount@yahoo.com
Ph - 09388607036, 0484 -2342902

email - prismount@yahoo.com
Ph - 09388607036, 0484 -2342902



ANATECH INSTRUMENTS

Office:

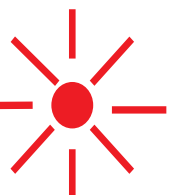
405, B-68, Crescent Tower,
 Off. New Link Road, Next to Dhiraj Heights,
 Andheri (W), Mumbai – 400053.

Tel.: 022-26730463/ 64, 022-26741619/ 20

Fax: 022-26730465/ 26392893

E-mail: anatecb@mtnl.net.in, anatechsales@mtnl.net.in, anatecbmarketing@yahoo.com

Website: www.anatechinstruments.in





Laser Science Services (I) Pvt. Ltd.

**Lasers | Ultrafast & THz Spectroscopy | Thin Film Deposition | Micromachining
CCD's | Streak Cameras | Photovoltaic | Optical Tables | Optics & Opto-mechanics**

Representing - World's leading companies in filed of Lasers, Spectrometers, Camera's & Optical Components for High Resolution Lifetime Spectroscopy & Microscopy applications.

Femtosecond Laser

- ❖ Terahertz Imaging
- ❖ CARS Microscopy
- ❖ Raman Spectroscopy
- ❖ Multiphoton Microscopy.



Time Resolved Ultrafast Spectrometers

- ❖ Transient Absorption
- ❖ Fluorescence Upconversion
- ❖ Flash Photolysis System
- ❖ Microsecond Flash photolysis



Excimer Lasers

- ❖ Pulsed Laser Deposition
- ❖ Micromachining
- ❖ Lithography
- ❖ FBG Writing



Single Frequency Laser

- ❖ Interferometry
- ❖ Test & Measurement
- ❖ Spectroscopy
- ❖ Metrology



THz Spectroscopy Kit

- ❖ THz Spectroscopy
- ❖ Imaging
- ❖ Explosive detection
- ❖ Material Inspection



Super Continuum Source

- ❖ Fluorescence Lifetime Imaging
- ❖ TIRF Microscopy
- ❖ Single Molecule Imaging
- ❖ Optical Coherence Tomography



Optical Tables & Components

- ❖ Mirrors, Lenses
- ❖ Optical Filters
- ❖ Manual & Motorized Stages
- ❖ Optical Tables



CCD & Streak Cameras

- ❖ Low Light Imaging
- ❖ Microscopy
- ❖ Spectroscopy
- ❖ High Speed Imaging



Laser Spectra Services India Pvt. Ltd. BANGALORE

Spectra-Physics
A Division of Newport Corporation

Newport
Optical Solutions

HORIBA JOBIN YVON

ULTRAFAST LASERS

- MaiTai, One Box Ti:Sapphire Oscillators
- Tsunami, Ultrafast, Ti:Sapphire Lasers
- SpitFire Ace, Ultrafast Ti:Sapphire Lasers
- TOPAS, Automated Ultrafast OPA
- OPA 800 Ultrafast OPA
- OPAL Femtosecond OPO
- PulseScout Autocorrelator/Spectrometer



P.V & PHOTONICS TOOLS

- Class AAA, Solar Simulator, I-V Tester,
- IQE, IPCE Systems
- Light Source & Spectroscopy
- Vibration Isolation Table
- Motion Controller
- Optics & Opto Mechanics



FLUORESCENCE

- Steady State Fluorescence Spectrometer
- Fluorescence Lifetime Spectrometer
- NanoLog
- Remote Sensing Instruments
- TCSPC Lifetime Instruments
- Fluorescence Microscopy



RAMAN SYSTEMS

- Lab-Ram, Analytical Raman System
- T64000/U1000, High Resolution Raman Systems
- Process Raman System
- Modular Raman System
- Fiber Raman Microscopes



M/s. Laser-Spectra Services India Pvt. Ltd.,
80/10, I Floor, Raj Towers,
M. S. Ramiah Main Road,
Mathikere,
BANGALORE-560 054.

Phone : +91(0)-80-23576 907
Fax : +91(0)-80-23576 904
Web : <http://www.laser-spectra.com>



LASER SPECTRA SERVICES



619, Nirmal Lifestyle Corporate Centre, LBS Marg, Mulund West, Mumbai 400080. Ph: 022-25613102, 022-25610903
 Web: www.advancedphotonicsindia.com
 Email: sales@advancedphotonicsindia.com

Complete Photonics Solutions For Research and Industry



Active Vibration Cancellation Technology
 Vibration Isolation Workstations
 Non-isolating Support Systems
 Isolators and Bread Boards
 Air Compressors & Acoustic Encloser



Lenses, Mirrors
 Prism, Beam Splitters
 Polarisers, Filters
Richardson Gratings

Manual / Motorized Motion Systems
 Translation / Rotation Stage
 Actuators / Goniometric Cradles
 PicoMotor stages / Actuators

Precision Custom Optical Components
 UV to IR material coatings
 Precision Metal Optics
 Laser Growth, Pockel Cells, Autotracker
 Reflective Coatings, UV VIS and IR coatings



Spatial Light Modulators
 Phase Modulators, Amplitude Modulators
 Applications: Laser Beam Shaping, Phase Shifting, Laser Pulse Modulation



Terawatt and Petawatt femtosecond laser
 High Power femtosecond KHz amplifier
 Beam Diagnostics and Beam Measurement System



CCD Detectors
 Monochromator & Spectrographs
 Flat Field Imaging Spectrographs
 Raman Spectroscopy



Alignment, attachment and packaging systems for fiber optic components



Spectroradiometer
 Photometer
 Videophotometer
 Colorimeter
 Integrating Sphere Calibration Standard

Luminance/ Radiance Standards
 Uniform Light System for Detector Calibration
 Lamp Measurement Systems
 LED & Laser Power Measurement Systems
 Reflectance/Transmittance Meas. System
 Integrating Spheres
 Light Source & Detectors

Fiber Optic Spectrometers
 Optical Fibers
 Thin Film Measurement

LIBS, reflectance and transmittance measurement



Auroal Studies, Sky Imaging System
 Low Light level measurements
 Imaging for Airglow (Mesosphere and Low Thermosphere)

Goniometers, Photometers
 Imaging spheres
 Light measurement for Luminaries, Single LEDs and Displays



InGaAs APDs, InGaAs arrays, Line scan Cameras
 High power multi mode and single mode lasers
 Single photon detectors, benchtop receivers



Total Solution provider in field of photonics

Radiometer/Photometer
 Spectroradiometers
 Systems for Photometry, Radiometry
 LED modules



Femtosecond Fluorescence Upconversion Spectrometer
 Femtosecond pump probe transient absorption spectrometer
 Femtosecond Oscillator (Ti:Sapphire laser and laser kits)
 Femtosecond Amplifiers



IR Cameras



UltraFast Pulse Shaper and Pulse measurement System
 UltraFast Pulse Energy Stabilization
 Pulse Optimization System

